STUDIES OF A GENOMIC FOSFOMYCIN RESISTANCE PROTEIN FROM

*PSEUDOMONAS AERUGINOSA*

By

Rachel Pharris Rigsby


Dissertation

Submitted to the Faculty of the

Graduate School of Vanderbilt University

in partial fulfillment of the requirements

for the degree of

DOCTOR OF PHILOSOPHY

in

Chemistry

August, 2005

Nashville, Tennessee


Approved:

Professor Richard N. Armstrong

Professor Lawrence J. Marnett

Professor Carmelo J. Rizzo

Professor Michael P. Stone

Professor Alan R. Brash

# ACKNOWLEDGEMENTS

I would like to thank my parents, husband, and family for their love and support. Without them I would never have succeeded. Thanks also to AW, AB, BL, and JB for their wonderful friendship. Everyone should have such a caring, honest network of support. I am forever indebted to ACH for introducing me to the wonders of science and for his encouragement which led me to pursue a career in chemistry. I am thankful for RWK, DFO, HCC, RHF, and WLM, the wonderful science professors who guided my undergraduate career. Special thanks to BRE for his support and assistance during those years and his continued friendship. Thanks to DKE, who taught me to not take myself so seriously and who was a wonderful instructor, mentor, and friend.

I have to thank KCF for patiently enduring me as an undergraduate research fellow. He must surely have thought I would never succeed. Thanks to Carmelo Rizzo, Larry Marnett, Alan Brash, and Michael Stone, my graduate committee. Their advice and kindness have been appreciated. I must thank my labmates, especially KLF, who was an exceptional mentor and great friend. Thanks to CLR, LCT, LAB, and DWB for helpful discussions and for making the lab much more fun.

Finally, I must thank my advisor, Richard Armstrong. He believed in me when I was ready to give up, and without his encouragement I surely would not have completed my degree. I truly owe him a great deal.

TABLE OF CONTENTS

# LIST OF TABLES

LIST OF FIGURES

# ABBREVIATIONS

| | |
|---|---|
| PEP | Phosphoenolpyruvate |
| UDPGlcNAc | uridine-5'-diphospho-*N*-acetyl-D-glucosamine |
| ANS | 8-anilino-1-naphthalene sulfonate |
| $\alpha$GP | L-$\alpha$-glycerolphosphate |
| GSH | reduced glutathione |
| VOC | Vicinal Oxygen Chelate |
| EPR | Electron Paramagnetic Resonance |
| EDTA | ethylenediamine tetraacetic acid |
| TRIS | tris(hydroxymethyl)aminomethane |
| HEPES | N-2-(hydroxyethyl)piperazine N'-2(ethanesulfonic acid) |
| MOPS | 3-(N-morpholino)-propanesulfonic acid |
| IPTG | isopropyl-$\beta$-D-thiogalactopyranoside |
| DTT | dithiothreitol |
| DEAE | diethyl aminoethyl |
| AQC | 6-aminoquinolyl-N-hydroxysuccinimidyl carbamate |
| HPLC | high pressure liquid chromatography |
| LB | Luria Broth |
| TMA | tetramethyl ammonium |
| FPLC | fast protein liquid chromatography |
| MALDI | matrix assisted laser desorption ionization |
| TOF | time of flight |

| | |
|---|---|
| SDS-PAGE | sodium dodecylsulfate polyacrylamide gel electrophoresis |
| CD | circular dichroism |
| NMR | nuclear magnetic resonance |
| $GSO_3^-$ | glutathione sulfonate |
| PCR | polymerase chain reaction |
| MIC | minimum inhibitory concentration |
| ENDOR | electron nuclear double resonance |
| Pf | phosphonoformate |
| AcP | acetyl phosphonate |
| PAA | phosphonoacetic acid |
| PEP | phosphoenolpyruvate |
| UV | ultraviolet |

CHAPTER I


INTRODUCTION


Antibiotics

In 1896, Ernest Duchesne discovered that *Penicillium* mold could effectively inhibit the growth of *E. coli* and prevent typhoid infections if injected concomitantly with the bacteria. Alexander Fleming's work in the 1920s on the same mold lead to a revolution in modern medicine. In a few years, for the first time in history, tuberculosis, pneumonia, and a myriad of other infections could be easily treated. Since Fleming's seminal observation, chemists and biologists have worked to isolate, characterize, and synthesize molecules capable of inhibiting microbial growth. Compounds have been designed to disrupt three main pathways necessary for bacterial survival. These include inhibition of DNA, protein, and cell wall synthesis (Figure 1). Quinolones interfere with topoisomerases, which regulate DNA supercoiling and thus transcription. Macrolides and related drugs disrupt protein synthesis by binding ribosomes. The third class targets enzymes involved in bacterial cell wall synthesis. These molecules have decreased risk of side effects since there are no equivalent human enzymes.

Cell wall biosynthesis is the process by which microbes assemble the complex molecular structure which allows them to resist osmotic pressure and other environmental stresses. It begins with the reaction of phosphoenolpyruvate (PEP) with uridine diphospho-N-acetyl-D-glucosamine, generating UDP-N-acetylenolpyruvyl glucosamine
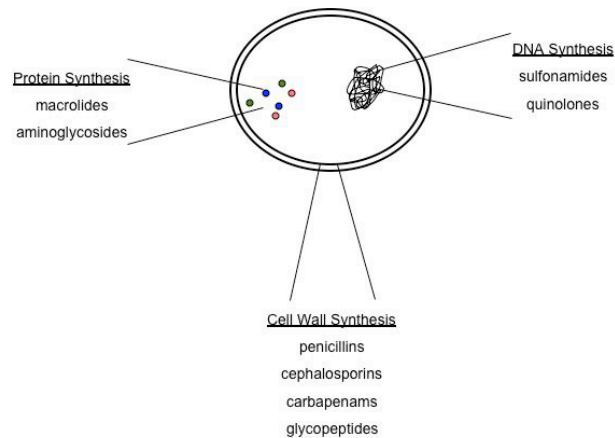
Figure 1. Cellular targets of the major classes of antibiotics.

(Figure 2) (*1*). This is reduced by NADPH to UDP-N-acetyl muramic acid. A series of amino acids are added sequentially by the MurC-MurF enzymes. The precursor is then localized to the cell membrane via transfer from the uridyl carrier to the phosphate group of a C55-isoprenoid alcohol phosphate by MraY, generating Lipid I. N-acetyl- D - glucosamine is then transferred from uridine to the lipid-linked *N*-acetylmuramic acid residue by MurG, generating Lipid II. A series of steps add peptide cross-links between lipid chains, leading to the generation of mature peptidoglycan.

Many steps in peptidoglycan synthesis have been targets of antimicrobial therapies. Penicillin and other β-lactams are structural analogs of D-alanyl-D-alanine and inhibit enzymes which recognize this moiety, preventing further catalysis toward mature cell wall. Vancomycin and related drugs bind to the D-alanyl-D-alanine portion of the cell wall precursor, also preventing further catalysis. Bacitracin inhibits MraY and prevents transfer of N-acetylmuramyl peptide to the cell membrane.

2
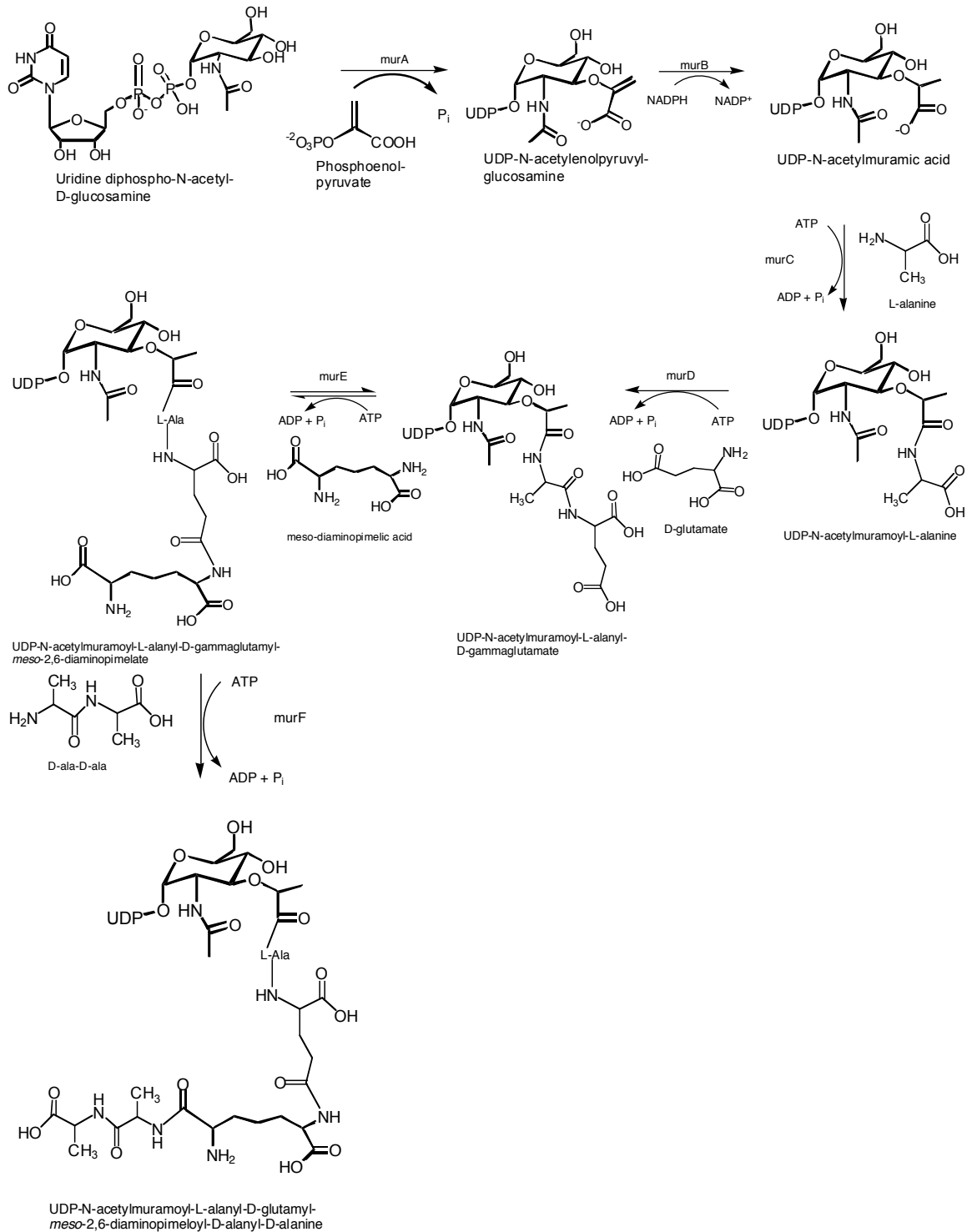
Figure 2. Reactions of the formation of bacterial cell wall components.

Antibiotic Resistance

Although antibiotics have undoubtedly cured countless infections and saved millions of lives world-wide, bacteria continue to wreak havoc in the medical community, creating a $25 billion market for antibiotics annually in the US alone (*2*). Resistance can be acquired from a variety of sources—plasmids, bacteriophage, and free DNA—containing transposons and other resistance elements (Figure 3A). Resistance genes may be incorporated into the genomic material or remain separate as a plasmid.

Resistance can be achieved through a variety of mechanisms. Spontaneous resistance can occur through random mutations in target proteins which are capable of carrying out their native function while resisting attack by an antibiotic. Alternatively, modulation of uptake or efflux systems by mutation of receptors expressed in the cell membrane can prevent antibiotic molecules from entering or hasten their export from the cell. Cytosolic proteins capable of sequestering antibiotic molecules can prevent them from reaching their cellular target. Finally, expression of proteins which can alter or decompose an antibiotic into an inactive form also protects the bacteria (Figure 3B).

The resistance problem has affected every class of antibiotic (Table 1). With the exception of vancomycin, bacterial resistance emerged within a few years of an antibiotic's introduction into the clinic. Identification of β-lactamases, which break down penicillin and related compounds, now limit the effectiveness of these wonder drugs. Even vancomycin, used as a last resort to treat resistant infections, is susceptible. A plasmid-encoded resistance cassette allows bacteria to produce a modified cell wall precursor (UDP-muramyl-tetrapeptide-D-lactate) which has low affinity for vancomycin (*3*).

A
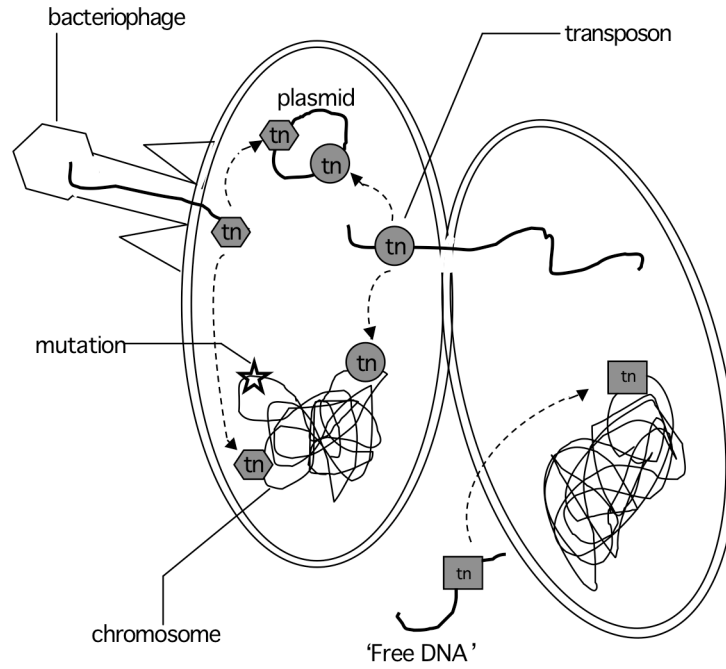


B
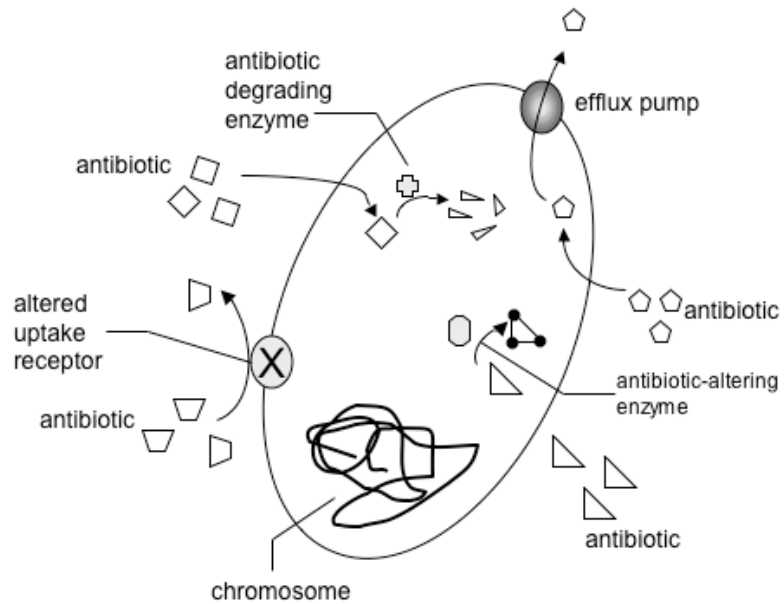


Figure 3.  A.  Modes of acquisition of antibiotic resistance elements.  B.  Methods bacteria utilize to protect themselves from antibiotic.  Adapted from (*4*).

5

**Table 1.** Relationship between discovery, introduction into the clinic, and identification of resistance for selected antibiotics. Taken from (*3*).

| Antibiotic | Discovered | Introduced in the clinic | Resistance identified |
|---|---|---|---|
| Penicillin | 1940 | 1943 | 1940 |
| Streptomycin | 1944 | 1947 | 1947 |
| Tetracycline | 1948 | 1952 | 1956 |
| Erythromycin | 1952 | 1955 | 1956 |
| Vancomycin | 1956 | 1972 | 1987 |

What is being done to resolve the resistance problem? Medical and scientific professionals are educating themselves and the public on the proper use of antibiotics. Some health professionals have also begun withholding treatment with new antibiotics such as Zyvox except as a last resort (*2*). New treatments include development of narrow-spectrum agents or enzyme inhibitors which could be utilized in combination therapies with resistant organisms (*5*).

Fosfomycin

In 1969 Hendlin and coworkers reported the discovery and synthesis of a novel phosphonate isolated from cultures of *Streptomyces* which was effective as an antibiotic against Gram positive and negative bacteria (*6, 7*). The compound, (1*R*, 2*S*)-1,2-epoxypropylphosphonic acid, or fosfomycin, acted by irreversibly inhibiting uridine-5'-diphospho-*N*-acetyl-D-glucosamine-3-enolpyruvyltransferase (MurA), the enzyme which catalyzes the first step of cell wall biosynthesis (Figure 2) (*8*). It is known that binding of substrate (UDPGlcNAc) to MurA induces large conformational changes, and it has been

shown that UDPGlcNAc binding is required for fosfomycin inactivation to occur. Inactivation by fosfomycin occurs in a bimolecular mechanism (Figure 4) involving the formation of a reversible enzyme-substrate complex followed by the irreversible covalent modification of the enzyme by fosfomycin (*9*).

Inactivation has been measured in two ways. MurA reacts with 8-anilino-1-naphthalene sulfonate (ANS) such that ANS fluorescence is quenched upon substrate binding to enzyme. Addition of fosfomycin to MurA•UDP-GlcNAc produces a structural change with a bimolecular rate constant $k^*_{struc}$ of 85 $M^{-1}s^{-1}$. Inactivation studies of the same complex in the presence of fosfomycin produces a similar rate constant $k^*_{inact}$ of 104 $M^{-1}s^{-1}$. The similarity of these independently measured rate constants indicates that fosfomycin-induced structural changes of MurA and enzyme inactivation occur in parallel.

$$MurA + S_1 \xrightleftharpoons[88\ \mu M]{K_{D(S1)}} E \cdot S_1 \xrightarrow{\ k^*\ (fosfomycin)\ } I\text{-}E^* \cdot S_1$$
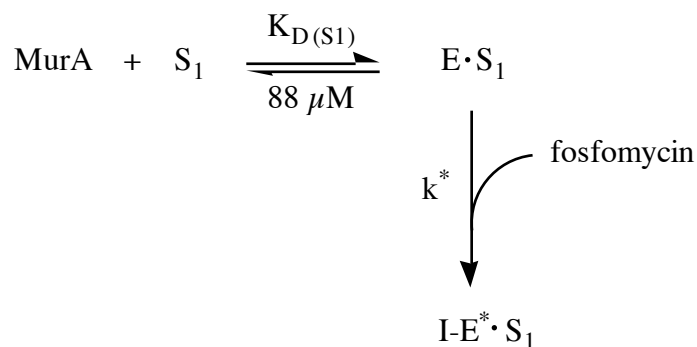
Figure 4. Mechanism for the inactivation of MurA by fosfomycin. $S_1$ is UDP-GlcNAc.

X-ray crystal structures obtained with UDP-GlcNAc and fosfomycin present in the MurA active site show the antibiotic adducted to Cys115 (Figure 5A). A variety of positive residues, necessary for binding phosphoenolpyruvate, coordinate to fosfomycin equally well (Figure 5B).

A

B
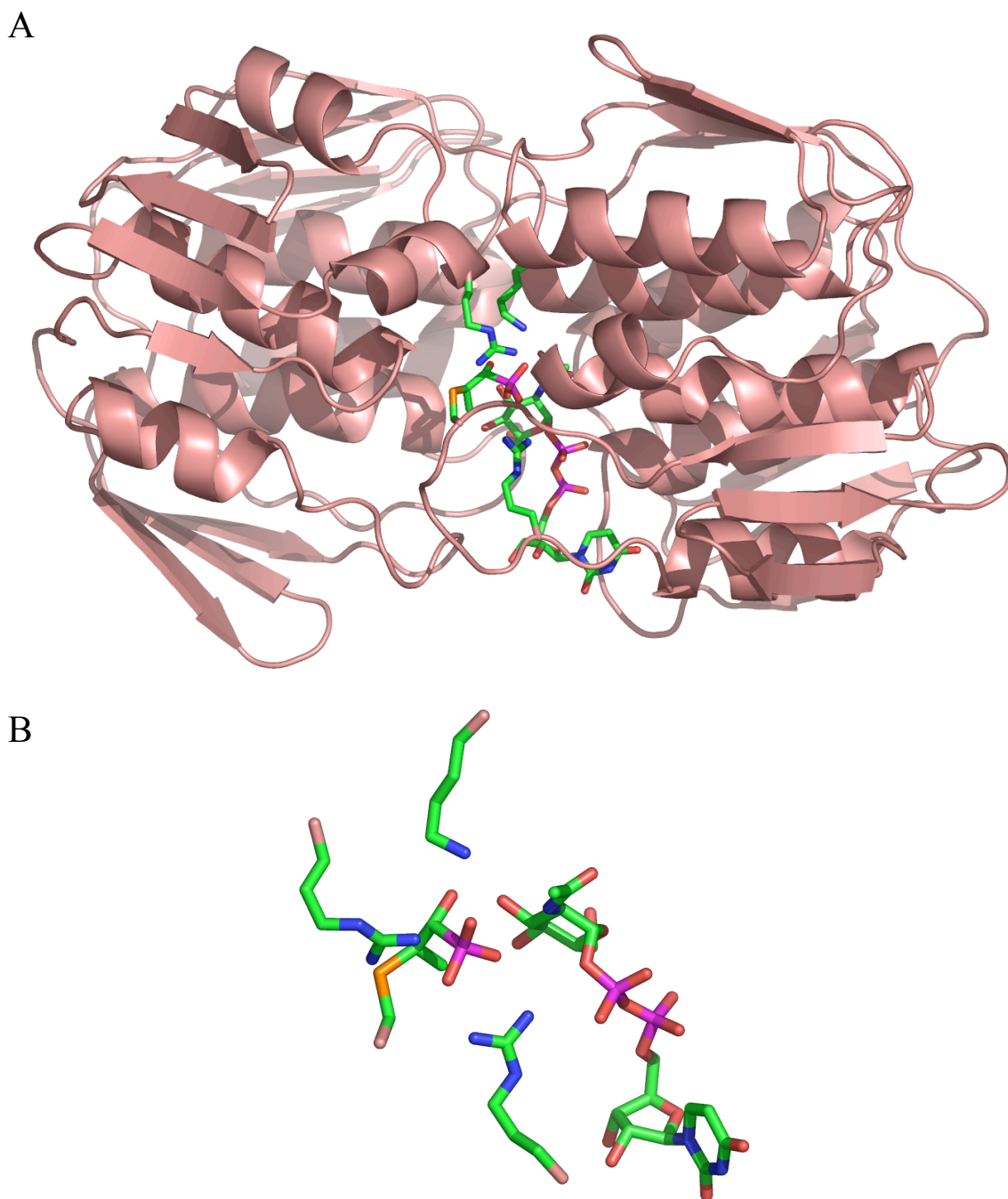
Figure 5. A. Ribbon representation of MurA (from 1UAE.pdb). UDP-GlcNAc, fosfomycin, and several active site residues are shown as sticks. B. Enlargement of the active site, showing fosfomycin bonded to Cys115. UDP-GlcNAc (top right) is shown, as are R120, R397, K22 and C115. Figures were made using PyMOL (*10*).

While fosfomycin is an excellent antibiotic—its mechanism of inactivation is irreversible and its target has no homologue in mammals, thus preventing side effects—it has not escaped the resistance problem. Means of resistance to fosfomycin appeared shortly after it was introduced into the clinic. Bacteria with mutations in the L-$\alpha$-glycerolphosphate ($\alpha$GP) and hexose phosphate transport systems, which were both shown to be utilized in fosfomycin uptake, appeared (*11-13*). Mutants of MurA also arose; these proteins were catalytically active but were resistant to modification and inactivation by fosfomycin (*14*). Later, a third type of resistance appeared. Researchers linked this resistance to a plasmid-encoded transposable element identified as Tn*2921* (*15*). This resistance element was a 16 kDa soluble protein which caused a modification of fosfomycin (*16*) later determined to be conjugation with the tripeptide glutathione ($\gamma$-Glu-Cys-Gly, GSH) (*17*).

Early purification and characterization of this resistance protein indicated that it was a dimeric protein whose activity increased in the presence of divalent cations such as $Mn^{++}$ and $Co^{++}$ (*18*). Subsequent research revealed that the protein, termed FosA, was a $Mn^{++}$-dependent GSH transferase unrelated to canonical GSH transferases (*19*). FosA also showed activation in the presence of monovalent cations such as $K^+$. The reaction catalyzed by FosA is shown in Figure 7.

Sequence homologies of FosA and other catalytically unrelated enzymes revealed the existence of a previously unrecognized enzyme superfamily. Enzymes in the family use conserved histidine and glutamate residues to bind metal ions which coordinate vicinal substrate oxygen atoms, thus facilitating catalysis (Figure 6). This common mechanistic imperative lead to the family being dubbed the Vicinal Oxygen Chelate

(VOC) superfamily (*20*).  The VOC proteins contain conserved βαββ structural motifs which pair to form a cupped-shaped metal binding site (Figure 6) (*21*).

Genomic FosA Homologues

After the identification and characterization of the plasmid-encoded fosfomycin resistance protein it was thought that other resistance proteins might exist in bacterial genomes.  To test this hypothesis, the FosA sequence was used to query bacterial genome databases in BLAST searches to identify any homologues.  This revealed the occurrence of a protein with approximately 30% identity to FosA in the genome of *Bacillus subtilis*.  The *yndn* protein has subsequently been expressed and characterized (*22*).  Studies have indicated that this protein, named FosB, is regulated by the σW class of transcription factors.  These proteins are known to be involved in regulation of bacterial defense mechanisms against antimicrobials.  FosB also catalyzes a thiol transferase reaction with fosfomycin but utilizes L-cysteine as a thiol donor.  This is not surprising since most Gram positive bacteria lack the genes necessary for GSH synthesis.  Also, the protein has little activity with Mn(II), preferring $Mg^{++}$ as its cofactor.  Unlike FosA, FosB shows no activation by monovalent cations.

As other microbial genomes have become available, FosA homologues have been identified in *Pseudomonas aeruginosa*, *Staphylococcus aureus*, and *Listeria monocytogenes*, among others.  Characterization of purified enzymes has shown that the resistance proteins fall into three classes based on sequence homology, metal preferred for catalysis, and choice of nucleophile conjugated to fosfomycin.  Figure 7 shows relationships between the proteins as well as the reactions catalyzed by each class.
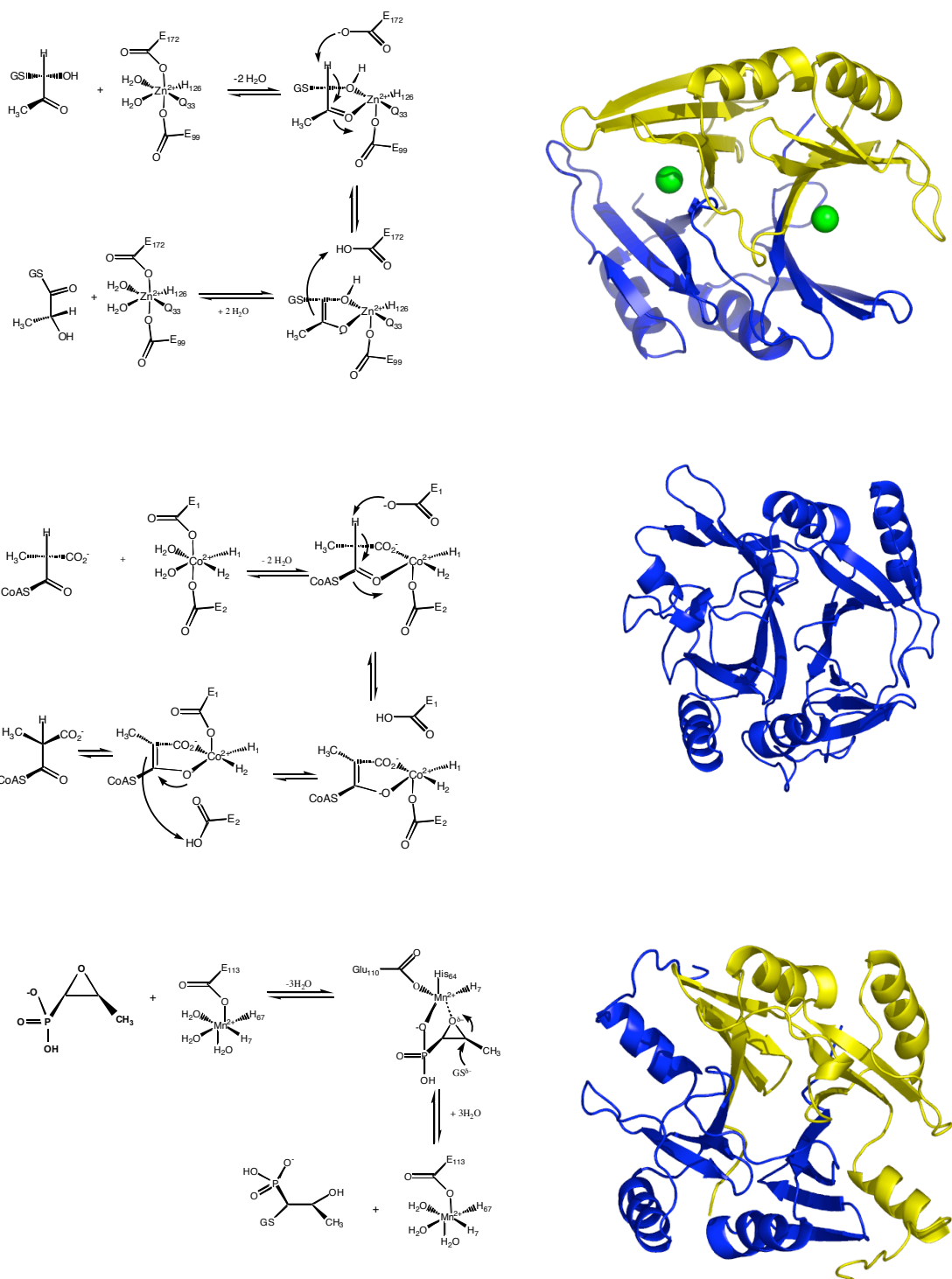
Figure 6. Ribbon diagrams and proposed mechanisms of VOC superfamily members. Note coordination of vicinal oxygen atoms in the substrates by the metal centers. From top to bottom, glyoxalase I, extradiol dioxygenase, and FosA. Generated from 1MPY.pdb, 1F9Z.pdb, and 1NPB.pdb, respectively. Glyoxalase I is shown with bound $Ni^{++}$ ions (green spheres). Ribbons colored by monomer.

A
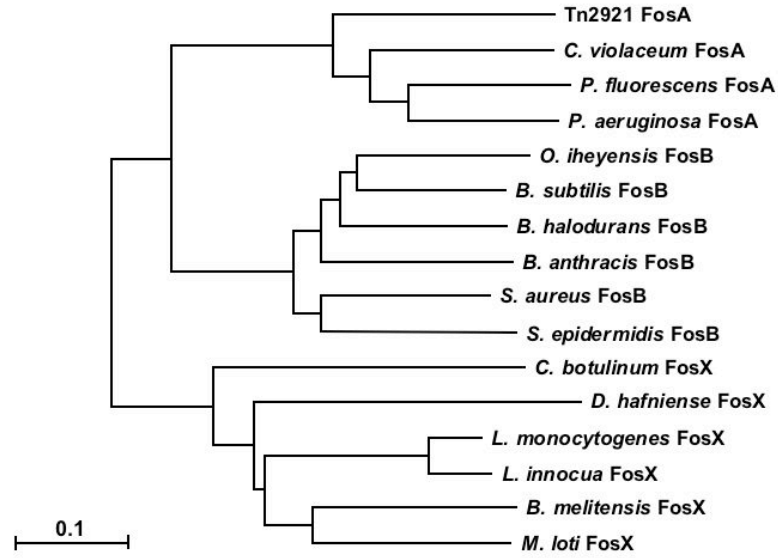


B
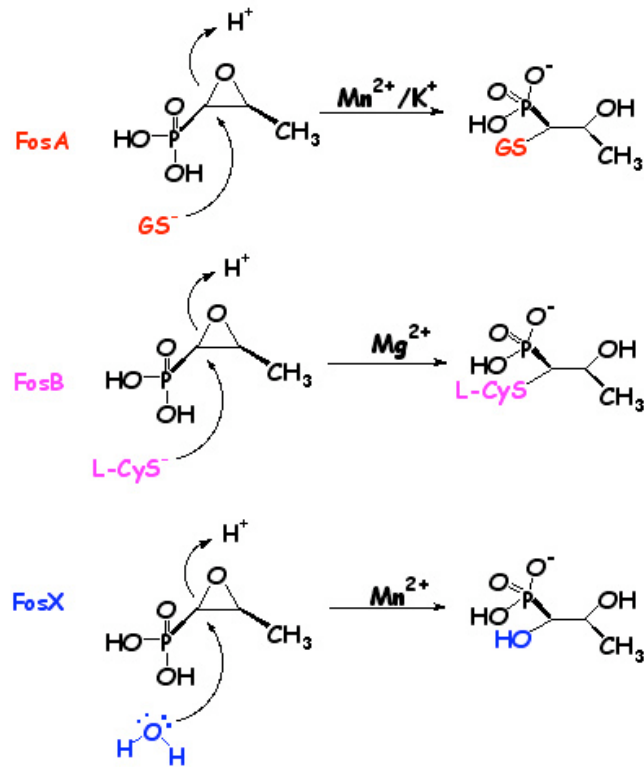


Figure 7. A. Relationships between the fosfomycin resistance proteins as generated by ClustalW. B. Reactions catalyzed by each type of resistance protein.

This Work

Research presented here reports experiments carried out to elucidate kinetic, structural, and mechanistic characteristics of the FosA homologue encoded in the genome of *Pseudomonas aeruginosa* as well as preliminary studies of a FosB protein from the genome of *Staphylococcus aureus*. The PA1129 gene from *P. aeruginosa* shares a 60% identity with FosA, and it was thought that this protein could in fact be a genomic fosfomycin resistance protein. Microbiological data support the existence of a resistance element in *P. aeruginosa*, as fosfomycin is often ineffective in treating urinary tract infections caused by the organism (*23*). Several studies report unusually high minimum inhibitory concentrations (MICs) for fosfomycin for strains of *P. aeruginosa* (*24-26*). The gene was cloned from genomic DNA and the protein expressed, purified, and characterized. Results indicate that, like the plasmid-encoded protein, PA1129 is a very efficient, manganese-utilizing GSH transferase specific for fosfomycin.

Prior to structural characterization of PA1129, electron paramagnetic resonance (EPR) spectroscopy was utilized to probe the metal coordination of the E•Mn(II)•K complex in the presence and absence of phosphonates. It had been shown previously that for FosA (Tn2921), the EPR spectrum of E•Mn(II)•K was dramatically altered upon the addition of fosfomycin but remained unchanged in the presence of glutathione (*27*). In the absence of structural data of several site-directed mutants, circular dichroism was used to compare secondary structures of mutants to native protein. Fosfomycin resistance could be mediated if effective inhibitors were developed for concomitant administration with the drug. Analysis of a crystal structure of PA1129 with fosfomycin bound in the active site indicated that small phosphonates might competitively inhibit the

13

resistance proteins (*28*).   Research presented here focused on analysis of a panel of potential phosphonate inhibitors (Figures 8 and 9) as well as an oxidized form of glutathione (GSO$_3$⁻) for inhibition of FosA.   Phosphonoformate, **2**, was of particular interest as a minimal transition state analogue (Figure 8).   Also investigated was the ability of PA1129 to catalyze formation of either an enolate or a 1,2-GSH adduct with acetyl phosphonate, **4**.



**2**
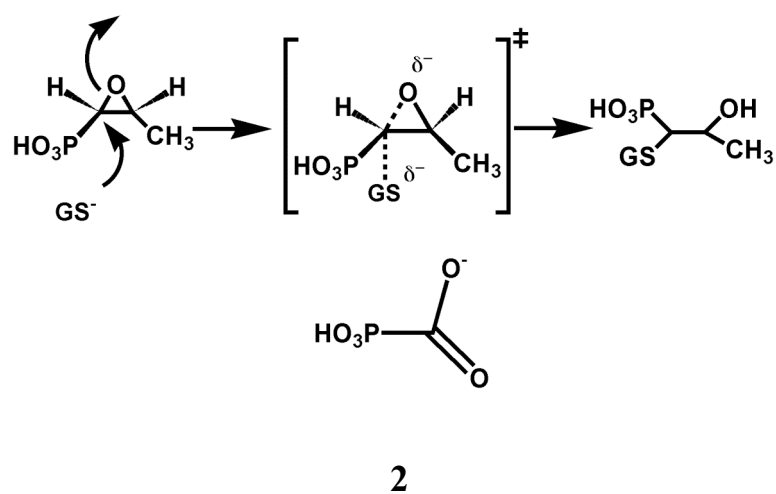
Figure 8.   Reaction catalyzed by FosA comparing a proposed transition state with phosphonoformate, **2**.
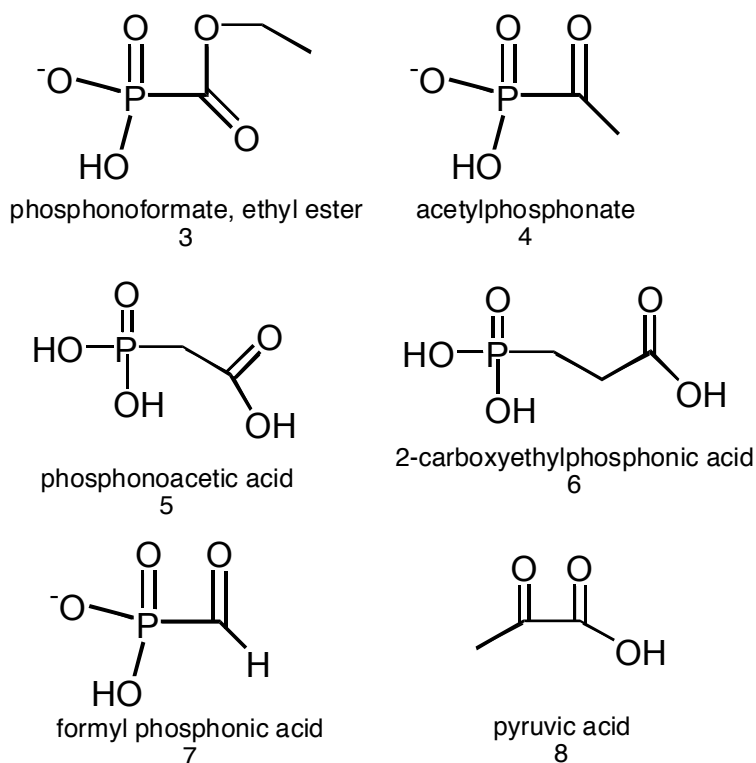
Figure 9. Compounds tested as inhibitors of FosA activity.

While various biochemical methods including x-ray crystallography (*28*), electron paramagnetic resonance spectroscopy (*29*), and kinetic characterization have answered many questions regarding how fosfomycin binds to FosA and is activated for nucleophilic attack, little has been learned about how GSH is conjugated to the antibiotic. Work presented here reports the elucidation of a potential GSH binding site through manual docking of GSH to a FosA crystal structure followed by energy minimization of the docked complex. Mutagenesis of potential binding and catalytic residues followed by kinetic characterization and GSH binding studies provide support for the proposed binding site.

Insight into the origin of this diverse protein family (Figure 7) has come from a FosX homologue from the genome of *Mesorhizobium loti*, a nitrogen-fixing bacterial symbiont of *Lotus* species. The *mlr3345* gene is located in a phosphonate utilization operon also found in *E. coli*, although an *mlr3345* homologue is missing. While presumably mlr3345 has a physiologic role in phosphonate metabolism, it has also been found to be a promiscuous fosfomycin resistance protein *in vitro* in that it catalyzes both hydrolase and GSH transferase reactions with fosfomycin. However, it is not capable of conferring significant resistance to *E. coli* transformed with an expression plasmid. It seems likely that this catalytically poor fosfomycin resistance protein evolved early in the divergence of fosfomycin resistance proteins from a common precursor. This research has attempted to elucidate residues of importance in determination of substrate specificity and catalytic proficiency between the FosA and FosX classes of resistance proteins.

The FosB proteins were identified as a class of fosfomycin resistance proteins which catalyze the addition of L-cysteine to fosfomycin in a $Mg^{++}$-dependent manner. A genomic protein from *B. subtilis* was cloned, expressed, and characterized previously (*22*). BLAST searches of bacterial genomes using FosA as a query identified the presence of a putative fosfomycin resistance protein in *Staphylococcus aureus* which showed 62% identity to BS_yndn from *B. subtilis*. This protein was cloned, expressed, purified, and characterized with respect to its substrate and metal preferences. Results show that it is in fact a cysteine-utilizing, $Mg^{++}$-dependent FosB.

CHAPTER II


MATERIALS AND METHODS


Materials

*Escherichia coli* BL21-DE3 cells were from Novagen (Madison, WI). Phosphonoacetic acid, 2-carboxyethylphosphonic acid, pyruvate, and tris(trimethylsilyl) phosphite were from Aldrich (Milwaukee, WI). Ampicillin, potassium chloride, potassium phosphate (monobasic), ethylenediamine tetraacetic acid (EDTA), tris(hydroxymethyl)aminomethane (TRIS), N-(2-hydroxyethyl)piperazine N'-(2-ethanesulfonic acid) free acid (HEPES), 3-(N-morpholino)-propanesulfonic acid (MOPS), potassium phosphate (dibasic), 5, 5'-dithiobis(2-nitrobenzoic acid), reduced glutathione, L-cysteine, and glutathione sulfonate were from Sigma (St. Louis, MO). Fosfomycin (disodium salt) was from Fluka (Ronkonkoma, NY). Sephacryl S100 was from Pharmacia. Isopropyl-β-D-thiogalactopyranoside (IPTG) and dithiothreitol (DTT) were from RPI (Mt. Prospects, IL). PEG 3350 (50% solution) was from Hampton Research. Hydroxylapatite, AG1-X8 resin, and Chelex 100 ($Na^+$ form) were from BioRad. DEAE Fast Flow and SP-sepharose resins were from Amersham Biosciences (Uppsala, Sweden). Metals (puratronic grade) were purchased as the chloride salts from Alfa Aesar (Ward Hill, MA). Tetramethylammonium hydroxide was from Acros. AQC reagent kit was from Waters (Milford, ME). Acetyl chloride, acetonitrile (HPLC grade), and diethyl ether were from Fisher. Triethylphosphonoformate was from Avocado Research Chemicals Ltd. Luria Broth Base (LB) was from Difco. Sephacryl S100 was

from Pharmacia.    Restriction nucleases were purchased from New England Biolabs (Beverly, MA).

## Methods

### Cloning of PA1129

The gene encoding the FosA from *Pseudomonas aeruginosa*, PA1129, was amplified by PCR from cosmid PMO013326 (Pseudomonas Genetic Stock Center, East Carolina University School of Medicine, Greenville, NC).  Primers (Life Technologies) were designed to incorporate NdeI and BamHI restriction sites at the 5' and 3' ends, respectively, of the coding sequence.  The PCR product was purified using the QiaQuick PCR purification kit (Qiagen Inc., Valencia, CA).  The purified PCR product and pET20b(+) DNA (Novagen, Madison, WI) were digested with the indicated restriction enzymes, purified by gel electrophoresis, and ligated to form the PA1129 expression plasmid.  DNA sequencing confirmed results.

### Protein expression

An expression plasmid was used to transform *E. coli* BL21(DE3) cells.  A 2 L of fermenter was inoculated with enough bacteria from an overnight starter culture grown to $OD_{600} < 1.2$ to make a final density of approximately 0.01-0.03.  Bacteria were grown with constant agitation and aeration at 37°C to an $OD_{600} = 0.8$, and protein expression was induced by the addition of 0.4 mM IPTG.  Protein was allowed to express for 4 hours.  Bacteria were harvested by centrifugation and stored at –20°C.

*Protein purification*

Typically a bacteria pellet from 1 L of culture was resuspended 80 mL 20 mM Tris/HCl (pH 7.5) (buffer A) and lysed by sonication. Cellular debris was removed by centrifugation (30,000 x $g$ for 30 min), and the supernatant was dialyzed against 2 L buffer A. All dialysis steps were conducted at 4°C, and all dialysis buffers contained 1 mM DTT. Crude lysate was passed through a 2.5 x 17 cm Fast Flow DEAE cellulose column equilibrated with buffer A, washed with A, and eluted with a linear gradient (20-500 mM) of NaCl over 8 column volumes. Fractions containing PA1129 as determined by the absorbance at 280 nm and SDS-PAGE were pooled and treated to remove any bound metal by dialysis for at least 8 hours against buffer A containing 5 mM EDTA and 3 g Chelex 100 resin ($H^+$ form)). This was followed by dialysis against buffer A. Protein was then passed through a 1 x 16 cm HiPrep Q column (Pharmacia, Piscataway, NJ) using an FPLC system. The column was equilibrated with buffer A prior to loading protein and was developed with a linear gradient of 0-220 mM NaCl in buffer A. Fractions containing PA1129 were pooled and dialyzed against buffer B [20 mM potassium phosphate (pH 6.8)] overnight. Protein was then passed through a 2 x 7.5 cm hydroxylapatite column equilibrated with B and eluted isocratically with the same buffer. Fractions containing PA1129 were pooled and treated to remove any bound metal by dialysis for at least 8 hours against buffer C [20 mM TMAHEPES (pH 8.0)] containing 5 mM EDTA and 3 g Chelex 100 resin ($Na^+$ form) followed by dialysis in buffer C. Protein was concentrated using a nitrogen pressure cell fitted with an Amicon 10K molecular weight cut-off membrane and stored at –80°C.

*Mass spectrometry of purified protein*

A solution of 25 µM protein in buffer was prepared. A sample (5 µL) of this was mixed with 15 µL 0.1% trifluoroacetic acid prior to desalting with a ZipTip (Millipore) following the manufacturer's protocol. Protein was spotted on a MALDI target by mixing 1 µL protein solution with 1 µL sinapinic acid solution (10 mg in 1 mL elution solution). The MALDI-TOF mass spectrometer was calibrated with standards spotted on the target prior to mass analysis of protein sample.

*Determination of reduced [GSH]*

Reduced [GSH] was determined using the technique of Ellman (*30*). After dissolving GSH in buffer (typically 20 mM TMAHEPES pH 8.0) solution pH was adjusted to 8.0 with TMAOH. Dilutions were prepared and 25 µL mixed with 950 µL 200 mM Tris (pH 8.0) and 25 µL 5 mM 5, 5'-dithiobis(2-nitrobenzoic acid) [prepared in absolute ethanol] and the absorbance at 412 nm recorded. Reduced [GSH] was calculated from Beer's law (equation 1) using the extinction coefficient for 5-thio-2-nitrobenzoate, 13,600 $M^{-1}cm^{-1}$.

$$A = \varepsilon bC \qquad\qquad (1)$$

*Preparation of TMAfosfomycin*

The tetramethylammonium (TMA) salt of fosfomycin was prepared from the disodium salt by dissolving typically 100 mg in $H_2O$ followed by chilling on ice. A 1.5 x 15 cm AG50W-X8 ($H^+$ form) column was prepared, equilibrated with $H_2O$, and chilled to

4°C.  The fosfomycin solution was acidified to approximately pH 3 by addition of 6 M

HCl and loaded immediately onto the column, which was maintained at 4°C.

Fosfomycin (acid) was eluted isocratically with $H_2O$ into tubes containing a small

volume of TMAOH solution.  Fractions containing fosfomycin were identified by the low

pH of the fractions.  These were pooled and the pH adjusted to approximately 7 prior to

lyophilization and resuspension in 20 mM TMAHEPES pH 8.0.  Solution was calibrated

by complete enzymatic conversion to GS-fos followed by HPLC analysis.


*Kinetic analysis*

Activity assays relied on the detection of the free amino group of the peptide

adduct of the antibiotic after derivatization with the fluorescent reagent 6-aminoquinolyl-

N-hydroxysuccinimidyl carbamate (AQC) and separation of the derivatives by reversed

phase HPLC.  Typically 50-150 nM enzyme was preincubated with $MnCl_2$ and KCl in 20

mM TMAHEPES pH 8.0 prior to mixing with glutathione (GSH).  Kinetic reactions were

equilibrated to 25°C and were initiated by the addition of fosfomycin

(tetramethylammonium salt, TMAfos).  Typical reactions contained 50 μM Mn(II), 100

mM $K^+$, 1-100 mM GSH, and 0.1-5 mM TMAfos in a final volume of 100 μL.  After 2-5

min, reactions were quenched by the addition of 200 μL 5% (w/v) trichloroacetic acid

followed by vortexing and addition of 100 μL each of 0.8 M NaOH and 1 mM valine

(internal standard).  A 5 μL aliquot was then added to 80 μL borate buffer and mixed

with 15 μL of the AQC reagent solubilized according to manufacturer's directions.

Reactions were heated for 10 min at 55°C and diluted with 400 μL 50 mM NaOAc pH

5.0 prior to injection onto a 0.046 x 25 cm Ultrasphere C-18 column (Beckman,

Fullerton, CA).  Samples were eluted with a linear 0-35% MeCN gradient with a flow rate of 1 mL/min over 15 min.  GSH-fos, GSH, and valine had retention times of 9.3, 11.2, and 14.7 min, respectively as illustrated in Figure 11.  The ratio of product to valine peak areas were used to calculate product concentrations from a calibration curve constructed from area ratios of product:internal standard versus substrate concentration.

*Determination of minimum inhibitory concentration for fosfomycin*

*E. coli* BL21(DE3) cells were transformed with empty pET20(b) vector as well as vector containing *PA1129*.  Liquid LB cultures containing 100 µg/mL ampicillin were inoculated from freshly streaked LB agar plates containing ampicillin and grown at 37°C with shaking.  After several hours, bacteria equivalent to an $OD_{600} = 0.02$ were streaked on LB agar plates containing 100 µg/mL ampicillin, 30 µM glucose-6-phosphate, and various concentrations of fosfomycin.  Bacteria were grown 16 hr at 37°C, and growth was recorded.

*$K^+$-free purification*

Protein was expressed and purified as described for native enzyme until after the HiPrepQ column.  Protein was then concentrated to 10 mg/mL and dialyzed in 20 mM Tris pH 7.5 containing 100 mM NaCl and 100 µM EDTA (Buffer C) containing 1 mM DTT.  Protein was passed through an S100 column equilibrated with buffer C and eluted with an isocratic gradient of buffer C.  Purity was confirmed using SDS-PAGE.  Protein was then dialyzed in 20 mM TMAHEPES pH 8.0 (Buffer B) plus 1 mM DTT, 3 g Chelex, and 5 mM EDTA followed by dialysis in buffer B.  Protein was then concentrated and stored in aliquots at -80°C.

*Circular dichroism spectroscopy*

Solutions of MnCl$_2$, KH$_2$PO$_4$, and protein in 20 mM MOPS pH 7.0 were passed through a 0.2 µM syringe filter to remove particulates. Protein concentrations were determined by measuring the absorbance at 280 nm and calculating concentration using Beer's Law and the extinction coefficient (native, T9V, T9S, G37E = 25,670 M$^{-1}$ cm$^{-1}$, W34A, W34AG37E = 20,030 M$^{-1}$ cm$^{-1}$). Measurements were taken using a Jasco J-80 CD spectrometer (VU Center for Structural Biology) maintained at 25°C. Spectra were recorded from 190-260 nm with 1 nm steps at 5 nm/min with 2 s averaging time. The instrument was autozeroed on buffer. Concentrations in the sample cuvette were: [E] = 40 µM, [MnCl$_2$] = 260 µM [K$^+$] = 100 mM, Similar samples containing 5 mM fosfomycin were also analyzed. Data were converted to molar ellipticity (θ) using equation 2, where c is [E] in mM, n is the number of amino acids, and l is the cell length in cm, and plotted.

$$[\theta] = \left[\frac{100(signal)}{cnl}\right] \qquad (2)$$

*Preparation of EPR samples*

Samples consisting of 5 mM PA1129 in the presence of 500 µM Mn$^{2+}$ alone or with 2 mM disodium fosfomycin were prepared in 20 mM HEPES pH 8.0. Spectra were collected from 11700-12700 Gauss at Vanderbilt University with the assistance of Dr. Al Beth. Samples of enzyme with bound metal and fosfomycin with either 100 mM K$^+$ or 20 mM Tl$^+$ were also prepared. Data for these samples as well as ENDOR spectra were collected by collaborators Brian Hoffman and Josh Telser (Northwestern University).

Deuterated samples were also prepared as follows. TMA HEPES (pH 8.0) as well as MnCl$_2$, TMAfosfomycin, and phosphonoformate were prepared, lyophilized to dryness, and resuspended in D$_2$O. Drying and resuspension was repeated. Enzyme was deuterated by concentrating in a Centricon spin concentrator followed by addition of deuterated TMA HEPES. This was repeated twice. Samples containing 5 mM E, 0.5 mM Mn$^{++}$, with or without 2 mM fosfomycin or 5 mM phosphonoformate were prepared, frozen, and shipped on dry ice to collaborators at Northwestern University.

*Synthesis of phosphonoformate*

Phosphonoformate was prepared from triethylphosphonoformate by a previously reported method (*31*). Triethylphosphonoformate (10 g, 48 mmol) was added to a solution of 11.42 g (285 mmol) of sodium hydroxide in 90 mL of water at 50°C. The solution was heated to 90°C. After being refluxed for 1 h, the reaction mixture was cooled to 20°C. Phosphonoformate was then filtered from the reaction mixture using a Buchner funnel fitted with Whatman #1 filter paper. The product was recrystallized from water and lyophilized to dryness. Elemental analysis: C: 4.83%; H: 2.71%, O: 52.74%.

*Synthesis of acetyl phosphonate*

Acetyl phosphonic acid was synthesized following methods previously described (*32, 33*). Tris(trimethylsilyl) phosphite was slowly added to a 2-fold excess of acetyl chloride in a flask immersed in an ice/EtOH bath. The mixture was stirred for at least 2 h on ice and then stirred at room temperature overnight. After removal of the volatile

silane products, the pH of the solution was adjusted to 4 with NaOH. The reaction mixture was extracted with diethyl ether several times. The aqueous layer containing the product was then taken to dryness by lyophilization: $^1$H NMR (300.1 MHz, D$_2$O) δ 2.22 (d, J$_{PCH}$ 3.72 Hz); $^{13}$C NMR (75.5 MHz, D$_2$O) δ 30.6 (d, J$_{CP}$ 43.8 Hz), 228.6 (d, J$_{CCP}$ 157.6 Hz).

*Synthesis of formyl phosphonic acid*

Synthesis of formyl phosphonic acid was attempted following a published protocol (*34*). Briefly, nitrilotris(methylene phosphonic acid) was mixed with hydrogen peroxide in the presence of vanadyl sulfate catalyst. A variety of pH and temperature conditions were tested.

*Inhibition assays*

Enzyme assays were carried out as described above. In a typical reaction mixture, enzyme (60-150 nM) was incubated with 100 mM KCl, 50 μM MnCl$_2$, and 15 mM GSH in 20 mM TMAHEPES (pH 8.0) at 25°C in the presence of 1, 2, 3, or 4 mM disodium fosfomycin and varying concentrations of phosphonoformate, acetylphosphonic acid, phosphonoacetic acid, or 2-carboxyethylphosphonic acid. Reactions were quenched; 1.0 mM valine was added as an internal standard, and the mixture was reacted with Waters AccQFluor reagent and analyzed by reversed-phase HPLC. Inhibition data were analyzed as a Dixon plot (1/V vs [I]) to determine K$_I$ (*35*).

*Inhibition by GSO₃⁻, pyruvate, or ethyl phosphonoformate*

Glutathione sulfonate ($GSO_3^-$) (0 or 12 mM) was added to enzyme reactions containing 150 nM PA1129, 50 μM Mn(II), 100 mM $K^+$, 6 mM disodium fosfomycin, and 7.5 or 15 mM GSH in 20 mM TMAHEPES pH 8.0. E•Mn(II)•$K^+$ was incubated with inhibitor prior to the addition of substrates. Similar reactions containing 2 mM TMAfosfomycin and GSH were carried out in the presence of 5 μM ethyl phosphonoformate. Reaction velocities were determined by measuring product formation as previously described. Pyruvic acid was analyzed for inhibition by adding 20 mM to enzyme reactions which were analyzed by $^{31}$P NMR after quenching and demetallation.

*In vivo inhibition by phosphonoformate*

*E. coli* BL21 (DE3) pLysS cells were transformed with a PA1129 expression vector. Cultures inoculated from a freshly-streaked LB agar plate containing 100 μg/mL ampicillin, 20 μg/mL glucose-6-phosphate (G6P), and 5 or 10 mg/mL phosphonoformate were grown at 37°C to mid-log phase. A volume equivalent to 0.005 $OD_{600}$ was used to inoculate a series of cultures containing similar concentrations of ampicillin, G6P, and phosphonoformate in addition to 5 or 10 mg/mL fosfomycin. These cultures were grown for 4 h while monitoring the $OD_{600}$. As a control experiment, bacteria were also grown on LB/agar plates containing varying concentrations of ampicillin (0.8 – 1 mg/mL) and 5 mg/mL phosphonoformate in the presence of G6P and chloramphenicol.

*Titration of FosA with fosfomycin and phosphonoformate*

A solution of 0.1 μM PA1129 in the presence of 50 μM MnCl$_2$ was prepared in 20 mM TMAHEPES (pH 8.0) containing 100 mM KCl.  A solution of 50 μM MnCl$_2$ in buffer was similarly prepared.  All solutions were filtered through a 0.2 μM filter. Phosphonates were added to both solutions incrementally while monitoring the change in fluorescence.  Measurements were made in triplicate on a SPEX Fluorolog-3 spectrofluorimeter (Jobin Yvon Horiba, Edison, NJ) in the constant-wavelength mode. Solutions were excited at 275 nm (3 mm slit width), and emission measurements were taken at 330 nm (2 mm slit width).  After data were corrected for fluorescence of the buffer solution, data were averaged and fit as the absolute value of the change in fluorescence to equation 3.

$$|\Delta F| = -\left[\frac{-(K_d + [P] + F_{max}) + \sqrt{\{K_d + [P] + F_{max}\}^2 - 4[P]F_{max}}}{2}\right] \quad\quad (3)$$

*Stopped-Flow Analysis of Binding Kinetics*

The PA1129 FosA incubated with MnCl$_2$ and phosphonoformate in 20 mM TMAHEPES (pH 8.0) was mixed with varying concentrations of fosfomycin in an Applied Photophysics SX17 stopped-flow spectrometer in absorbance mode.  The change in absorbance at 245 nm was monitored as a function of time; 1000 data points were collected in 100 ms using the oversampling method.  Concentrations in the observation cell were as follows: 5 μM FosA, 50 μM MnCl$_2$, 100 mM K$^+$, 25 μM phosphonoformate, and 5, 10, 15, and 20 mM fosfomycin.  Data were fitted to a single exponential, floating

end point equation using the instrument software to obtain $k_{obs}$.  The first 2 ms of data were omitted from the data analysis.  The off rate for fosfomycin was measured in a similar manner by trapping with phosphonoformate.

*Enolization of acetyl phosphonate*

Potassium phosphate (20 mM, pH 7.5) was deuterated by taking a 100 mM solution to dryness, resuspending in $D_2O$, drying, and repeating.  Deuterated buffer was sparged with Ar to remove dissolved oxygen prior to sample preparation.  A solution of 0.5 µM PA1129 in the presence of 100 mM KCl and 50 µM $MnCl_2$ in deuterated buffer was incubated with acetyl phosphonate (25 mM) for several days.  A similar solution lacking enzyme was also prepared.  At various times, aliquots were removed, and the ^{1}H NMR was recorded.

*Adduct formation between GSH and acetylphosphonate*

A solution of 1 µM PA1129 in deuterated, Ar-sparged KPi (20 mM, pH 7.5) containing 5 µM $MnCl_2$, 25 mM GSH, and 25 mM acetyl phosphonate was allowed to incubate at room temperature.  A similar solution lacking enzyme was prepared.  At various times, aliquots were removed, demetallated with Chelex 100 resin, and analyzed by ^{1}H NMR.

*GSH docking and minimization*

This work was done in collaboration with Eric Dawson, Ph. D. in the lab of Terry Lybrand, Ph. D. at Vanderbilt University.  An initial conformation of GSH was taken

from coordinates found in a co-crystal structure of a porcine glutathione S-transferase containing $GSO_3^-$ in the active site (2GSR) (*36*). The $GSO_3^-$ was changed to GSH and manually docked into the active site of FosA (1LQP) (*28*) using the interactive molecular graphics program PSSHOW (E. Swanson, University of Washington, 1995). To allow favorable positioning of the GSH substrate in the enzyme's active site, a fosfomycin molecule bound at the entrance to the enzyme's active site (in 1LQP) was removed and sidechain dihedral angles for residues K90 and Q36 were changed to the first most probable rotamer from a backbone-dependant amino acid rotamer library (*37*). All crystallographic waters were retained during the manual docking steps; however, waters having Van der Waal's radii overlapping with atoms of manually docked GSH were removed prior to energy minimization calculations. The resulting structure retained a significant 'droplet' of crystallographic water molecules. Molecular mechanics parameters for the GSH and fosfomycin substrates were developed (see below) to enable energy minimization calculations following molecular docking. Partial charges for both substrates were generated using *ab initio* electrostatic potential calculations with a 6-31G* basis set, followed by fitting to an atom-centered point charge model with the RESP program (*38*). Use of the unionized thiol form of GSH limited the need for development of molecular mechanics parameters for this ligand to the γ-glutamyl residue of GSH. The amino acid residue type (ILG) was created in the LeaP module of AMBER using parameters derived from methyl-glutamine (used as a model compound). Parameters for FosA as well as for the catalytic ion-cofactors were available in public databases. Hydrogen atoms were added to the enzyme-substrate complex, which was then refined to remove any residual bad steric interactions or backbone conformational strain

29

using a combination of limited (200 steps) steepest descents and conjugate-gradient energy minimization. The calculations were performed *in vacuo* with a distance-dependent dielectric model, using standard AMBER all-atom potential functions in AMBER 8.0 (*39*).

*Molecular Mechanics Parameter Development*

The following lists parameters and .prp files developed and utilized for energy minimization.

**------ILG - amino-terminal monomer from glutathione (GSH)------------------**
ILG.prp
ILG  INT  0
 CORRECT  OMIT  DU  BEG
 0.0
　 1 DU1  DU  M   0    0    0   0.0000   0.0000   0.0000
　 2 DU2  DU  M   1    0    0   1.0000   0.0000   0.0000
　 3 DU3  DU  M   2    1    0   1.0000  90.0000   0.0000
　 4 N    N3  M   3    2    1   1.2624 149.1681 315.3131  -0.8689
　 5 H1   H   E   4    3    2   1.0049 133.6152 120.5899   0.3395
　 6 H2   H   E   4    3    2   1.1096  83.0337 220.7611   0.3395
　 7 H3   H   E   4    3    2   1.0069 111.4414 327.2653   0.3395
　 8 CA   CT  M   4    3    2   1.4802  29.1957  65.4978   0.2825
　 9 HA   HP  E   8    4    3   1.0853 107.1225 107.8812   0.0238
　10 C    C   B   8    4    3   1.5360 107.3531 354.0461   0.6306
　11 O    O2  E  10    8    4   1.3392 113.4132  20.6207  -0.5382
　12 OXT  O2  E  10    8    4   1.2029 123.8519 198.9541  -0.5382
　13 CB   CT  M   8    4    3   1.5334 113.8678 229.1416   0.0122
　14 HB2  HC  E  13    8    4   1.0810 108.8775 311.1876   0.0095
　15 HB3  HC  E  13    8    4   1.0846 109.3753  68.0776   0.0095
　16 CG   CT  M  13    8    4   1.5331 113.3891 190.4032  -0.0498
　17 HG2  HC  E  16   13    8   1.0779 110.0078 294.9958   0.0086
　18 HG3  HC  E  16   13    8   1.0876 109.9151  53.5195   0.0086
　19 CD   C   M  16   13    8   1.5188 110.5419 171.8841   0.5449
　20 OD   O   E  19   16   13   1.2217 122.4343 343.4974  -0.5536

DONE

STOP

```
##############################################################################
##  Parameters for Fosfomycin and Glutathione (ILG) developed in collaboration  ##
##          with the research group of Professor Terry Lybrand                ##
##############################################################################

------Fosfomycin ---------------------------------------------------
fos.prp
FCN  INT  0
 CORRECT  OMIT  DU  BEG
 0.0
  1 DU1  DU   M    0    0   0    0.0000    0.0000    0.0000
  2 DU2  DU   M    1    0   0    1.0000    0.0000    0.0000
  3 DU3  DU   M    2    1   0    1.0000   90.0000    0.0000
  4 C1   CT   M    3    2   1    0.5588  119.2199  156.2674  -0.0043
  5 H11  HC   E    4    3   2    1.0900  126.9068  305.7325  -0.0119
  6 H12  HC   E    4    3   2    1.0917  119.7220   97.6411  -0.0119
  7 H13  HC   E    4    3   2    1.0911   73.0795  203.6849  -0.0119
  8 C2   CT   M    4    3   2    1.5112   33.2379   14.9290   0.0434
  9 H2   H1   E    8    4   3    1.0827  116.2593  184.2278  -0.0280
 10 O3   OS   M    8    4   3    1.4686  114.6385   49.0908  -0.4633
 11 C4   CT   M   10    8   4    1.5177   59.5838  247.7705   0.0872
 12 H4   H2   E   11   10   8    1.0821  108.8855  253.7460  -0.0113
 13 P    P    M   11   10   8    1.8765  124.3382  116.2854   1.0550
 14 O2P  O2   E   13   11  10    1.5043  103.3487   74.6816  -0.8810
 15 O3P  O2   E   13   11  10    1.5186  104.5741  313.1847  -0.8810
 16 O1P  O2   E   13   11  10    1.5082   98.4772  194.0102  -0.8810

LOOP
C2   C4

DONE

STOP
```

31

```
######################################################################
##  Parameters for Mn2+ and Fosfomycin taken from Amber Parameter Database  ##
##          Website - http://pharmacy.man.ac.uk/amber/                      ##
######################################################################
```

**Mn²⁺ vdw parameters** (from Concanavalin A study by G.M. Bradbrook et al.)

```
MASS
MN    55.00    0.00


NONB
MN     1.6900    0.0140
```

--------------------------------------------------------------------------------

**Fosfomycin parameters** (calix[4]arenes: PhD Thesis of Marc Baaden - 250800)

```
MASS


BOND
CT-P  331.    1.82


ANGLE
CT-P -O2   60.     104.6     angles from gopt / force const. (Baaden) - esd
CT-CT-P    35.     113.1          "           "
OS-CT-P    50.     124.3          "           "
P -CT-H2   60.     127.3          "           "


DIHEDRAL
X -CT-P -X   9        3.51        0.    3.  tpl - JPC 94


NONBOND

------manganese-----------------------------------------------------------
mn.prp
MNG  INT  0
CHANGE OMIT DU  BEG
 0.0
  1 DUMM  DU  M  0 -1 -2  0.000     0.000     0.000    0.000
  2 DUMM  DU  M  1  0 -1  1.0000    0.0000   0.0000   0.000
  3 DUMM  DU  M  2  1  0  1.0000   90.0000  0.0000    0.000
  4 MN       MN  M  29.683 127.561 -18.450  2.00


DONE


STOP
```

*Generation of Mutants*

Site-directed mutagenesis was performed on the PA1129 expression plasmid using the QuikChange site-directed mutagenesis kit (Stratagene, La Jolla, CA). Oligonucleotide primers (Life Technologies) were designed to change codon 9 from ACC to GTC (T9V) and TGC (T9S), codon 34 from TGG to GCG (W34A) and CAC (W34H), codon 37 from GGC to GAA (G37E), codon 39 from TAT to TTT (Y39F), codon 48 from TGC to GCC (C48A), and codon 50 from TCC to ATG (S50M) and TGC (S50A). Multiple mutants W34A/G37E, W34A/G37E/S50M and W34A/G37E/Y39F/S50M were also created. A disrupted $K^+$-binding loop mutant was prepared by inserting RVE residues (CGC GTC GAG) between residues 93 and 94. The W34A/G37E/Y39F/S50M mutant was also created in the $K^+$-binding loop mutant background. Site-directed mutagenesis was also performed on the *B. subtilis* FosB expression plasmid using primers designed to change codon 40 from TAT to TTT (Y40F). Mutations were confirmed by DNA sequencing.

*Expression and purification of mutants*

Mutants were expressed and purified as described for native protein. Briefly, for PA1129 mutants, bacteria were lysed by sonication followed by centrifugation to pellet debris. Lysate was dialyzed in 20 mM Tris pH 7.5 prior to loading onto a DEAE column equilibrated with this buffer. Protein was eluted with a salt gradient, and fractions containing PA1129 were pooled and dialyzed in 20 mM KPi pH 6.8. Protein was passed isocratically through a hydroxylapatite column equilibrated with the same buffer. Fractions containing PA1129 were pooled and dialyzed against 20 mM TMAHEPES

pH 8.0 containing Chelex resin and EDTA followed by dialysis in 20 mM TMAHEPES pH 8.0. For FosB, protein was passed through a DEAE column and eluted with a NaCl gradient prior to dialysis followed by isocratic elution from a hydroxylapatite column. Protein was then demetallated and passed isocratically through an S100 gel filtration column. Protein was dialyzed in 20 mM HEPES pH 8.0, concentrated, and stored at -80°C.

*Kinetic analysis of mutant enzymes*

The kinetic assay for native protein was followed as described to determine kinetic parameters for mutants. Briefly, enzyme was incubated with the appropriate metal(s) prior to addition of thiol and fosfomycin (disodium or TMA salt). Reactions were quenched and derivatized with a fluorescent reagent (AQC) prior to HPLC analysis.

*Fluorescence titration of enzyme with glutathione*

A solution of 5 µM PA1129 in the presence of 50 µM $MnCl_2$ and 100 mM KCl was prepared in 20 mM TMAHEPES (pH 8.0) which had been filtered through a 0.2 µm filter. A solution of buffer containing $MnCl_2$ and KCl was prepared similarly. GSH was added to both solutions incrementally while monitoring the change in fluorescence. Titrations were also done in the presence of phosphonoformate. Titration measurements were made in triplicate on a SPEX Fluorolog-3 spectrofluorimeter (Jobin Yvon Horiba, Edison, NJ) in the constant-wavelength mode. Solutions were excited at 275 nm (3 mm slit width), and emission measurements were taken at 340 nm (3 mm slit width). After

correction for fluorescence of buffer, data were averaged and fit to a hyperbola to obtain

a $K_d$.


*Estimation of turnover number by $^{31}P$ NMR Spectroscopy*

In typical reactions, enzyme was equilibrated with Mn(II) in 20 mM HEPES (pH

7.5) prior to the addition of 25-150 mM GSH. Reactions were initiated by the addition of

25 mM fosfomycin and allowed to proceed at room temperature for several minutes to

several hours. Reactions were quenched by vortexing with $CHCl_3$ followed by freezing

on dry ice. After thawing and centrifugation, the aqueous layer was removed to a fresh

tube and incubated with a small amount of Chelex 100 resin ($H^+$ form) for at least 3 hr to

remove Mn(II), which causes a paramagnetic line broadening of the $^{31}P$ signal. Reactions

were centrifuged to pellet the Chelex resin followed by removal of the supernatant to a

fresh tube. The Chelex was washed with distilled, deionized $H_2O$, centrifuged, and the

supernatant removed and combined with the first supernatant. After addition of $D_2O$, the

proton-decoupled $^{31}P$ spectra of the reactions were collected at 121 MHz. GS-fos, 1,2-

dihydroxypropylphosphonic acid, and fosfomycin had $^{31}P$ chemical shifts of 18.1, 16.9,

and 11.1 ppm, respectively. Following the law of conservation of mass, product and

substrate peak heights are measured and amount of product formed calculated from the

ratio between peak heights and total substrate used in the reaction.


*Purification of the FosB from B. subtilis*

Protein was overexpressed in BL21-DE3 *E. coli* cells grown from an

LB/ampicillin (100 μg/mL) plate freshly streaked from a glycerol stock. A 100 mL

LB/ampicillin culture was inoculated with one colony and grown overnight (typically 12 hr at 27°C and 150 rpm). A volume of overnight culture was added to 2 L LB containing ampicillin and antifoam in a 2 L fermentor to make the final $OD_{600}$ = 0.006. Bacteria were grown to $OD_{600}$ = 0.8, when 400 mM IPTG was added to induce overexpression. Bacteria were grown for 4 hr, harvested by centrifugation, and cell pellets stored at -20°C prior to purification. Cells were resuspended in approximately 80 mL 20 mM TRIS pH 7.5, lysed by sonication [4 x 3 min at duty cycle 7 and output control 8], and centrifuged to pellet cell debris. All dialysis was done in 2 L buffer at 4°C in the presence of 1 mM dithiothreitol (DTT). Protein was dialyzed in 20 mM TRIS pH 7.5 prior to being passed through a 1.6 x 60 cm DEAE FastFlow column equilibrated with buffer. Protein was eluted with a 20-250 mM NaCl gradient over 8 column volumes. Fractions containing FosB as identified by $A_{280}$ and SDS-PAGE were pooled and dialyzed against 20 mM KPi pH 6.8. Protein was then passed through a 2 x 7.5 cm hydroxylapatite column equilibrated with buffer, washed with buffer, and eluted with an 8 column gradient of 50-350 mM KPi. Fractions containing FosB were pooled and dialyzed in 20 mM TRIS pH 7.5 containing 3 g Chelex ($H^+$ form), 100 μM EDTA, and 100 mM NaCl prior to isocratic elution from a Sephacryl S100 gel filtration column. Protein was diluted in half with buffer and dialyzed in 20 mM TRIS pH 7.5 containing 3 g Chelex and 5 mM EDTA prior to dialysis in 20 mM HEPES pH 8, concentration, and storage at -80°C.

*Kinetic analysis of the FosB from B. subtilis*

Kinetic reactions were carried out for $FosB^{Bs}$ in reaction mixtures containing 600 nM enzyme, 1 mM $Mg^{++}$, 0.1-10 mM fosfomycin, and 2-50 mM cysteine in 20 mM

HEPES pH 8.0. Reactions were done at 25°C in 100 µL volume for sufficient time to allow approximately 15% product formation. Reactions were quenched and derivatized as previously described (see Chapter 3 Methods). Data were fit to the Michaelis-Menten equation using the program Prism to obtain $K_m$ and $k_{cat}$.

*Crystallization of the FosB from B. subtilis*

Several attempts were made to crystallize purified protein at ambient temperature using the hanging drop method. Conditions were identified which produced needles and small crystals. These were typically 2-4% glycerol or ethanol and 12-14% PEG 3350 in 100 mM Tris pH 8.5. Enzyme (5 mg/mL) was incubated with $MgCl_2$ (10 mM) and Cys-fos product (10 mM) prior to mixing equal volumes (2-4 µL) of enzyme solution with well solution on cover slides.

*Cloning, expression, and purification of the FosB from S. aureus*

The gene encoding the FosB protein from *S. aureus* was amplified from genomic DNA by PCR using gene-specific primers. NdeI and EcoRI sites were added to the 5' and 3' ends, respectively. A silent mutation (CA**T** to CA**G**) was incorporated in codon 134 to remove an NdeI site from the coding sequence. An expression vector was prepared as described for FosA$^{PA}$. This plasmid was used to transform BL21-DE3 *E. coli* cells. Protein was expressed as described for PA1129 except after induction with IPTG (0.2 mM) cells were grown at 30°C for 5 hours. Bacteria harvested from 2 L of culture were suspended in 100 mL 20 mM KPi pH 6.8, lysed by sonication, and the resulting suspension centrifuged for 30 min at 35,000 x *g*. The supernatant was stirred with

Benzonase Nuclease (Novagen, Madison, WI) according to the manufacturer's directions [50 μL Benzonase, 2 mM $MgCl_2$, and 10 mg BSA for 2 h at 25°C], thereby reducing or eliminating undesired interactions of FosB with nucleic acids. Benzonase treatment was followed by dialysis against 20 mM KPi pH 6.8. All dialysis was performed at 4°C, and all buffers contained 1 mM DTT. Protein was passed through a 1.6 x 60 cm SP-Sepharose column equilibrated with buffer (20 mM KPi pH 6.8). The column was then washed with buffer, and protein was eluted with a 10-500 mM NaCl gradient (in buffer) over 8 column volumes. Fractions containing FosB were identified by the absorbance at 280 nm and SDS-PAGE. These fractions were pooled and dialyzed against buffer. Protein was then loaded onto a 2 x 7.5 cm hydroxylapatite column equilibrated with buffer and eluted with a linear phosphate gradient (20-500 mM) in buffer. Fractions containing FosB$^{SA}$ were pooled and dialyzed against 20 mM MOPS (pH 7.0) containing 5 mM EDTA and 3 g Chelex 100 (H$^+$ form, 100-200 mesh) to remove protein-bound metal, followed by dialysis against 20 mM MOPS pH 7.0. Protein was concentrated and stored at -80°C.

*Preliminary kinetic analysis using $^{31}P$ NMR*

Enzyme incubated with Mg$^{++}$ was mixed with fosfomycin and various thiol substrates (typically 25 mM each) for product analysis. Reactions were quenched by vortexing with $CHCl_3$ prior to mixing with $D_2O$ (20% final concentration) followed by analysis by proton-decoupled $^{31}P$ NMR (121 MHz).

*Kinetic analysis with L-cysteine and fosfomycin*

Preliminary assays were done in the presence of a variety of metal ions. Transition metals were at 50 μM, and Mg$^{++}$ was at 1 mM. Typical kinetic reactions contained 300 nM enzyme preincubated with 1 mM MgCl$_2$, 0.1–10 mM fosfomycin, and 1–80 mM cysteine in 20 mM HEPES pH 8.0. Protein concentration was determined using the absorbance at 280 nm and the extinction coefficient as calculated from the tyrosine and tryptophan content (*40*) using Equation 1 with ε = 21,280 M$^{-1}$cm$^{-1}$. Reactions were quenched, neutralized, and derivatized as described in prior to analysis by HPLC.

*Crystallization of the FosB from S. aureus*

Attempts to crystallize purified FosB$^{Sa}$ were largely unsuccessful. Small crystals were obtained in typical conditions of 12-14 % PEG 3350, 2% glycerol, 10 mM cys-fos, 500 μM Mg, and 5 mg/mL E in 100 mM Tris pH 7. The crystals obtained exhibited diffraction to only about 3 Å, and data was not collected. Instead, further optimization was pursued.

CHAPTER III


CLONING, PURIFICATION, AND CHARACTERIZATION
OF PA1129, THE FOSA HOMOLOGUE FROM
*PSEUDOMONAS AERUGINOSA*


Results


*Purification*

The developed purification protocol produced high yields (100 mg/L culture) of very pure protein (Figure 10). The molecular weight agreed with the calculated mass of 15,114 Da. As expected, the protein interacted well with DEAE resin, since the calculated pI was 6.2 (EMBL WWW Gateway to Isoelectric Point Service).


*Kinetic analysis*

Protein concentrations were accurately determined prior to kinetic assays by measuring the $A_{280}$ and using the extinction coefficient 21,280 $M^{-1}cm^{-1}$ as calculated from the tryptophan and tyrosine content (*40*) and Beer's Law. Reactions were analyzed via HPLC using a calibration curve to correlate peak areas for product and internal standard (valine). A typical HPLC chromatogram is shown in Figure 11.
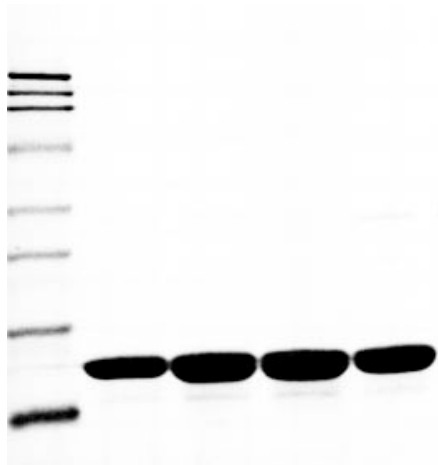
**A**
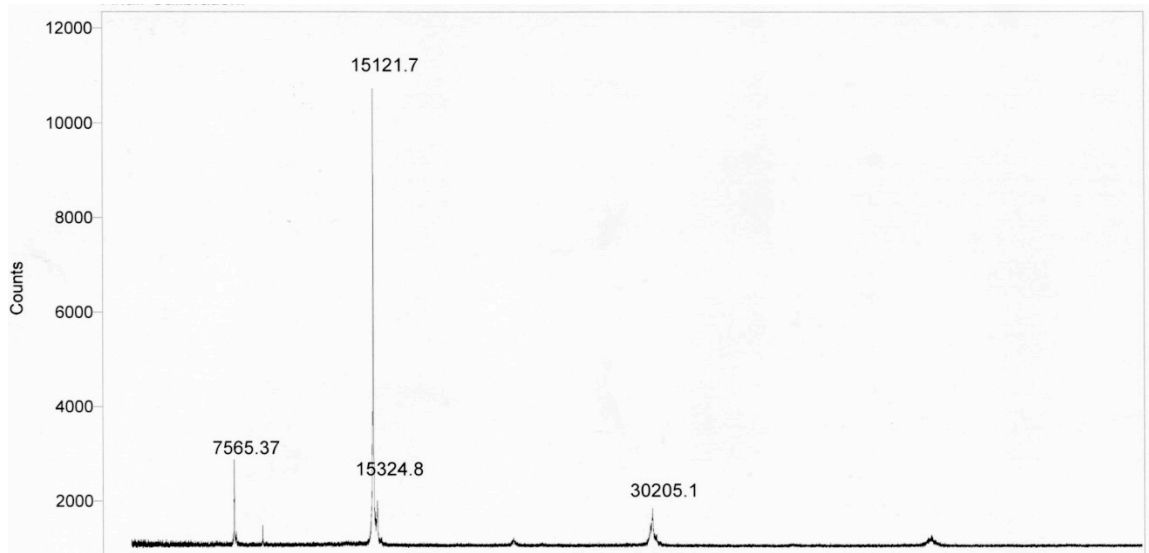


**B**



Figure 10.  A.  MALDI mass spectrum of purified PA1129.  B. SDS-PAGE showing protein standards (first lane) and fractions containing PA1129 from a hydroxylapatite column.  PA1129 bands (15,114 Da) are between molecular weight markers aprotinin (6,894 Da) and lysozyme (19,374 Da).
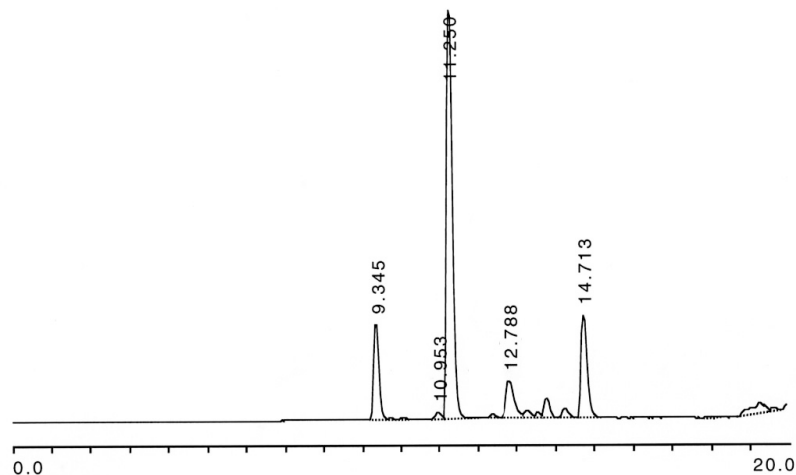
Figure 11. HPLC chromatogram of a typical FosA reaction mixture. GS-fos, GSH, and valine have retention times of 9.3, 11.2, and 14.7 min, respectively.

Preliminary studies indicated that PA1129 utilized $Mn^{++}$ preferentially for catalysis and was activated in the presence of $K^+$. Figure 12 shows fits of kinetic data to determine $K_{act}^{K+}$, $k_{cat}$, and $K_m$ for both substrates; table 2 lists these results as well as $k_{cat}/K_m$ for substrates.

**Table 2.** Kinetic parameters determined for PA1129.

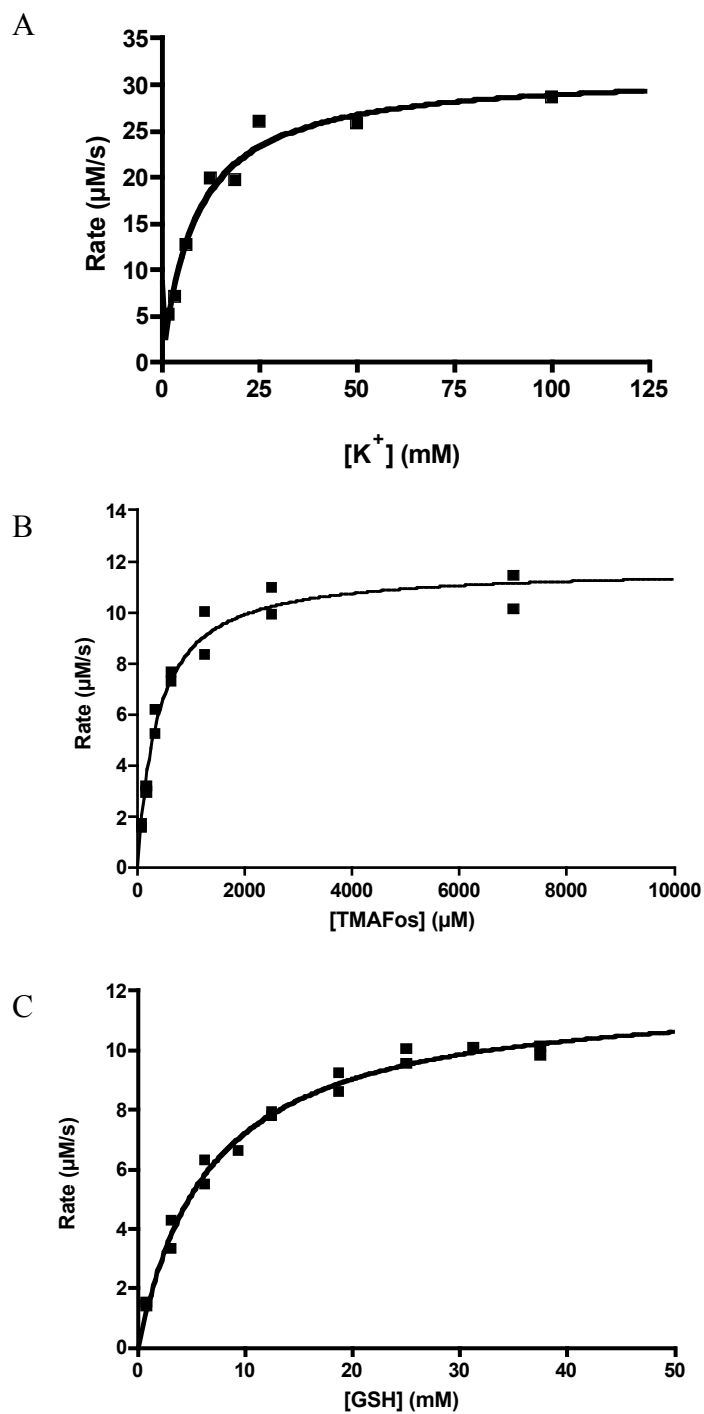| | |
|---|---|
| $K_{act}^{K^+}$ (mM) | $8.7 \pm 1.5$ |
| $k_{cat}$ (s$^{-1}$) | $175 \pm 6$ |
| $k_{cat}/K_m^{Fos}$ (M$^{-1}$s$^{-1}$) | $(9.0 \pm 1.4) \times 10^5$ |
| $k_{cat}/K_m^{GSH}$ (M$^{-1}$s$^{-1}$) | $(3.5 \pm 0.9) \times 10^4$ |

Figure 12. A. Activation of PA1129 in the presence of increasing $[K^+]$. B and C. Michaelis-Menten plots of steady-state kinetic data for fosfomycin (B) and GSH (C).

*MIC determination*

The ability of PA1129 to confer resistance to fosfomycin in the biological context of *E. coli* was determined by growing bacteria transformed with a PA1129 expression plasmid in varying concentrations of fosfomycin. The minimum inhibitory concentration (MIC) was determined as the concentration of fosfomycin at which bacteria no longer grew. This could not be accurately determined for PA1129, as bacteria grew at antibiotic concentrations > 45 mg/mL, the saturation limit for making solid agar plates for the experiment. Figure 13 shows bacterial growth on plates as well as MIC for fosfomycin for each protein tested. MIC values obtained are shown in Table 3.

**Table 3.** MIC values obtained for the fosfomycin resistance proteins in mg/mL.

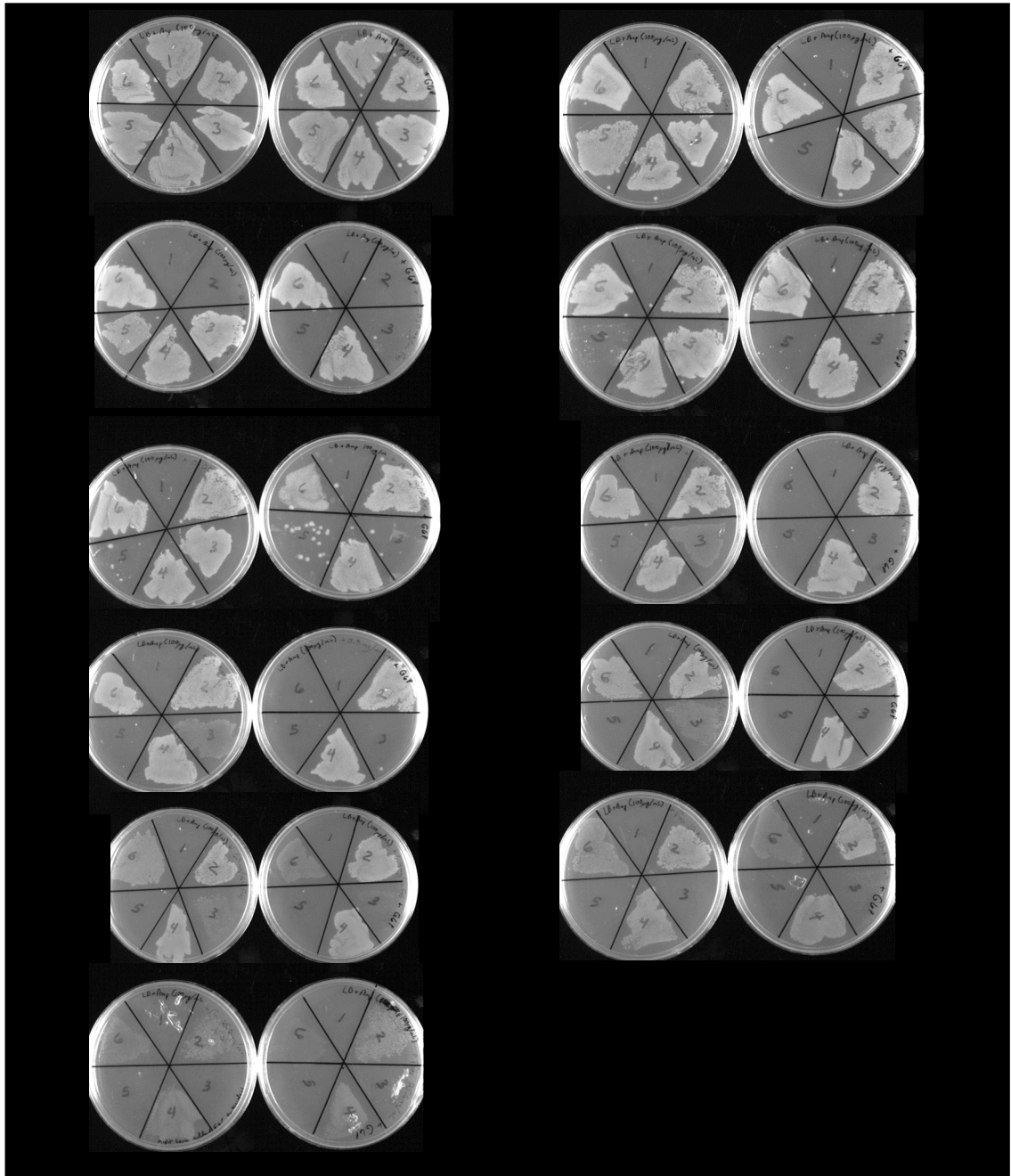| | - G6P | + G6P | $K_{cat}/K_m^{Fos}$ ($M^{-1}s^{-1}$) |
|---|---|---|---|
| pET 20 (control) | < 0.025 | < 0.025 | --- |
| Tn2921 | > 25.6 | > 25.6 | $(1.4 \pm 0.1) \times 10^7$ |
| Bs_yndn | 25.6 > MIC > 12.6 | 1 > MIC > 0.05 | $(4.0 \pm 0.6) \times 10^3$ |
| PA1129 | > 25.6 | > 25.6 | $(9.0 \pm 1.4) \times 10^5$ |
| mlr3345 | 0.40 > MIC > 0.20 | < 0.025 | $(5.0 \pm 0.6) \times 10^2$ |
| FosB$^{Sa}$ | > 25.6 | 0.40 > MIC > 0.20 | $(9.2 \pm 0.1) \times 10^3$ |

Figure 13.    Bacterial growth of *E. coli* transformed with 1.    pET-20b  or  pET-20b containing sequences for 2.  Tn2921 3.  Bs_yndn 4.  PA1129 5.  mlr3345 6.  FosB$^{Sa}$. Plates contained 100 µg/mL ampicillin, and those on the right contained 40 µM glucose-6-phosphate.  From the top, left to right, plates contained 0, 0.025, 0.05, 0.1, 0.2, 0.4, 1.6, 3.2, 6.4, 12.8, and 25.6 mg/mL fosfomycin.

*K⁺-free purification*

Protein eluted from the gel filtration column was of high purity (gel filtration chromatogram, Figure 14, and SDS-PAGE gel, data not shown). This protein exhibited equivalent activity to protein purified via the previous protocol.
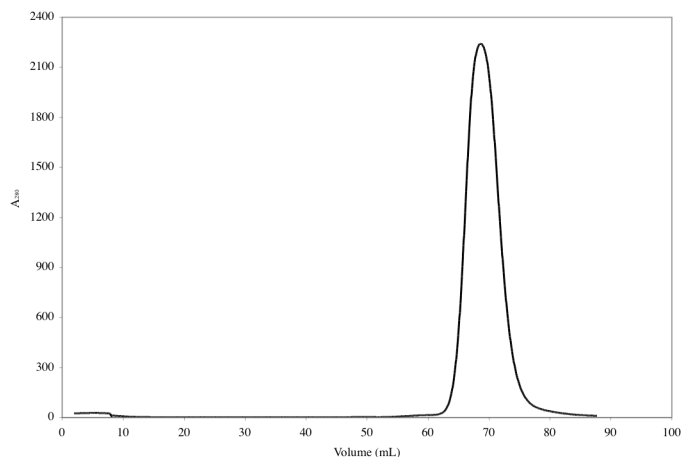


Figure 14. Chromatogram of the absorbance at 280 nm of the eluate from an S100 column in a typical FPLC run. PA1129 is shown as a single peak with no contaminants visible.

*EPR spectroscopy*

EPR spectra of PA1129 in the presence of Mn(II) was compared to the E•Mn(II)•fosfomycin complex (Figure 15A). As shown previously for Tn2921, the addition of substrate greatly perturbs the metal coordination (*29*). Structural information indicates that this is the result of a change in metal coordination by addition of a phosphonate oxygen into the coordination sphere. Collaborators have also collected absorbance EPR and $^{31}$P ENDOR spectra of PA1129 with bound metal and phosphonate (Figure 15B and C) (*41*). These results indicate that the oxirane oxygen of fosfomycin is
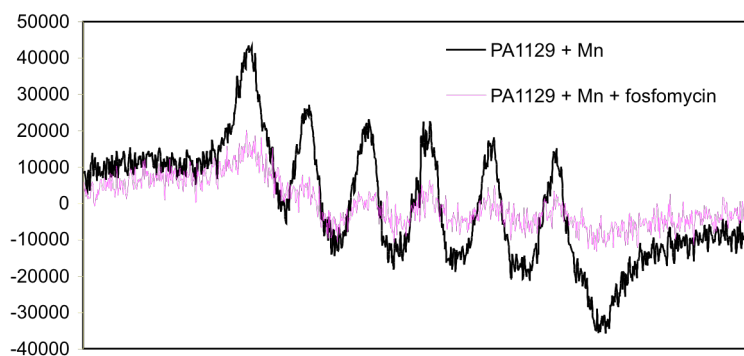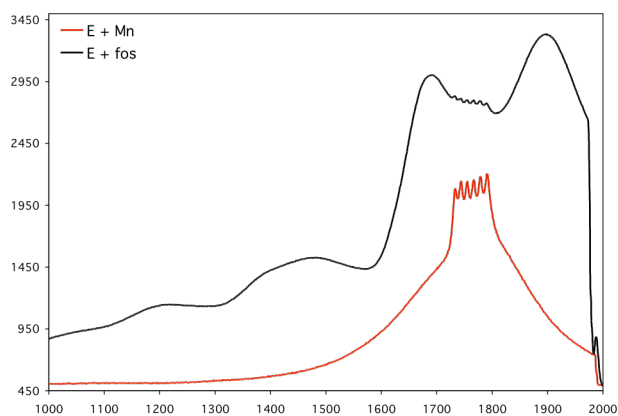
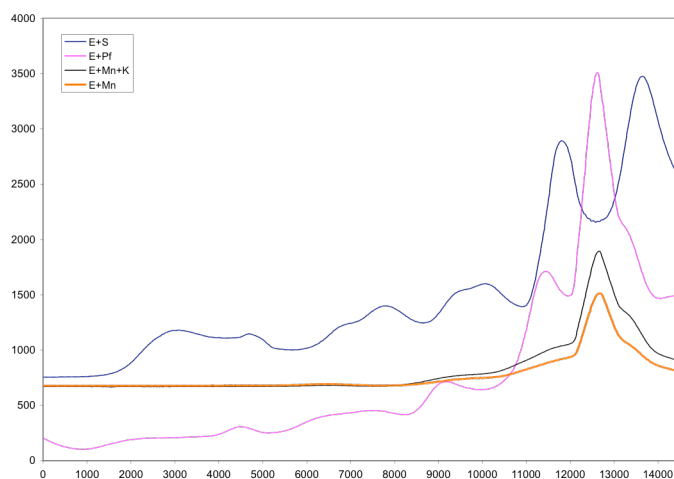Figure 15. A. Derivative EPR spectra of PA1129•Mn(II) and PA1129•Mn(II)•fos recorded at Vanderbilt University. B. Derivative EPR spectra of the same recorded by collaborators. C. 35GHz Continuous wave EPR spectra taken at 2 K and 30 dB microwave power of 5 mM PA1129 with bound Mn(II) (500 µM), $K^+$ (100 mM), fosfomycin (S), and phosphonoformate (Pf). B and C were recorded by collaborators at Northwestern University.

also coordinated to the metal center, although distances taken from the crystal structure do not support this (*28*).

*Circular dichroism spectroscopy*

CD spectra of PA1129 and several mutants in the presence of Mn(II) and K$^+$ and substrate are shown in Figure 16. There were no apparent differences between native protein and mutants. Also, no structural changes were apparent upon the addition of substsrate.
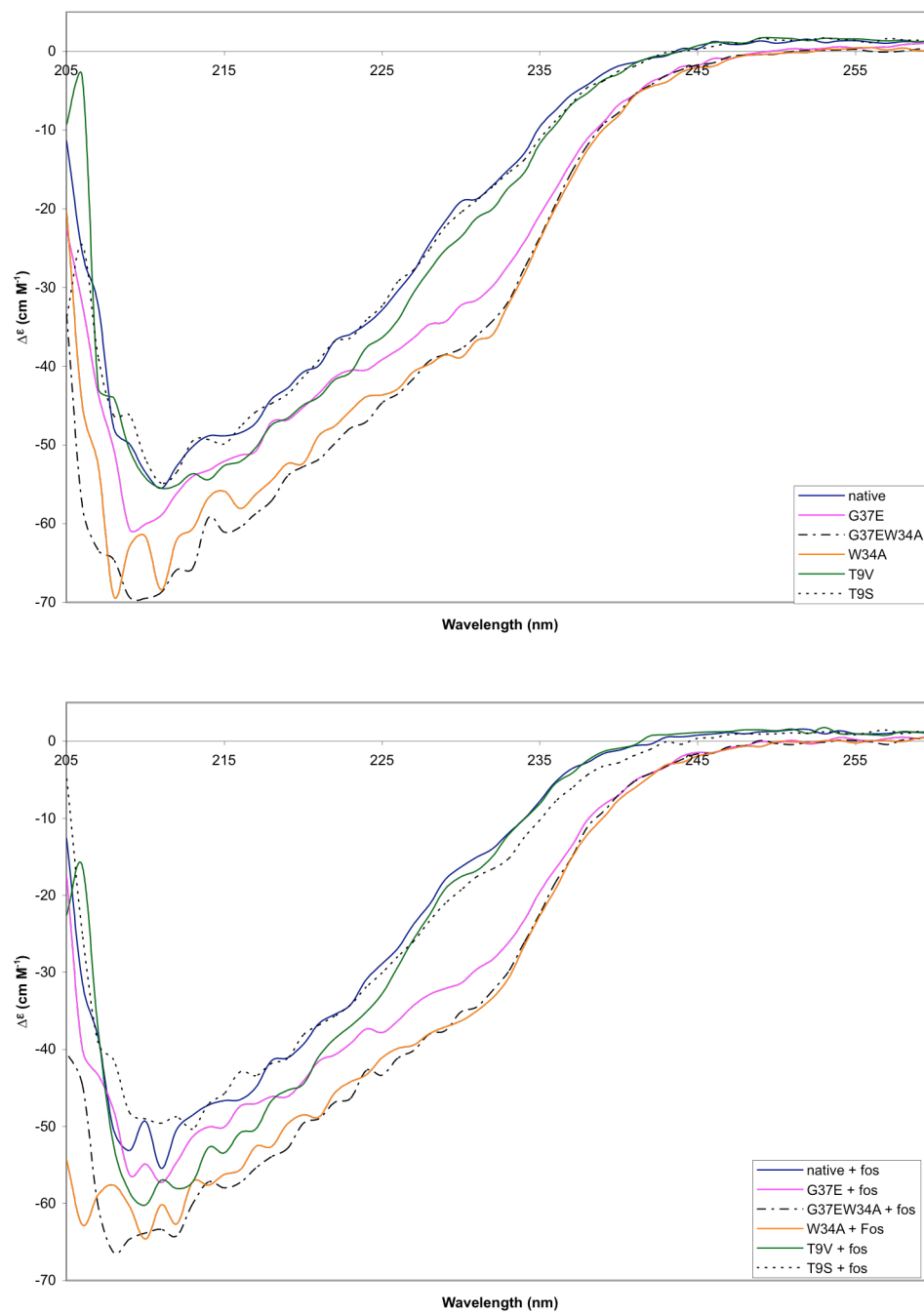
Figure 16.  Circular dichroism spectra of PA1129 and indicated mutants in the presence of $Mn^{++}$ and $K^+$ (top panel) and plus fosfomycin (bottom panel).

Discussion

The initial report of fosfomycin (*6*) hinted at the occurrence of a genomically-encoded resistance element in *P. aeruginosa*, as the $ED_{50}$ (the dose of antibiotic necessary to protect 50% of infected animals) was significantly higher than for other bacteria used in efficacy assays (with the exception of *Streptococcus pyogenes*). More recent studies have shown that strains of *P. aeruginosa* are highly resistant to fosfomycin as compared to *E. coli* (Figure 17).
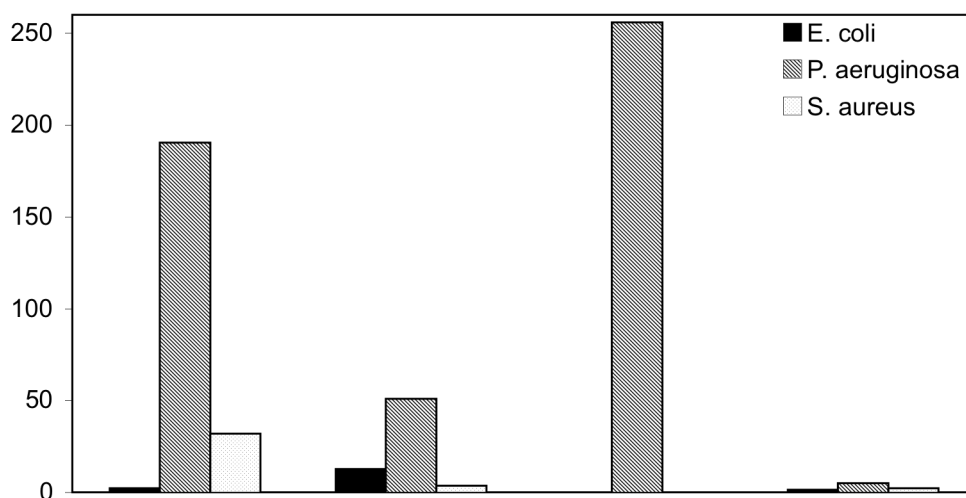


Figure 17. Reported MIC values (in μg/mL) for fosfomycin for various strains of *E. coli*, *P. aeruginosa*, and *S. aureus*. Taken from (*23-25, 42*). Where a range for the MIC was given, the average was taken.

Indeed, our own in vitro studies indicate that the protein provides high levels of resistance when expressed in *E. coli*. Kinetic data reveals that PA1129 falls just short of the superb catalytic efficiency of the plasmid-encoded homologue (TN2921) but is an excellent catalyst nonetheless.

Prior to the availability of structural data for the fosfomycin resistance proteins, circular dichroism spectroscopy was used to characterize native enzyme as well as

several mutants. In addition, electron paramagnetic resonance spectroscopy was used to probe the Mn(II) environment in the presence of $K^+$, substrate, and inhibitor bound to the enzyme. CD spectra indicated that native protein was well folded, with negative ellipticity characteristic of $\alpha$-helical content. Addition of substrate had no significant effects on enzyme secondary structure. Also, several mutants (discussed in more detail in Chapters V and VI) exhibited spectra similar to native protein, indicating that they are probably folded in a similar manner.

EPR spectroscopy is a valuable tool for observing changes in Mn(II) coordination environments. The derivative EPR spectra Mn(II) produces a signature sextet splitting pattern resulting from a hyperfine coupling between the electron spin and the spin (I=5/2) of the 100% natural abundance $^{55}$Mn nucleus (*43*). The spectrum of PA1129•Mn(II)•$K^+$ exhibited the six-line pattern typical of $Mn^{++}$ (Figure 15A and B). Upon addition of fosfomycin, this signal is almost obliterated due to line broadening. This corresponds to a change in metal coordination, either through changes in ligands or coordination geometry. EPR absorbance spectra (Figure 15C) reveal further differences in zero field splitting parameters (Discussed in (*41*)).

The x-ray crystal structure of PA1129 (Figure 18) was solved during the course of this work (*28*). These results further supported a membership in the VOC superfamily as the $\beta\alpha\beta\beta$ structural motif and metal binding mode are conserved. As predicted from EPR studies and mechanistic details of VOC relatives, PA1129 uses its metal center to coordinate substrate oxygens. A phosphonate oxygen is clearly coordinated to the manganese, being 2.1 Å from the metal. It was anticipated that the oxirane oxygen would also coordinate to metal (*20*), but the distance (2.35 Å) between the atoms in the crystal
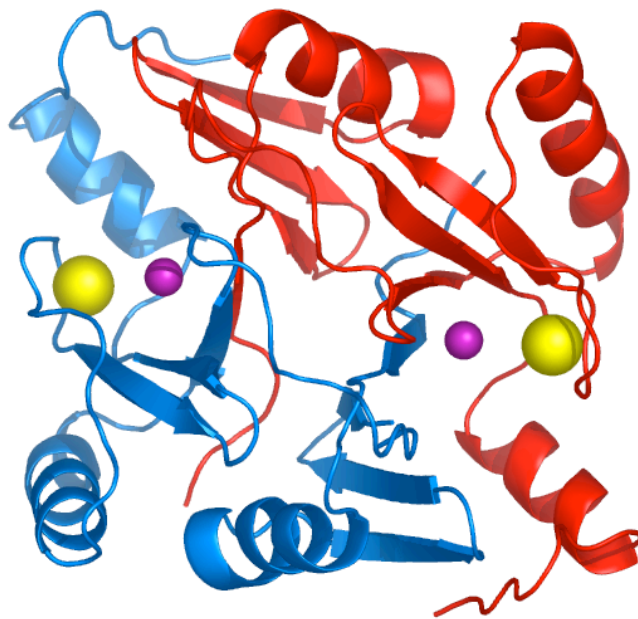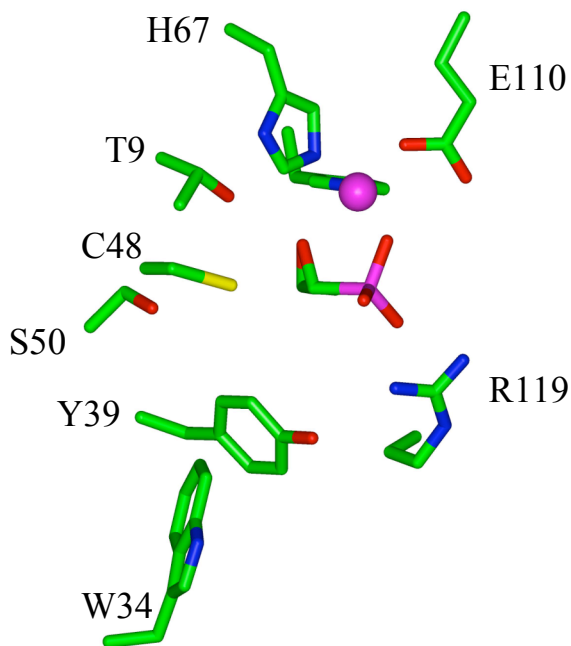
**A**



**B**



Figure 18. A. Ribbon diagram of PA1129 colored by monomer. Mn(II) and K$^+$ ions are purple and yellow spheres, respectively. B. Enlargement of the active site showing metal ligands (His7, His67, Glu110) as well as fosfomycin, Arg119, Thr9, Cys48, Ser50, Tyr39, and Trp34. Figure generated from 1LQP.pdb using the program PyMOL (*10*).

structure was outside the accepted range for Mn(II)--O coordination. However, detailed ENDOR studies (data not shown) indicate that the oxirane oxygen is coordinated with a longer-than-expected distance, probably due to the poor electron-donating ability of the oxygen (*41*). Spectra indicate that, in solution, fosfomycin coordinates Mn(II) only through the phosphate moiety. However, in the enzyme active site, spin density on the $^{31}$P is reduced by transfer via $^{31}$P—C—O$_{oxirane}$—Mn(II). This is in agreement with other VOC enzymes, as it serves to activate the epoxide for attack by a nucleophile, thus facilitating catalysis.

Comparison of catalytic efficiency (Table 3) revealed that this value correlates well with MIC for fosfomycin in *in vitro* studies. Although the method used does not allow for variations in protein expression levels, it provides an assay for analysis of putative fosfomycin resistance proteins.

CHAPTER IV


DEVELOPMENT AND ANALYSIS
OF POTENTIAL FOSA INHIBITORS


Results


*Inhibition assays*

The panel of phosphonate inhibitors (Figure 9) tested were found to inhibit PA1129 to a varying degree depending primarily on the length of carbon chain linking the phosphonate and carboxyl moieties (Table 3). Formyl phosphonic acid could not be successfully synthesized for testing in inhibition assays. Phosphonoformate, the proposed transition state analogue, was also tested for inhibition of the plasmid encoded FosA. Data indicate that it is a competitive inhibitor of both FosA enzymes. Figures 19 and 20 show Dixon plots of inhibition data. Since lines intersect in quadrant II, it is apparent that the inhibitors are competitive with respect to fosfomycin.


*Other inhibitors*

Assays carried out in the presence of glutathione sulfonate and pyruvate produced insignificant inhibition at the concentrations tested. Ethyl phosphonoformate, however, inhibited reactions nearly as well as phosphonoformate. These compounds were not pursued past preliminary tests for inhibition.
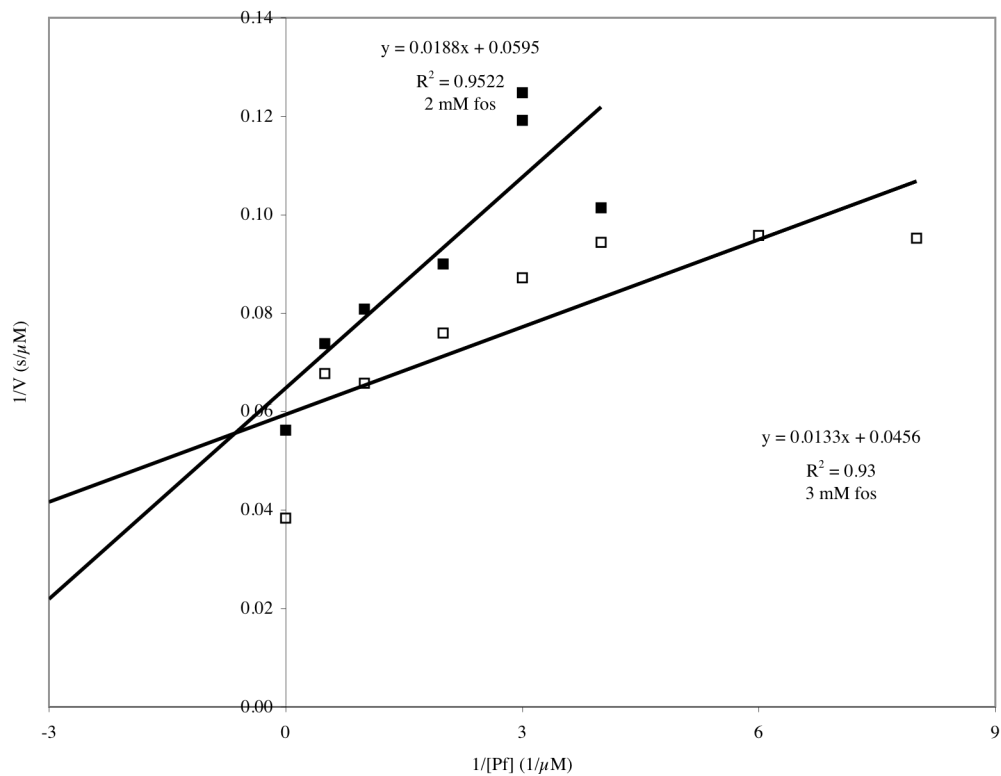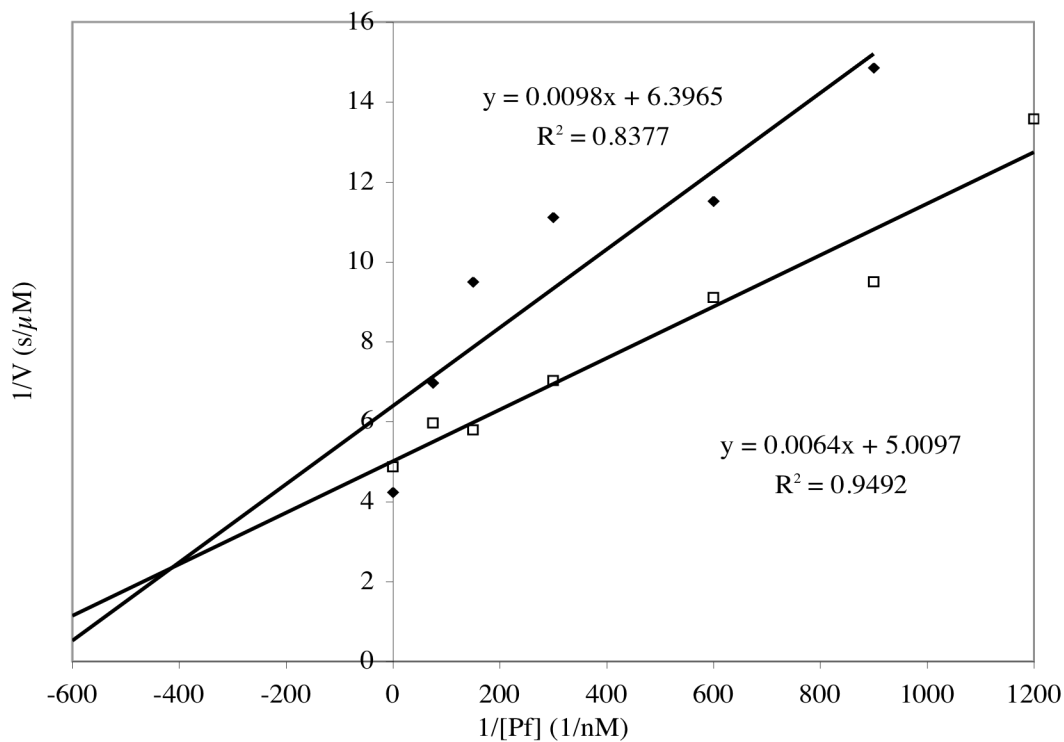
Figure 19. Dixon plots of inhibition data of PA1129 (top) and FosA (bottom) with phosphonoformate (Pf).
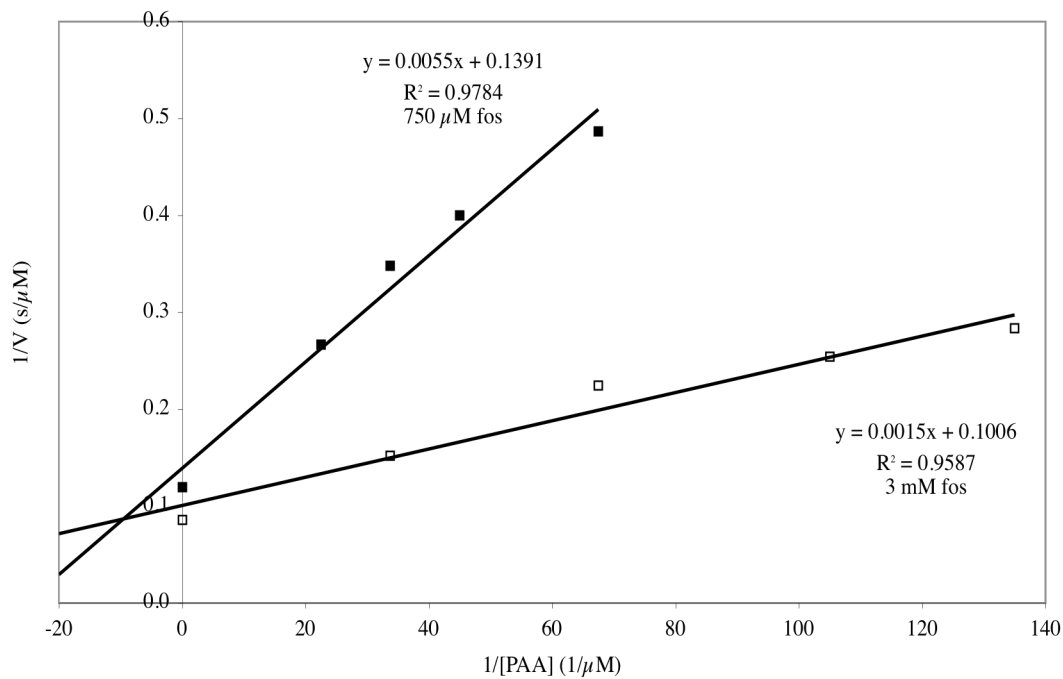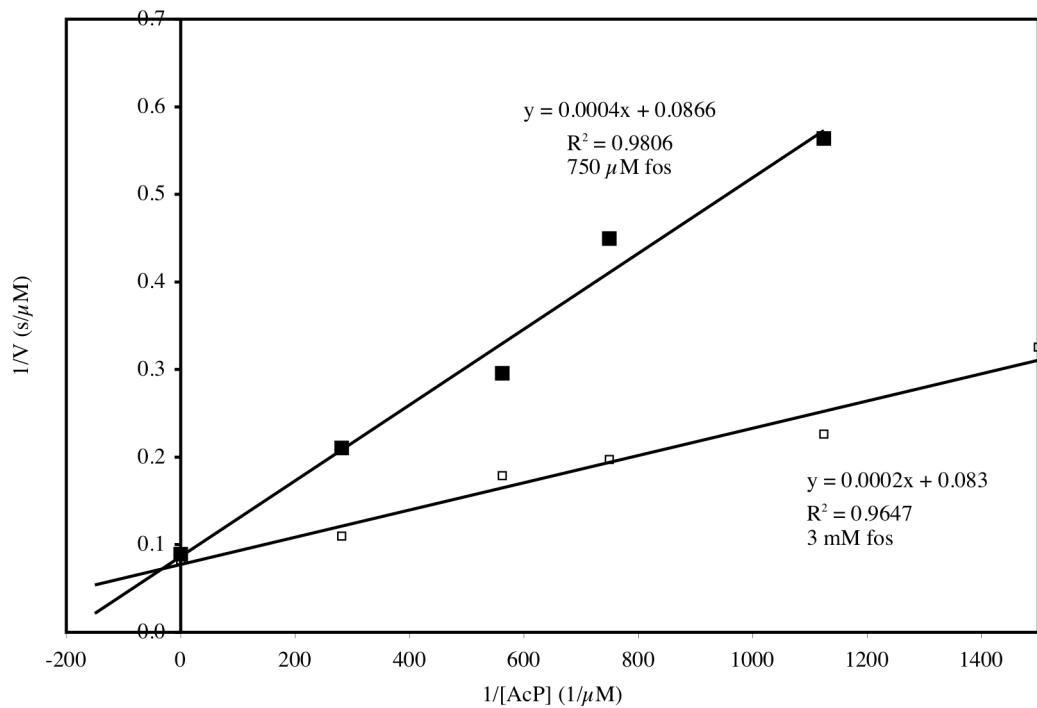
55

Figure 20.  Dixon plots of inhibition assays of PA1129 with acetyl phosphonate (AcP) and phosphonoacetic acid (PAA).

**Table 4.** Inhibition constants for a panel of phosphonates tested with PA1129.

| Compound | $K_I$ (μM) |
| --- | --- |
| Phosphonoacetic acid | $10 \pm 1$ |
| Phosphonoformate | $0.41 \pm 0.09$ |
| Acetyl phosphonate | $18 \pm 2$ |
| 2-carboxyethylphosphonate | $> 100$ |
| Pyruvate | n.d.[*] |
| $GSO_3^-$ | n.d. |

*n.d. = none detectable

*In vivo inhibition by phosphonoformate*

While phosphonoformate (Pf) proved to be a very effective inhibitor *in vitro*, it proved to be ineffective in lowering the MIC for fosfomycin when added to cultures of *E. coli* BL21-DE3 pLysS cells transformed with a FosA expression plasmid (Figure 21). In fact, addition of Pf to cultures actually lowered the MIC for ampicillin in the absence of fosfomycin from 1 mg/mL to approximately 0.7 mg/mL, indicating the inhibitor may be acting on cells in a fosfomycin-independent manner. The mechanism of action is not understood, although the molecule could be acting as an analogue of a small cellular phosphonate such as PEP and competitively inhibiting a variety of enzyme activities in the cell.
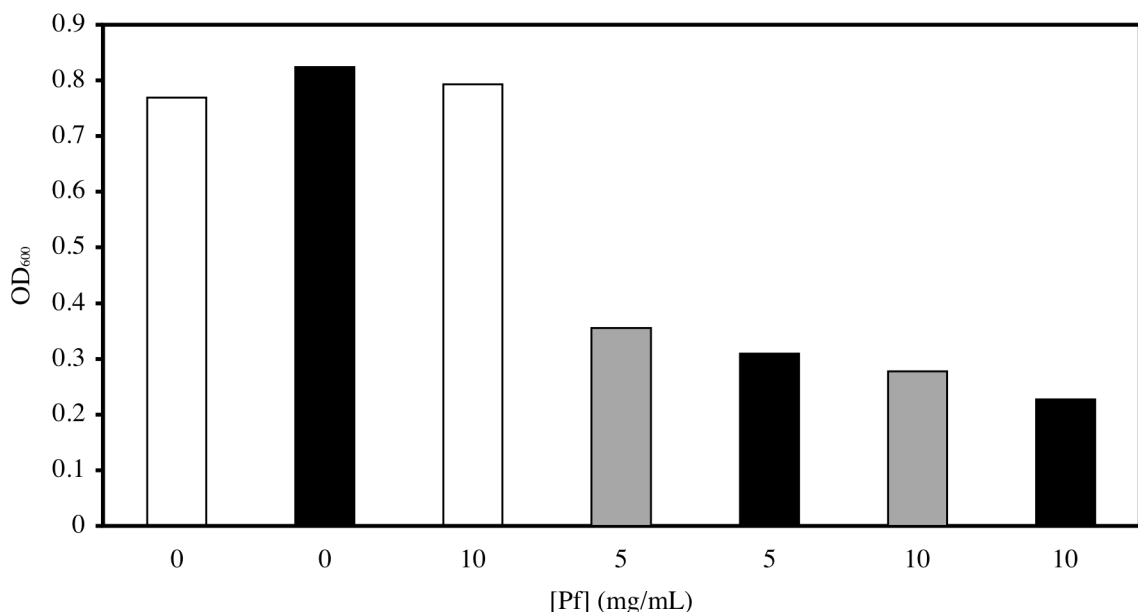
Figure 21. Results of bacterial growth in the presence of varying concentrations of Pf in the presence of 0 (open) 5 (gray), or 10 (black) mg/mL fosfomycin.

*Enolate and GSH adduct formation*

In addition to being a likely FosA inhibitor, it was possible that acetyl phosphonate could form a 1,2-adduct with GSH in the FosA active site (Figure 22B). Alternatively, FosA could catalyze formation of an enolate and enhance deuterium incorporation in the AcP methyl group (Scheme 1). Acetyl phosphonate in the presence of GSH and E•Mn(II) was monitored for the formation of a GSH-acetyl phosphonate adduct. This adduct would likely not be stable enough to be isolated from a reaction mixture. NMR analysis of reaction mixtures revealed that adduct was not formed to a measurable extent. E•Mn(II) and AcP incubated in $D_2O$ up to several days indicates that FosA cannot catalyze this reaction under the conditions tested (Figure 23).

A                                                                                   B



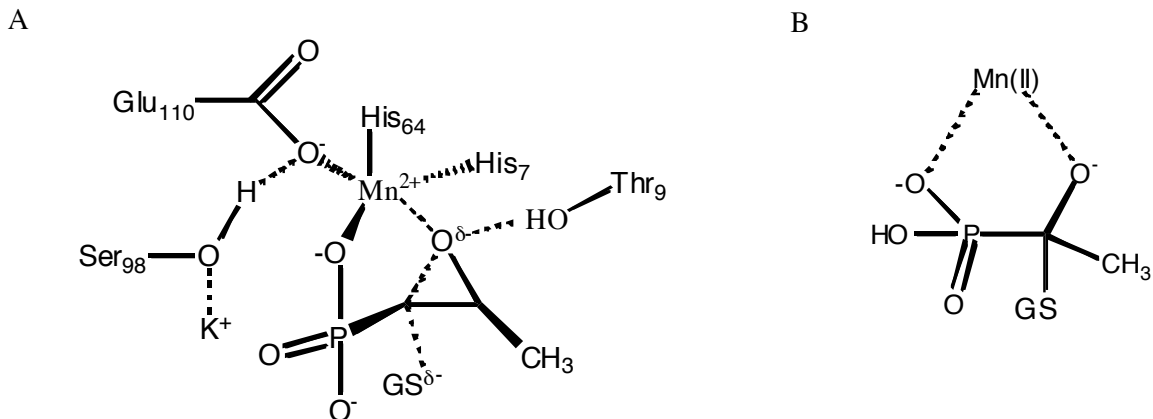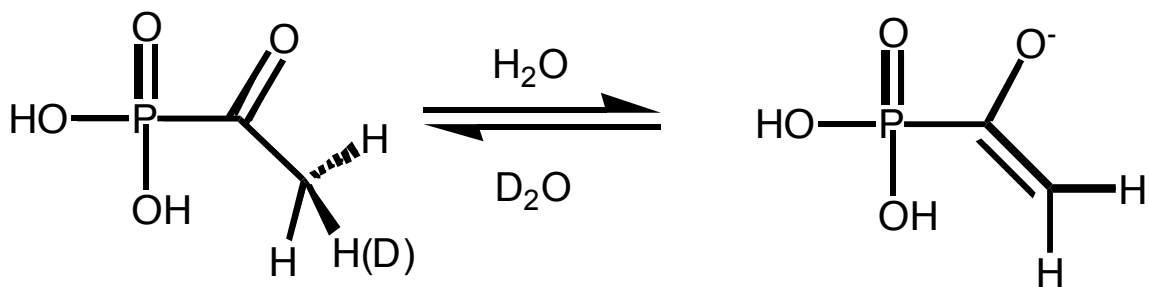Figure 22.  A.  Coordination geometry of a proposed transition state in FosA.  B.
Possible adduct of GSH and acetyl phosphonate in the FosA active site.



Scheme 1.  Formation of the enolate of acetyl phosphonate showing incorporation of
deuterium in the methyl group.
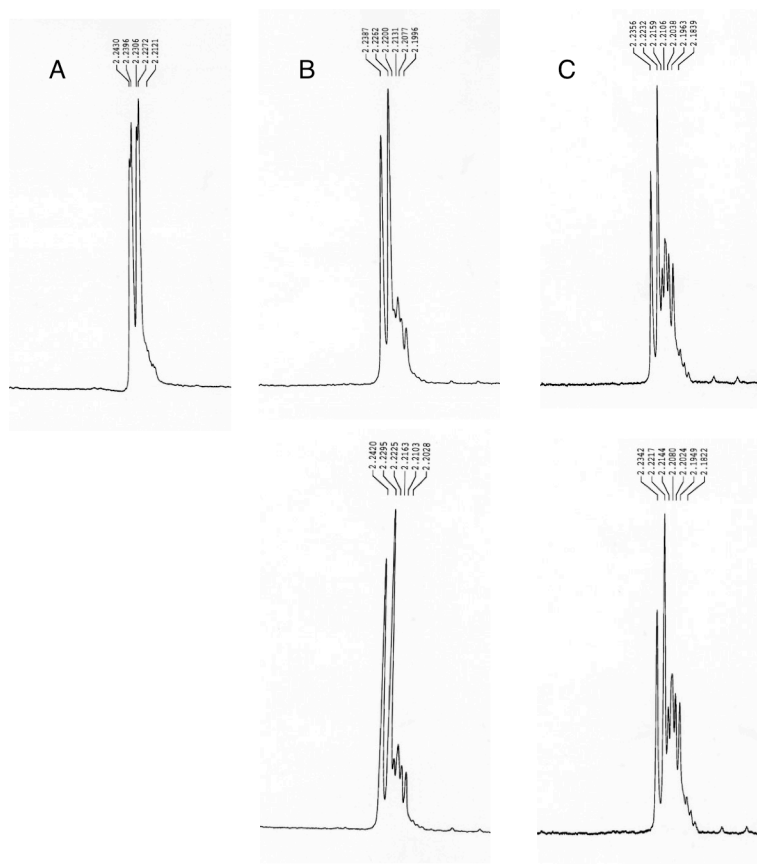
Figure 23. $^1$H NMR spectra showing incubation of acetyl phosphonate with E•Mn(II) in D$_2$O (top) and in reactions lacking enzyme (bottom) for 48 hr (A), 7 days (B), and 15 days (C). No differences from the control were observed.

*Binding of substrate and Pf to FosA*

Binding of substrate or Pf to PA1129 produced a characteristic change in the A$_{245}$ (Figure 24A). This was utilized to obtain information about their rates of binding to enzyme. Although binding rates were too large to be measured directly, differences in the ε$_{245}$ were used to obtain $k_{off}$ for Pf from FosA•Mn(II)•K$^+$•Pf by mixing with an excess of fosfomycin (Figure 24B). The $k_{off}$ for fosfomycin from FosA•Mn(II)•K$^+$•fosfomycin was determined in a similar manner by mixing with Pf (Figure 24C). Binding events followed single-exponential behavior, indicating that, in both cases, the phosphonate used

in excess successfully trapped FosA•Mn(II)•K$^+$ upon dissociation of bound ligand. Fits of the data to a single exponential gave $k_{off}$ values of 5 and 30 s$^{-1}$ for Pf and fosfomycin, respectively.


*Steady state phosphonate binding*

Although changes in the UV spectra were useful for obtaining pre-steady state binding information, the enzyme concentration (5 µM) necessary to produce measurable spectroscopic changes was in excess of estimated dissociation constants. However, changes in intrinsic protein fluorescence upon phosphonate binding were observed (Figure 25A), allowing the use of lower enzyme concentrations. Accordingly, steady-state titrations of FosA•Mn(II)•K$^+$ with fosfomycin and phosphonoformate were carried out while observing fluorescence changes at 330 nm (Figure 25B). Equilibrium dissociation constants of 0.74 ± 0.01 µM for fosfomycin and 0.17 ± 0.01 µM for phosphonoformate were obtained.
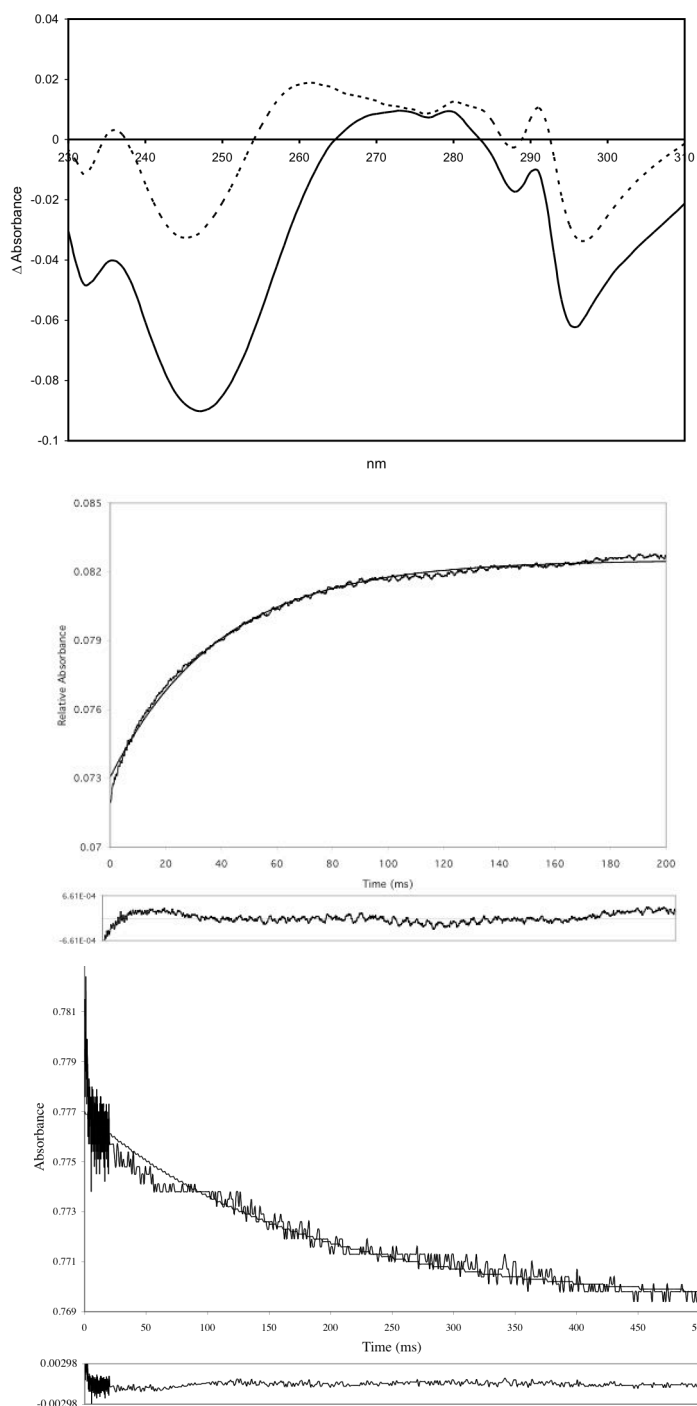
Figure 24. A. UV difference spectra of the complexes: (---) FosA• Mn(II)•**1** - FosA•
Mn(II) ($\Delta\varepsilon_{245}$ = -1690 $M^{-1}$ $cm^{-1}$) ; — FosA• Mn(II)•**2** - FosA• Mn(II) ($\Delta\varepsilon_{245}$ = -4560 $M^{-1}$
$cm^{-1}$)  B.  Change in $A_{245}$ upon rapid mixing of 5 μM FosA•Mn(II)•$K^+$•**2** with 10 mM **1**.
The solid line is a fit of the data to a single-exponential equation with a $k_{obs}$ of 5.06 ±
0.02 $s^{-1}$.  The bottom trace is the residual to the fit.  C.  Change in $A_{245}$ upon rapid mixing
of 5 μM FosA•Mn(II)•$K^+$•**1** complex with 5 mM **2**.  The solid line is a fit of the data to a
single-exponential equation with a $k_{obs}$ of 29 ± 3 $s^{-1}$.  The bottom trace is the residual to
the fit.
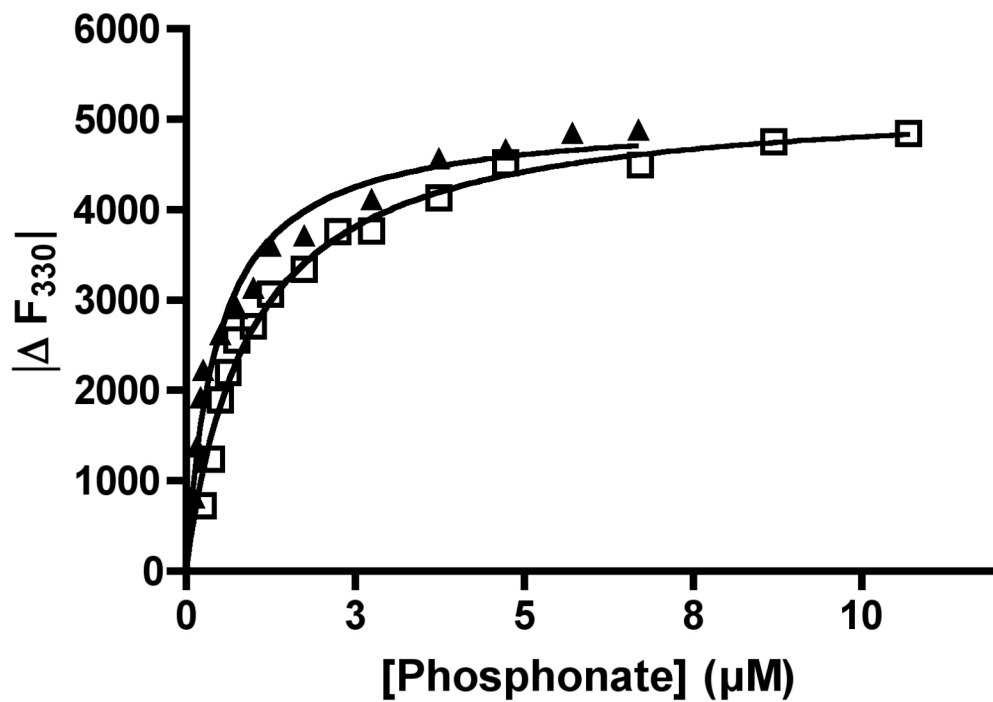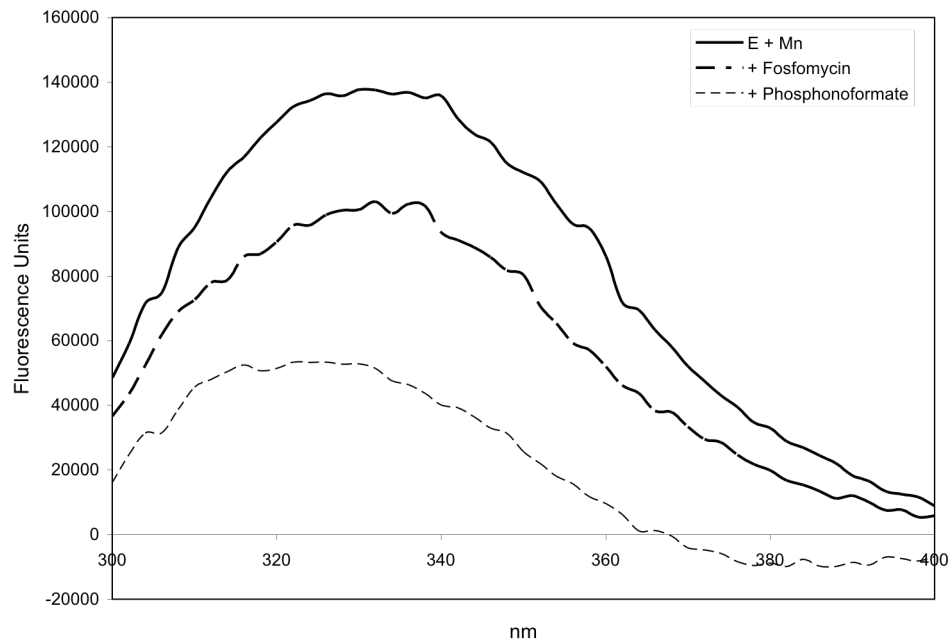
Figure 25. A. Fluorescence emission spectra of FosA•Mn(II) (—) and after addition of substrate (— —) and Pf (---). B. Fluorescence titrations of FosA•Mn(II)•K$^+$ with fosfomycin (□) and Pf (▲). Solid lines are fits of the data to equation 3 with dissociation constants of $0.74 \pm 0.01$ μM for fosfomycin and $0.17 \pm 0.01$ for Pf.

Discussion

The high-resolution structure of PA1129 with bound Pf has been reported (*28*). Figure 26A shows the location of Pf with respect to the metal center and residues providing hydrogen-bonding interactions. In this structure, the metal is five-coordinate. The angular structural parameter, $\tau$, for describing trigonality (*44*) was calculated from metal—ligand geometries according to equation 4, where $\alpha$ is the angle between equatorial ligands and $\beta$ is the angle between axial ligands.

$$\tau = (\beta - \alpha) / 60 \qquad (4)$$

Calculations using $\alpha = 119.39°$ (angle between Glu110 and Pf carboxylate) and $\beta = 174.82°$ (average of angles between His7 and His64, His64 and phosphonate oxygen, and phosphonate oxygen and His7) produced a value for $\tau$ of 0.92. This indicates nearly perfect trigonal bipyramidal geometry ($\tau = 1.0$). This is in contrast with the coordination of fosfomycin, which has a longer $Mn(II)—O_{oxirane}$ distance, moving the ligand out of the inner coordination sphere.

Structural results supported kinetic data implicating Pf as a competitive inhibitor, as it is bound in exactly the same position as fosfomycin (Figure 26B). Note the significant movement of Tyr62 between the substrate and inhibitor complexes. This motion may account for the spectral differences observed between E•Mn(II)•fosfomycin and E•Mn(II)•Pf and could provide a means of recognition of product by the enzyme, leading to its release during turn-over.
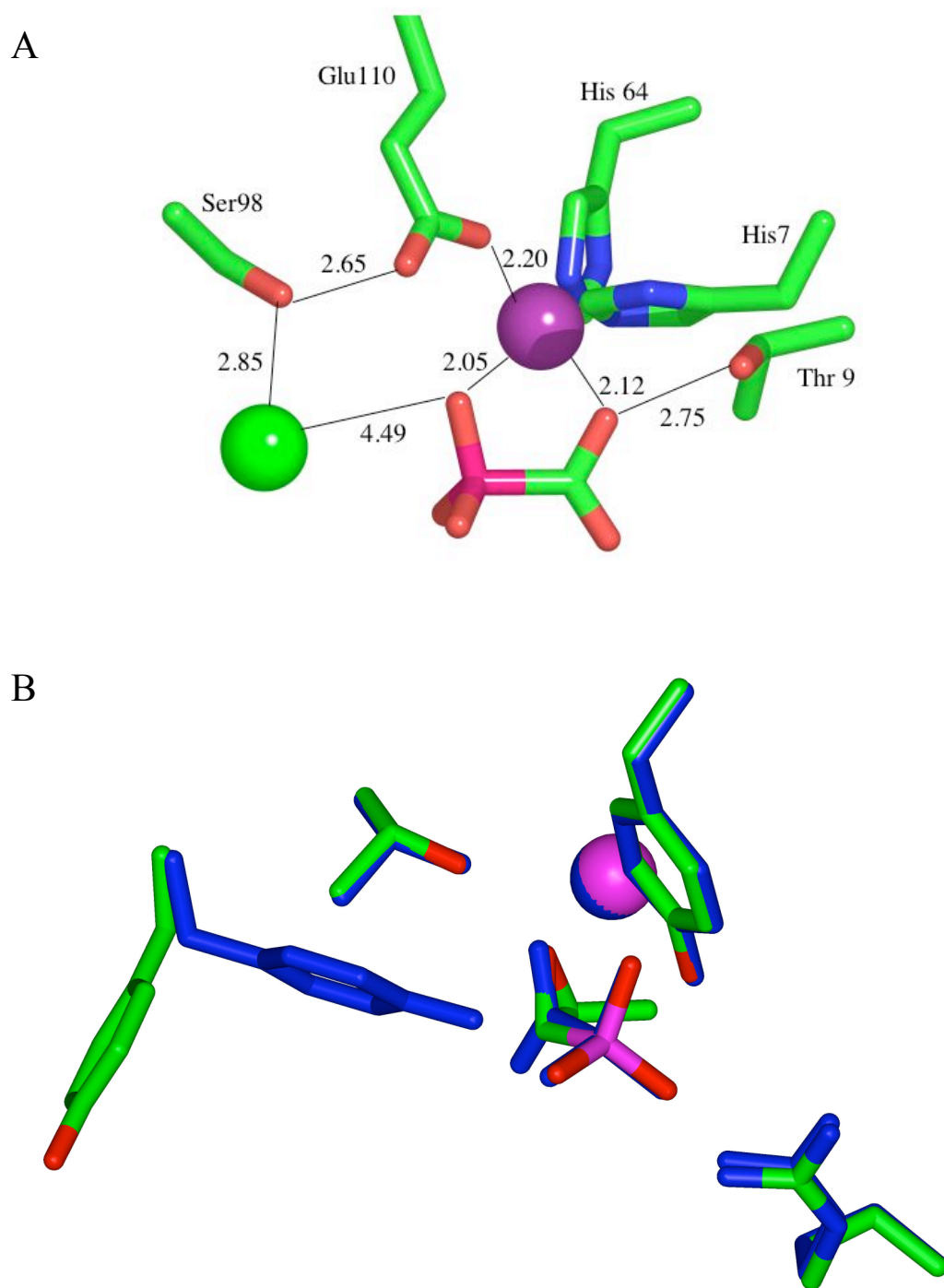
Figure 26. A. Phosphonoformate (Pf) bound in the PA1129 active site. Mn(II) and $K^+$ ions (purple and green spheres, respectively) are shown. Metal ligands E110, H7, and H64 as well as T9 and S98 are shown. Distances are in Å. B. Overlay of PA1129 with substrate or Pf bound in the active site. Note overlay of the phosphonates and the difference in orientation of Tyr62. Figure generated in PyMOL (*10*) from 1LQP.pdb and 1NKI.pdb.

*Inhibition of FosA*

Several simple phosphonates were modestly effective competitive inhibitors of the FosA enzyme encoded in the genome of *P. aeruginosa*. Phosphonoformate, acetyl phosphonate (AcP), and phosphonoacetate (PAA) were chosen as possible substrate or transition state analogues of the addition reaction based on the suggestion that the Mn(II) center acts as a Lewis acid to facilitate breaking of the C—O bond of the oxirane (*19, 28*). Oxirane ring-opening reactions typically occur with early transition states so that the geometry of the proposed five-membered chelate ring (Figure 22) is very close to that observed in the complex with Pf. Indeed, analysis of inhibition data indicated that inhibition by Pf was competitive (data lines crossed in quadrant II) and had a reasonable $K_i$. Transition state analogue inhibitors typically bind much more tightly than the corresponding substrate does. The fact that Pf binds only ~6-fold more tightly than substrate may reflect the fact that the reaction has a very early transition state with little charge build-up on the oxirane oxygen. Taken together, these observations suggest that Pf can be viewed as a minimal transition state inhibitor for FosA given that it lacks any of the structural elements of the second substrate GSH.

Phosphonoacetate, with the chelate ring expanded by a methylene group, binds ~20 fold less tightly than Pf. This compound resembles the structure of a very late transition state in which the C-O bond is almost completely broken. Acetylphosphonate (AcP), has a neutral oxygen adjacent to the phosphonyl group in place of the charged carboxylate. This compound has a $K_i$ that is significantly higher than the $K_d$ for fosfomycin. AcP was of particular interest because of its potential to form an enolate complex, Scheme 1, or a metal-stabilized 1,2-adduct with GSH (Figure 22B) in the FosA

active site. Catalysis of enolate formation by FosA is not unlikely, since other VOC superfamily members (e.g. extradiol dioxygenase) efficiently carry out catalysis via an enolate intermediate. Although deuterium incorporation in the methyl group is observed, the FosA•Mn(II) complex does not promote enolate formation over and above that observed with Mn(II)•6$H_2$O. Since AcP is not a very good inhibitor of FosA, it is unlikely that the enolate, if formed on the enzyme, is a particularly stable or highly populated species. Formation of an adduct with GSH was investigated, as it could be stabilized and trapped by coordination with the metal center. No adduct was apparent in NMR spectra of reaction mixtures. However, the adduct may form but not be stable enough to accumulate to sufficient concentration to be visible by NMR.

It is probable that formyl phosphonic acid would inhibit FosA, but this compound could not be synthesized for analysis. 2-Carboxyethyl phosphonic acid, with two methylene groups added to the carbon chain, is presumably too long to bind well in the active site since it does not inhibit enzyme activity. Glutathione sulfonate and pyruvate failed to inhibit PA1129 to any appreciable extent. The anionic sulfonate may not be accommodated well in the active site, although it is an effective inhibitor of the soluble glutathione transferases. Although pyruvate contains a carboxylate moiety which could presumably bind in the site typically filled by fosfomycin's phosphate group, an oxyanion group (e.g. sulfate, phosphate) may be required for binding in this site.

*In vivo inhibition*

*E. coli* transformed with the expression plasmid for FosA exhibit robust resistance to fosfomycin. Unfortunately, none of the inhibitors examined here were effective in

enhancing the efficacy of fosfomycin toward these transformants either in liquid culture or on agar plates. The reason for the lack of activity *in vivo* is unclear but may be due to ineffective transport of the molecules into the cytosol of the bacterium. The triethyl ester of Pf was tested for improved *in vivo* activity with the assumption that the esterified compound might enter cells more readily, where esterases would quickly cleave the ester bonds to form the active molecule. It is not known if the compound enters the cell or if cleavage actually occurs. These attempts at *in vivo* inhibition were also unsuccessful.

*Kinetics of Binding of Fosfomycin and Phosphonoformate*

Binding of phosphonates to PA1129 produced a characteristic change in the UV absorbance of the protein (Figure 24). Compared to E• Mn(II), E• Mn(II)•fosfomycin produced a $\Delta\varepsilon_{245}$ of -1690 $M^{-1}$ $cm^{-1}$ and E• Mn(II)•Pf a $\Delta\varepsilon_{245}$ of -4560 $M^{-1}$. These changes in extinction coefficient were utilized in stopped-flow experiments to observe dissociation of fosfomycin from E• Mn(II)•fosfomycin by trapping as E•Mn(II)•Pf and vice versa.

The equilibrium dissociation constant $K_d$ for each phosphonate could not be measured by absorbance due to the high enzyme concentration required for these experiments. In addition to the absorbance change, phosphonate binding produced a decrease in intrinsic protein fluorescence which could be utilized in steady state fluorescence titration experiments. Interestingly, addition of Pf to the enzyme produced a blue shift in the emission spectrum which was not seen with fosfomycin. The reason for this is unknown but could reflect minor changes in protein structure due to the transition-state nature of the inhibitor. Titration data revealed a dissociation constant of 0.2 μM and

$k_{off}$ of 5 s$^{-1}$ for Pf, suggesting that Pf binding occurs near the diffusion limit. A $k_{off}$ of 30 s$^{-1}$ and $K_d$ of 0.7 μM are consistent with a diffusion-controlled binding of fosfomycin as well. This rapid binding prevented the direct measurement of $k_{on}$. However, $k_{on}$ could be estimated from equation 5, giving $k_{off}/K_d \approx 10^7 - 10^8$ M$^{-1}$ s$^{-1}$.

$$K_d = k_{off} / k_{on} \tag{5}$$

The one clearly measurable difference in the equilibrium binding of Pf is the smaller rate constant for dissociation of the bidentate chelate. It seems evident that candidates for fosfomycin resistance protein inhibitors should retain this feature to facilitate binding to the enzymes.

CHAPTER V


GLUTATHIONE BINDING AND ACTIVATION IN FOSA


Results


*GSH docking and energy minimization*

After repeated attempts to identify a GSH binding site in FosA through protein crystallization trials using GSH, glutathione sulfonate, and GS-fosfomycin, a potential binding site was identified in PA1129 through manual molecular docking followed by energy minimization of the docked complex. Favorable intermolecular hydrogen bonding interactions to the docked GSH in the model include Arg93, Lys90, Ser50, Tyr39, Gln36, and Trp34. Figure 27 shows the location of GSH in a ribbon diagram of FosA (PA1129) as well as a diagram of hydrogen bonding interactions between GSH and protein.


*Kinetic analyses of native and mutant enzymes*

Glutathione transferases are known to use tyrosine or serine residues to assist in ionization of GSH during catalysis (*45*). It has been suggested that cysteine residues might also be involved in GSH ionization. A series of mutants was prepared and analyzed to identify a potential residue serving this purpose in FosA. Although Cys48 and Ser50 were preliminary candidates, mutation of either residue to Ala had little effect

on catalysis (Table 5).  The S50A mutant displayed substrate inhibition with fosfomycin. The equilibrium constant $K_i$ for inhibition as calculated from equation 6 was 2.4 mM.

$$v = \frac{V_{max}[S]}{K_m + [S]\left(1 + \dfrac{[S]}{K_i}\right)} \tag{6}$$

Results from the energy-minimized docked enzyme-substrate complex indicated that Tyr39 was in a favorable position to ionize GSH, being 3.45 and 3.48 Å from the unionized thiol of GSH and the C1 group of fosfomycin, respectively.  The Y39F mutant displayed a 10-fold reduction in turnover and 100-fold decrease in catalytic efficiency. Mutagenesis of the corresponding residue in FosB, also a thiol-utilizing enzyme, had similar effects on catalysis.

W34A and W34H mutants were also prepared and analyzed for activity since Trp34 was within hydrogen bonding distance to GSH in the model.  W34A exhibited a substantial increase in $K_m^{GSH}$.  The W34H mutant, however, had recovered native kinetics.  These mutations had minimal effect on fosfomycin kinetics.  All kinetic results are summarized in Table 5.

**Table 5.** Kinetic parameters for selected proteins.

| | $k_{cat}$ ($s^{-1}$) | $k_{cat}/K_m^{thiol}$ ($M^{-1}s^{-1}$) | $k_{cat}/K_m^{fos}$ ($M^{-1}s^{-1}$) | $K_d^{GSH}$ ($\mu M$) |
|---|---|---|---|---|
| M1-1 GST[a] | $18 \pm 2$ | $1.1 \times 10^5$ | n.a. | $26 \pm 3$ |
| PA1129 FosA | $180 \pm 6$ | $(4.1 \pm 0.8) \times 10^4$ | $(9.0 \pm 1.4) \times 10^5$ | $130 \pm 30$ |
| C48A | $177 \pm 8$ | $(1.3 \pm 0.3) \times 10^4$ | $(1.6 \pm 0.3) \times 10^6$ | |
| S50A | $134 \pm 2$ | $(6.2 \pm 0.4) \times 10^4$ | $(9.1 \pm 5.3) \times 10^5$ | |
| Y39F | $14 \pm 2$ | $(8.7 \pm 1.0) \times 10^2$ | $(1.0 \pm 0.6) \times 10^5$ | |
| W34A | $32 \pm 3$ | $(2.0 \pm 0.4) \times 10^2$ | $(1.3 \pm 0.3) \times 10^4$ | |
| W34H | $30 \pm 4$ | $(5.4 \pm 1.1) \times 10^3$ | $(1.1 \pm 0.3) \times 10^4$ | $100 \pm 20$ |
| B. subtilis FosB | $4.8 \pm 0.3$ | $122 \pm 37$ | $(4.0 \pm 0.6) \times 10^3$ | |
| Y40F | $0.02$ | | | |

n.a.:  not applicable

a.  Taken from (*46*).
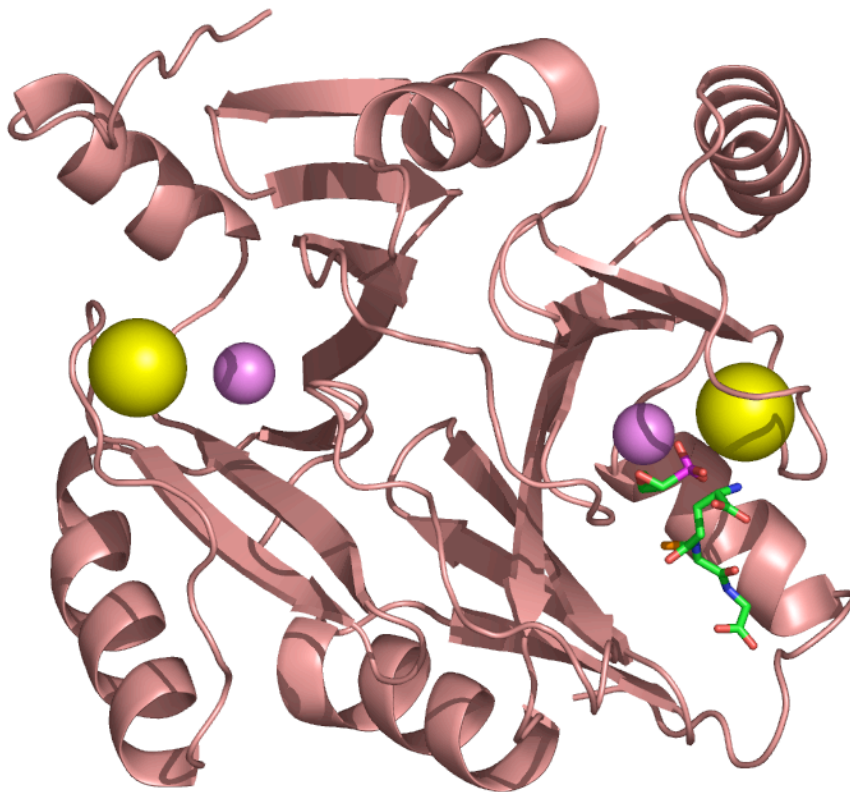
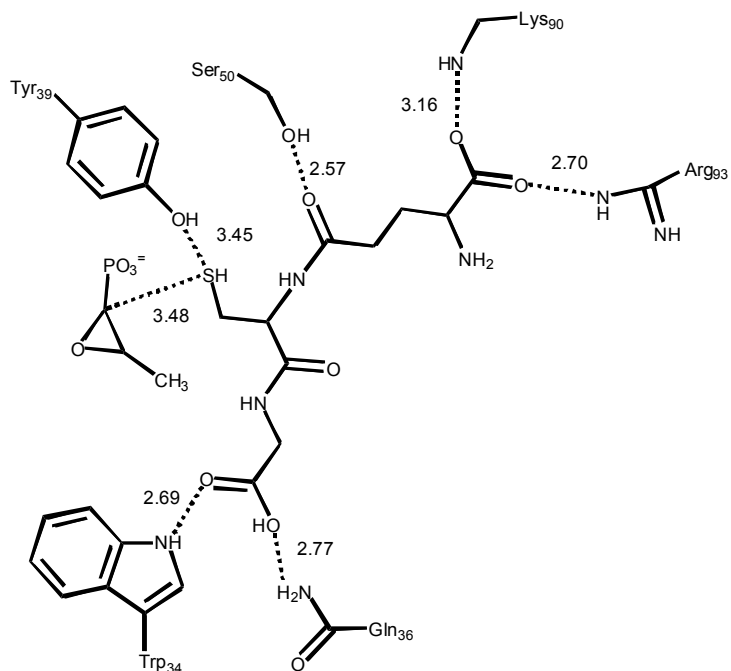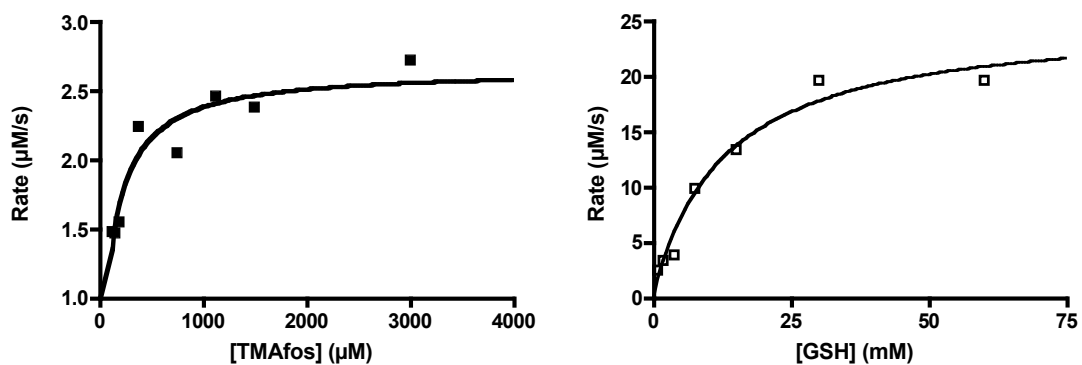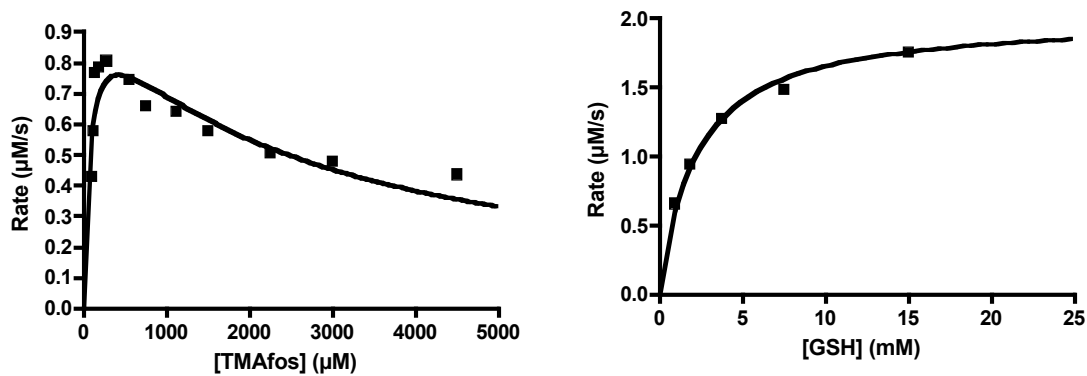Figure 27. A. Ribbon diagram of FosA (PA1129) with GSH shown in the docked position. B. Diagram of residues participating in hydrogen-bonding with GSH. The position of the GSH thiol relative to Tyr39 and fosfomycin C1 is indicated.

**A**

**B**

**C**
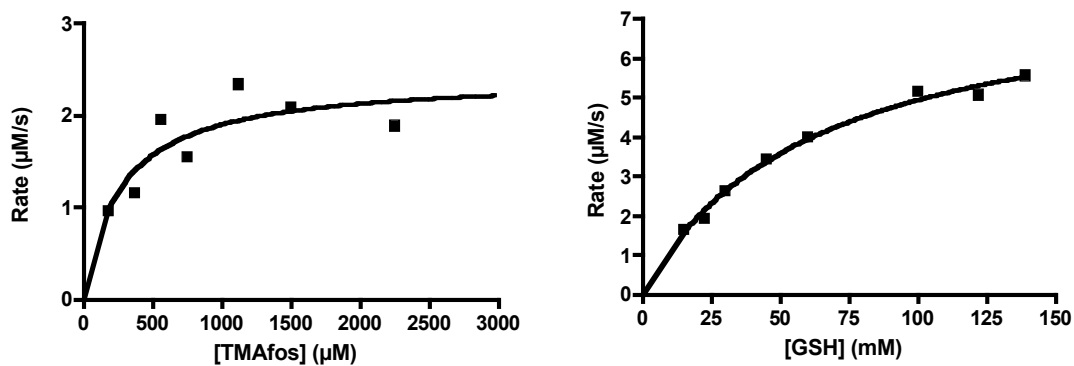
Figure 28.  Plots of kinetic data for C48A (A), S50A (B), and Y39F (C).
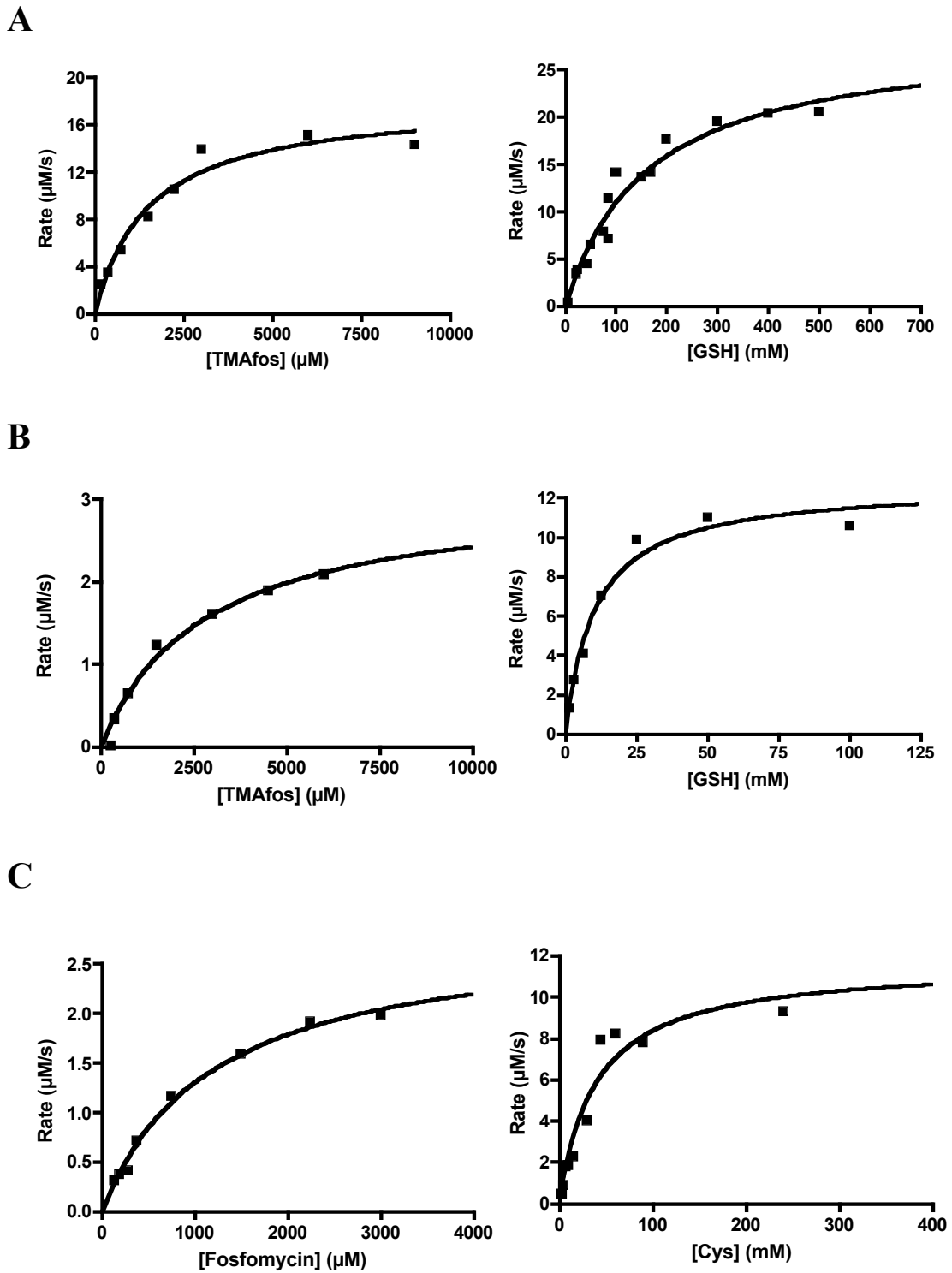
Figure 29. Plots of kinetic data for W34A (A), W34H (B), and FosB<sup>Bs</sup> (C).

*Fluorescence titration of enzyme with GSH*

Addition of GSH to E•Mn(II) produced a characteristic decrease in intrinsic protein fluorescence (Figure 30A). Interestingly, this change was lost upon pre-incubation of E•Mn(II) with phosphonoformate (Figure 30B). Titration of PA1129 with GSH revealed that the fosfomycin resistance proteins have equilibrium dissociation constants for GSH similar to the unrelated canonical GSH transferases (Table 5 and Figure 31A). Results from molecular docking indicated hydrogen bonding could occur between Trp34 and the C-terminal carboxyl oxygen of GSH. Attempts were made to measure the dissociation constant for GSH for the W34A mutant. However protein precipitation at relatively low [GSH] precluded an accurate determination of $K_d^{GSH}$ for this mutant. The W34H mutant, featuring an imidazole NH group, has potential to serve as a hydrogen-bond donor. Compared with the W34A mutant, functional rescue was observed in W34H to near-native levels of GSH binding affinity (Figure 31B).

Figure 30. A. Fluorescence scans of — PA1129•Mn•K and --- + GSH upon excitation at 275 nm. B. Fluorescence scans of PA1129•Mn•K•Pf (■) and PA1129•Mn•K•Pf plus GSH (□).

**A**



**B**



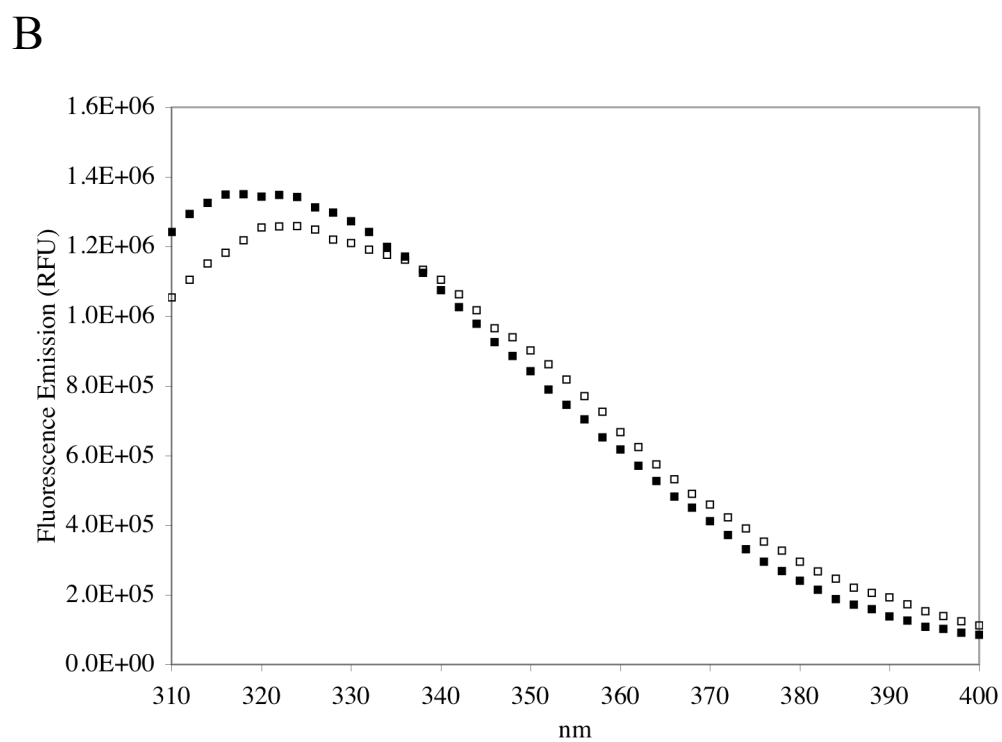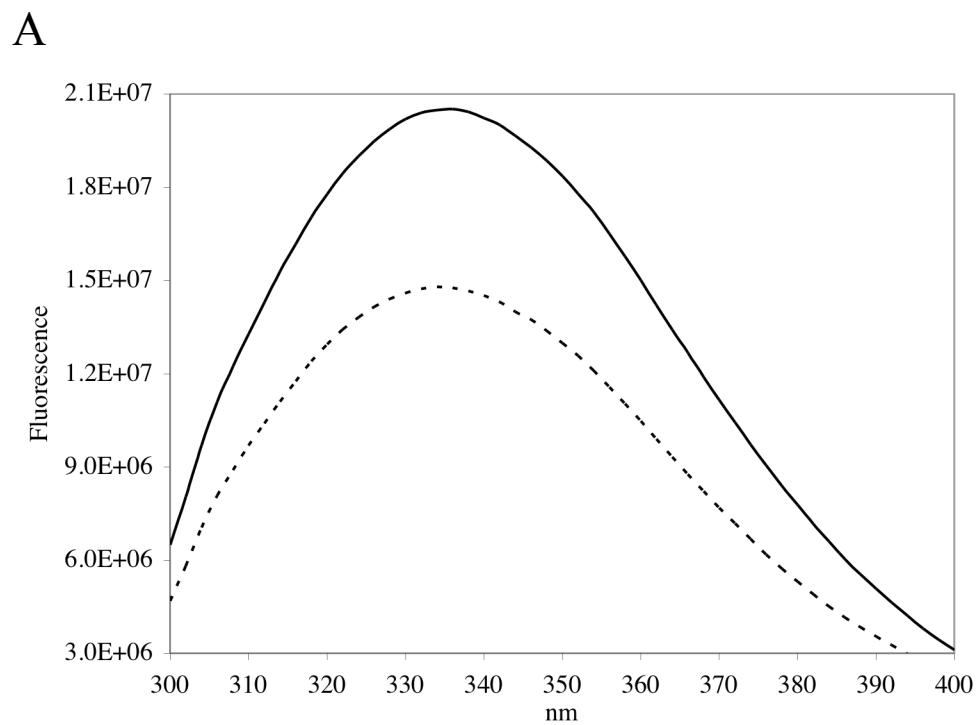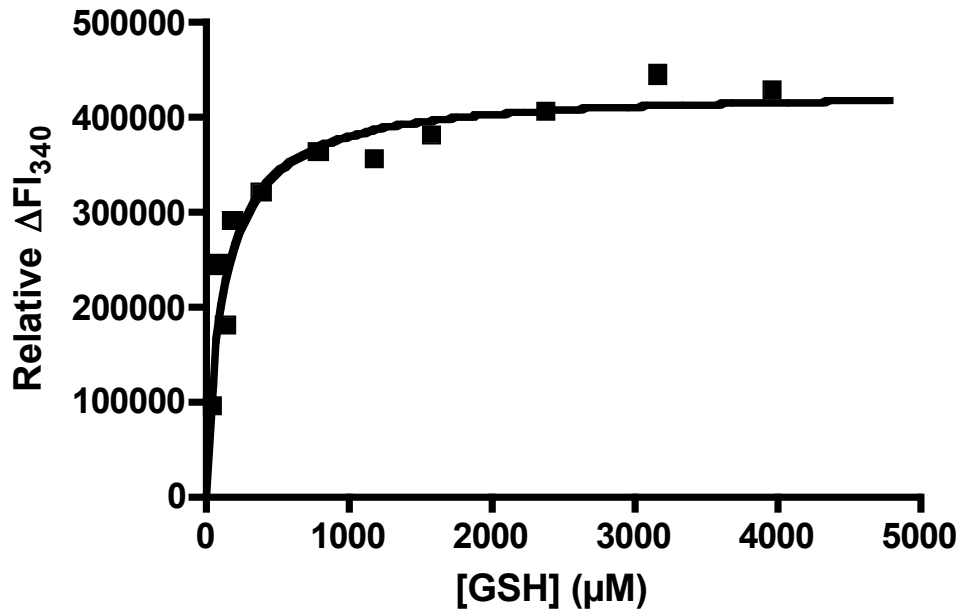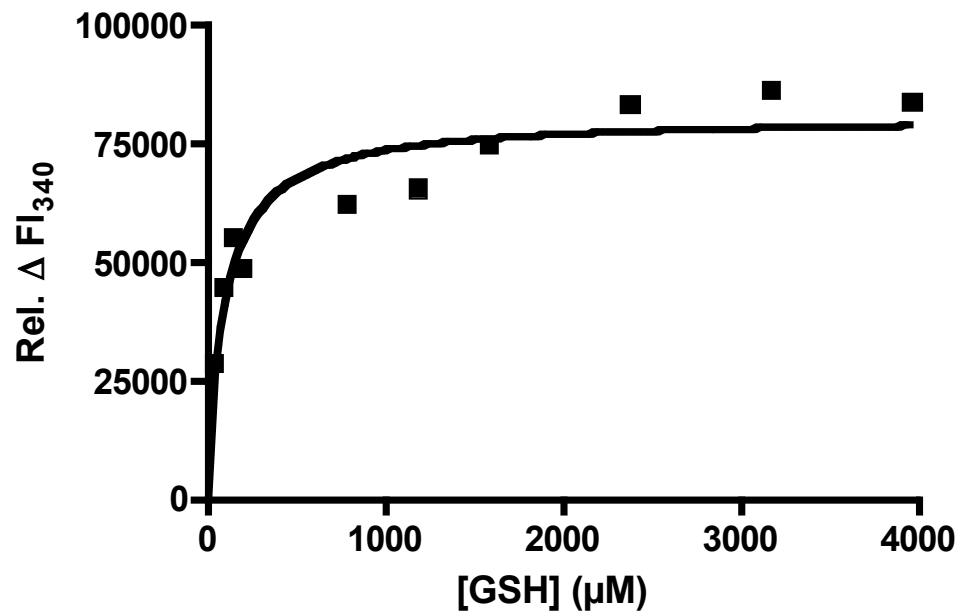Figure 31. Relative change in intrinsic protein fluorescence at 340 nm upon GSH titration of native (A) and W34H (B).

Discussion

*Glutathione transferases*

Many studies have provided information on GSH binding by the soluble or canonical GSH transferases (*36, 45*). Unfortunately, the FosA proteins, although they are efficient GSH transferases, share no sequence similarity with any of these enzymes. A third class of GSH transferases, which are trimeric, membrane-bound enzymes involved in cellular detoxication and other mechanisms, are also unrelated to FosA. As a result, none of the information resulting from years of research on these proteins was particularly useful in determining a mechanism of GSH binding and activation in FosA.

*Potential GSH binding site*

A potential mode of GSH binding was identified by manual docking of GSH into the active site of PA1129 followed by energy minimization of the resulting complex. Docking was initially influenced by only a few pieces of data. Early studies of FosA indicated that GSH was added to C1 of fosfomycin (*47*), indicating the sulfur must be positioned near this atom. Also, conservation of Tyr39 in FosA and FosB enzymes as well as kinetic studies of the Y39F mutant (and Y40F in FosB) indicated this residue might play a primary role in thiol ionization. Based on these points, the GSH sulfur was localized between the ionizing group and fosfomycin C1. Finally, the W34A mutant displayed a 10-fold increase in $K_m^{GSH}$, indicating it could be involved in hydrogen bonding and thus binding affinity of the substrate. Attempts were made to provide a potential for hydrogen bonding with Trp34 in the docked complex. The complex was

considered minimized after only 200 steps (20 steps of steepest descent followed by 180 steps of conjugate gradient descent) as no improvement in potential energy scores was obtained upon further minimization.

*GSH ionization*

FosA proteins contain several active site residues which could serve to facilitate GSH ionization prior to catalysis. Ser50 and Cys48, both likely candidates from early analysis of the active site containing fosfomycin, seemed to play minor roles in catalysis, as alanine mutants had activity comparable to native enzyme. Interestingly, the S50A mutant displayed substrate inhibition with relatively low levels of fosfomycin. This type of inhibition typically results from the binding of a second substrate molecule to E•S, producing an inactive ternary complex (S•E•S). Figure 32 shows the location of a second molecule of fosfomycin bound to PA1129 in the crystal structure. While no direct contacts with Ser50 are visible, it is interesting that the residue is in two conformation. Removal of the serine hydroxyl may allow for binding in solution of a molecule of fosfomycin to the enzyme in a manner similar to that observed in the crystal structure. The reason for this inhibition remains unclear.

Tyr62 and Tyr100, both conserved throughout the fosfomycin resistance protein family, have previously been indicated in phosphonate binding (*48*). In addition to these strictly conserved tyrosines, Tyr39 seemed a possible candidate for participation in thiol ionization due to its location in the FosA active site in our model and its conservation in the FosB cysteine-utilizing proteins. A recent study probing the ability of random FosA mutants to grow on fosfomycin-containing media revealed that Tyr39 was essential for

80
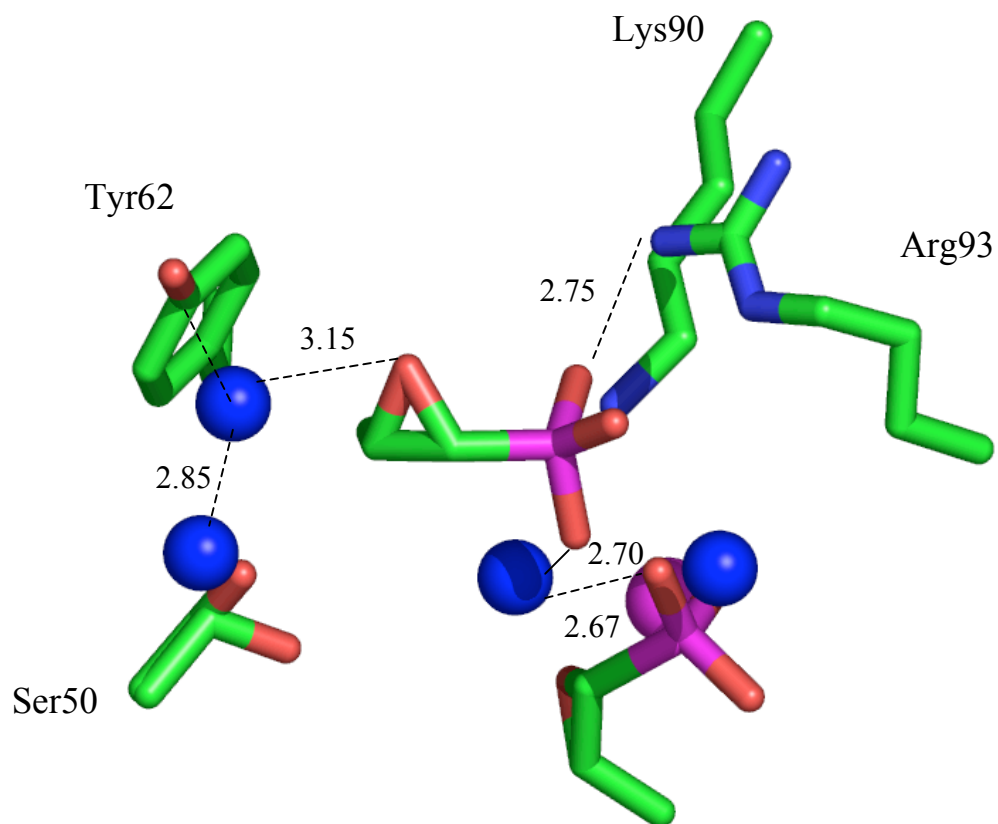
Figure 32. Diagram showing a second molecule of fosfomycin bound at the entrance of the PA1129 active site. Note the two conformations of Ser50. Ordered water molecules and Mn(II) ions are shown as blue and purple spheres, respectively. Distances are shown in Å. Distance from Lys90 and the nearest phosphonate oxygen is 2.82 Å (omitted for clarity). Figure prepared from 1LQP.pdb using the program PyMOL.

resistance, as no mutations were tolerated at this position (*49*).    Available data from canonical GSH transferases indicates that first-sphere hydrogen bonding to the thiol can lower the pK$_a$, thus facilitating catalysis.  Second-sphere interactions provided by protein residues can further lower the pK$_a$ by enhancing the stability of the resulting thiolate (*45*).
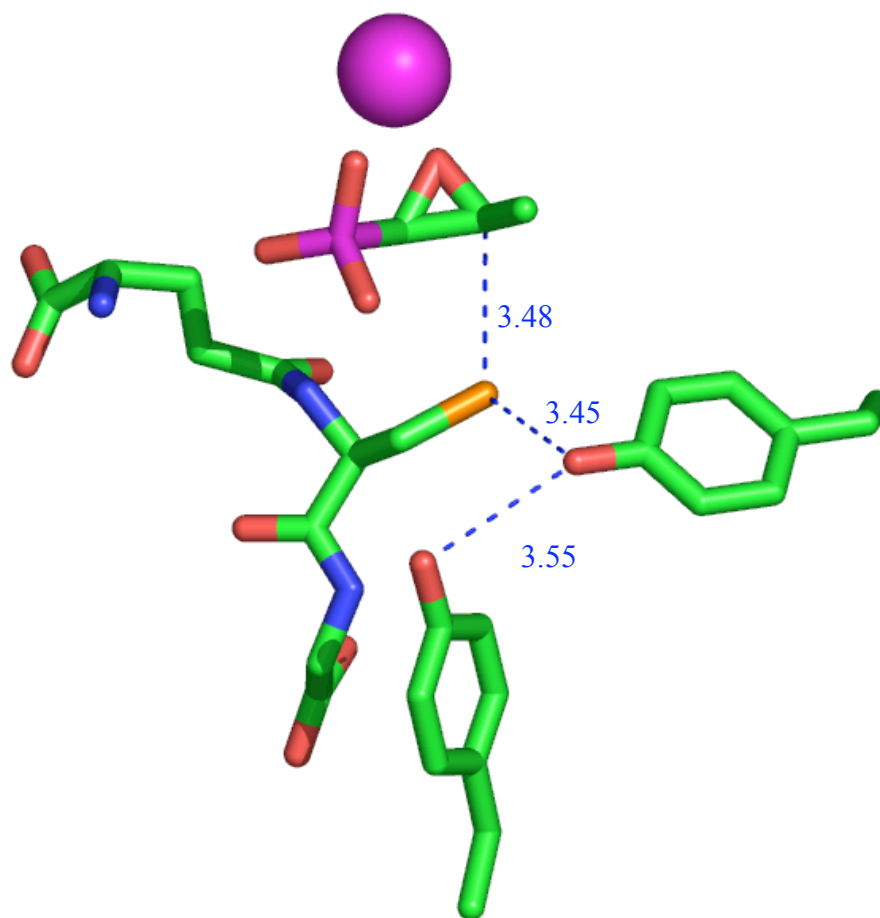


Figure 33.  Hydrogen bonding interactions between (from top to bottom) fosfomycin and GSH sulfhydryl, GSH sulfhydryl and Tyr39, and Tyr39 to Tyr128.  Distances between heavy atoms are shown in Å.

Such a second-sphere hydrogen bond between Tyr39 and Tyr128, which is conserved in the FosA proteins, is consistent with a role of Tyr39 in ionization (Figure 33). Indeed, a 10-fold reduction in activity was observed for the Y39F mutant. While this reduction is not as great as seen in equivalent mutants of canonical GSH transferases, activation of substrate in fosfomycin resistance proteins by the metal center increases its electrophilicity and could decrease the effect of thiolate anion formation on catalysis.

*GSH binding*

In our model for substrate binding, residues forming intermolecular hydrogen bonds to the docked GSH include Arg93, Lys90, Ser50, Tyr39, Gln36, and Trp34 (Figure 27). None of these residues are conserved in the other classes of resistance proteins with the exception of Tyr39 in the FosB proteins. Only one residue, Gln36, is modestly conserved in FosX as a lysine, which is capable of supplying the $NH_2$ functionality. This could explain why FosX mutants capable of catalyzing the FosA reaction do so only at high [GSH] (Fillgrove and Armstrong, unpublished data). Of the GSH interacting residues, Lys90 is particularly interesting as it ion-pairs with a terminal carboxyl of GSH. This seems essential for GSH binding, as canonical glutathione transferases consistently retain a positive residue for this purpose.

Although FosA proteins apparently arose from a convergent evolutionary pathway with respect to the canonical GSH transferases, many similarities in GSH binding are apparent. Initial comparison with crystal structures of alpha, pi, mu, and sigma GSH transferases reveals a comparable extended conformation of GSH (Figure 34). A primary determinant of GSH recognition and binding conserved in the canonical

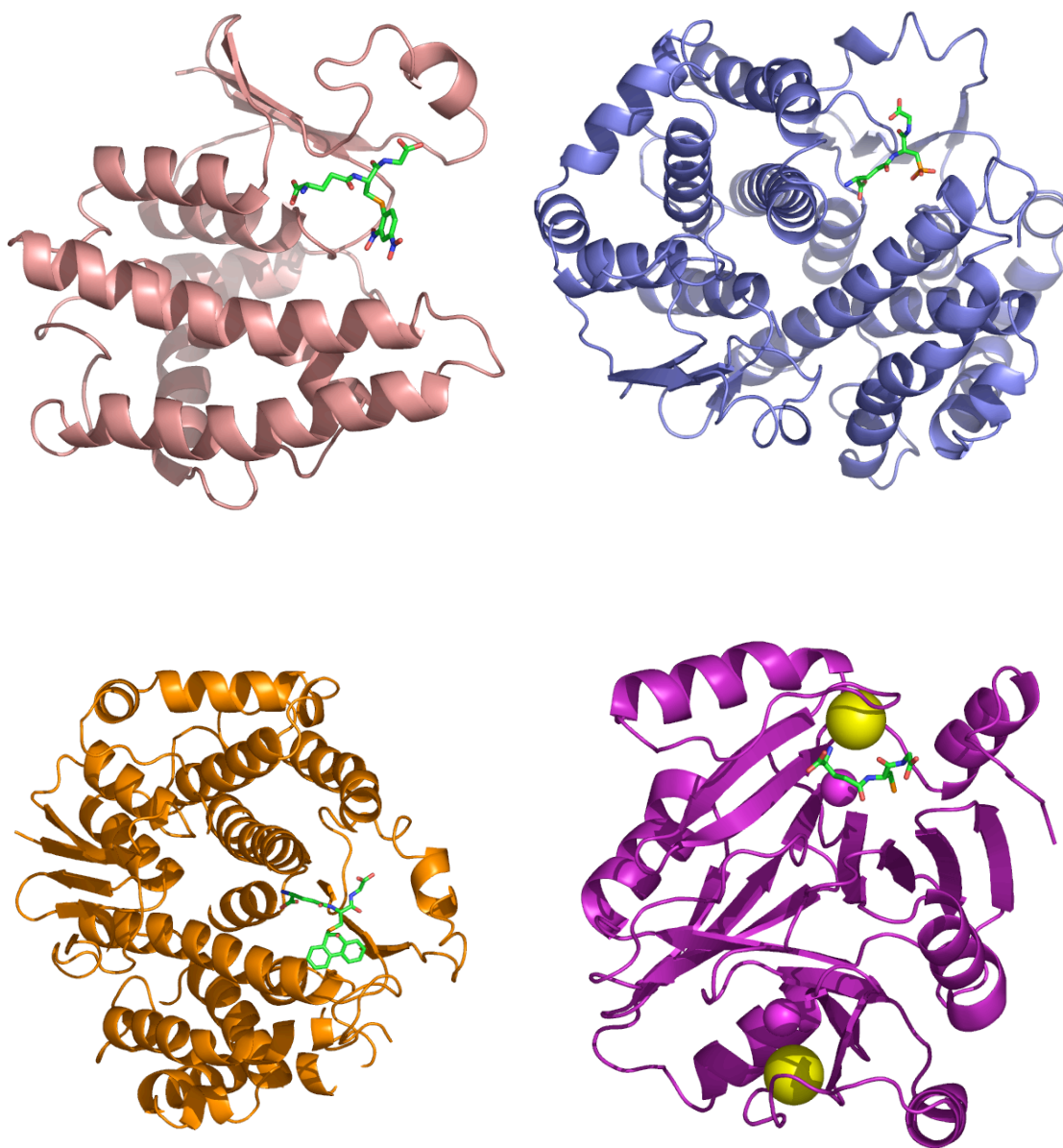Figure 34.   Ribbon diagrams of 1GSQ (salmon), 2GSR (blue), 2GST (orange), and PA1129 (purple) containing bound 1-(*S*-glutathionyl)-2,4-dinitrobenzene, glutathione sulfonate, (9*S*, 10*S*)-9-(*S*-glutathionyl)-10-hydroxy-9-10-dihydrophenanthrene, and glutathione, respectively, in stick representation.  In PA1129, $K^+$ and Mn(II) are shown as yellow and purple spheres, respectively.  Figures generated using PyMOL (*10*).
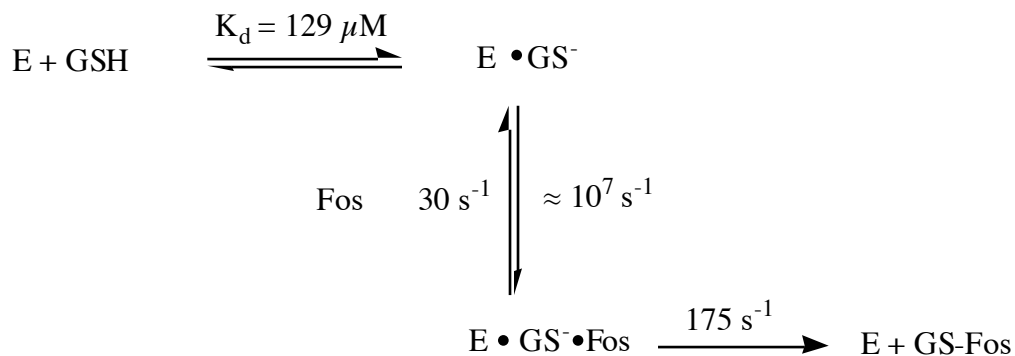
enzymes involves coordination of both GSH carboxylate functionalities by enzyme residues, typically Trp and Lys (*36*).  This appears in FosA as well, since, in addition to Gln and Arg residues, a Trp and Lys are used to supply hydrogen bonds to the substrate (Figure 27).  One significant difference from the canonical enzymes involves the number of contacts between enzyme and substrate.  These proteins typically have a dozen or so interactions, while in our model only half that many were identified. This could partially account for the approximately 5-fold decrease in GSH affinity exhibited by PA1129 as compared to a GSH transferase from the mu class (Table 5).

Attempts were made to study the effects of removing the hydrogen bond supplied by Trp34 to GSH by mutation to Ala.  While a value for the GSH equilibrium dissociation constant could not be determined for this mutant, circular dichroism spectroscopy (Chapter III) indicates that the protein is folded in a manner similar to native enzyme.  The W34H mutant exhibited GSH affinity similar to native protein, and there was a recovery in $K_m^{GSH}$.  In addition to our results, recent functional resistance assays of random mutant enzymes showed a requirement for Trp34 and for a positively charged residue at position 90 (*49*), indicating these residues may be critical for GSH binding to occur.

Addition of GSH to PA1129 produced a characteristic change in intrinsic protein fluorescence (Figure 30A).  However, when protein was pre-incubated with phosphonoformate, a transition-state analogue, the fluorescence change upon GSH binding was lost (Figure 30B).  This indicates that phosphonate binding could poise the enzyme for GSH binding and catalysis.  As bacteria must respond quickly to attack by antibiotics, using fosfomycin binding to prime the enzyme for GSH, which is always

present in the cell, could lead to more efficient catalysis and therefore a better chance of survival.

Titration of PA1129 with GSH revealed that the enzyme has a $K_d^{GSH} << K_M^{GSH}$. This could indicate that the E•GS⁻ complex may not reach equilibrium due to turnover being faster than substrate binding (Scheme 2). Attempts were made to measure rates of GSH binding via changes in intrinsic protein fluorescence as observed in steady state experiments. However, changes were too rapid to obtain values for $k_{obs}$, supporting a very rapid establishment of GSH binding equilibrium. An alternate experiment to measure binding was attempted by monitoring changes in absorbance at 239 nm, as this is a signature of thiolate formation (*50*). Unfortunately, no changes could be observed in direct binding assays or in competition experiments of E•Mn(II)•K⁺•GSH plus GSO₃⁻. Fosfomycin binds to FosA at near the diffusion limit, (*48*) and subsequent turnover is very rapid. Since the off-rate for fosfomycin is much slower than turnover, GSH binding cannot reach equilibrium (Scheme 2). This lack of equilibrium produces the observed discrepancy between $K_d$ and $K_m$.

$$E + GSH \xrightleftharpoons{K_d = 129\ \mu M} E\ \bullet GS^-$$

$$Fos \quad 30\ s^{-1} \Updownarrow \approx 10^7\ s^{-1}$$

$$E \bullet GS^- \bullet Fos \xrightarrow{175\ s^{-1}} E + GS\text{-}Fos$$

Scheme 2. Proposed steps in the mechanism of PA1129.

CHAPTER VI


ROLE OF THE K$^+$-BINDING LOOP AND SELECTED ACTIVE
SITE RESIDUES IN THE EVOLUTION OF THE FOSFOMYCIN RESISTANCE
PROTEINS


Results


*Conserved threonine provides important hydroxyl moiety*

FosA Thr9 is interesting in that it is conserved in FosA and X proteins but not in

the FosB family.  X-ray crystal structures of FosA revealed that Thr9 is within hydrogen

bonding distance of the oxirane oxygen of fosfomycin (Figure 35) (*28*).  T9V and T9S

mutants were prepared to analyze the role of the hydroxyl functionality in substrate

binding and catalysis.  Results show that the valine mutant, which lacks the hydroxyl, has

only slightly impaired substrate affinity (Figure 37 and Table 6) but an almost 100-fold

decrease in catalytic efficiency.  Both are restored in the serine mutant (Figure 37 and

Table 7).


*K$^+$-binding loop*

Early studies of the plasmid-encoded FosA revealed that it was activated by

monovalent cations (*27*), but the role of K$^+$ in this activation has remained poorly

understood.  To more fully elucidate how activation occurs, analyses of substrate binding

and catalysis of native protein in the absence of small monovalent ions and a mutant

protein containing a disrupted, non-functional binding loop were carried out (Tables 6
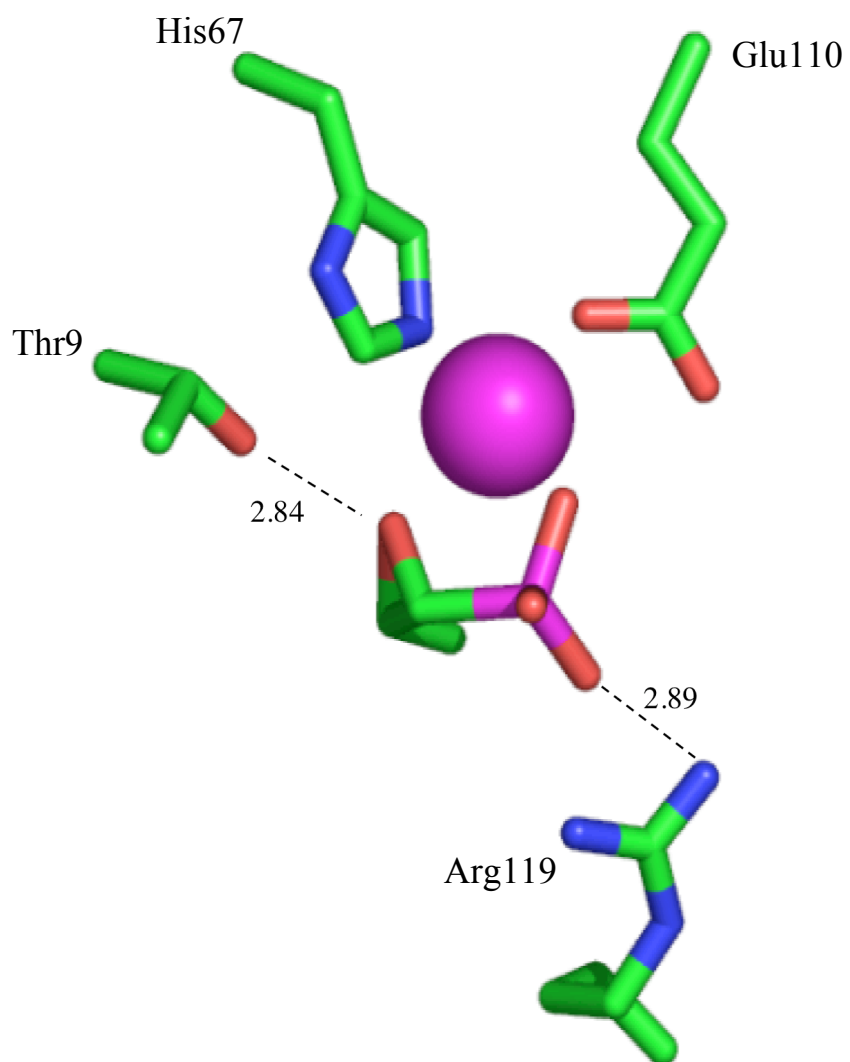
Figure 35. Active site of PA1129 showing bound Mn(II) [purple sphere] and fosfomycin. Side-chains of His7, Glu110, Arg119, and Thr9 are shown in stick representation. Distances are shown in Å. Figure generated from 1LQP.pdb using PyMOL (*10*).

and 7; Figure 39). Results show that fosfomycin binding in the mutant and for native enzyme in the absence of $K^+$ is identical to native in the presence of $K^+$. Turnover supported by the non-functional binding loop mutant is similar to that of native enzyme in the absence of $K^+$; this is 100-fold lower than native enzyme with bound $K^+$.

*Reciprocal FosA and X mutants*

Although several active site residues overlay in superpositions of FosA and FosX crystal structures, several important differences in the active sites are readily apparent (Figure 41). For example, Tyr39, conserved in FosA proteins, is a Phe in FosX. FosX Met57 projects a bulky sulfur into the active site, which is a much smaller serine in FosA. FosX Glu44, the proposed active-site base which activates water for hydrolysis of fosfomycin, is a glycine (Gly37) in FosA. Reciprocal mutants of these residues were prepared in PA1129 and mlr3345 to study the effects on catalytic ability as well as reaction selectivity (thiol transferase vs. hydrolase). Trp34 appeared to block a G37E mutation, so this residue was converted to Ala to create the W34A/G37E double mutant. Several multiple mutants were also prepared to study the collective effects of the mutated residues. These include W34A/G37E/S50M and W34A/G37E/Y39F/S50M. Reciprocal mlr3345 FosX mutants include E44G and E44G/F46Y/M57S. A mutant designed to incorporate tryptophan at a structurally-equivalent location as compared to FosA was prepared, but the mutant appeared to be misfolded (Fillgrove and Armstrong, unpublished data). Results of kinetic analyses are recorded in Table 7.

**A**
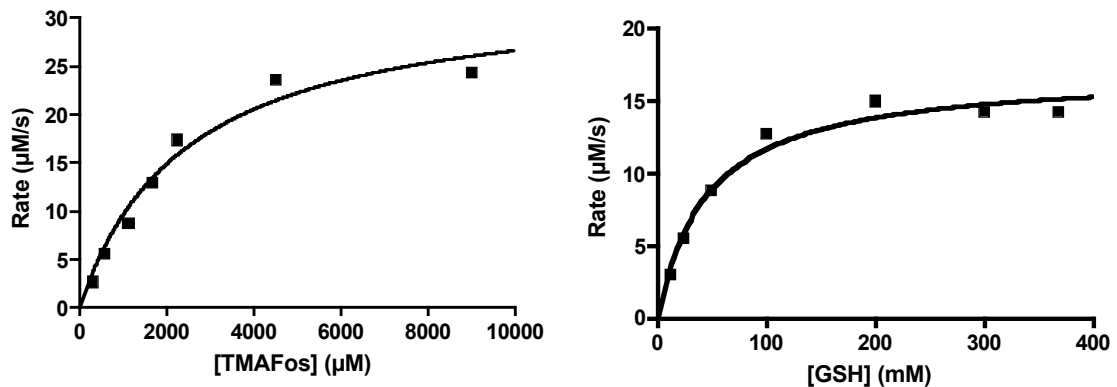


**B**
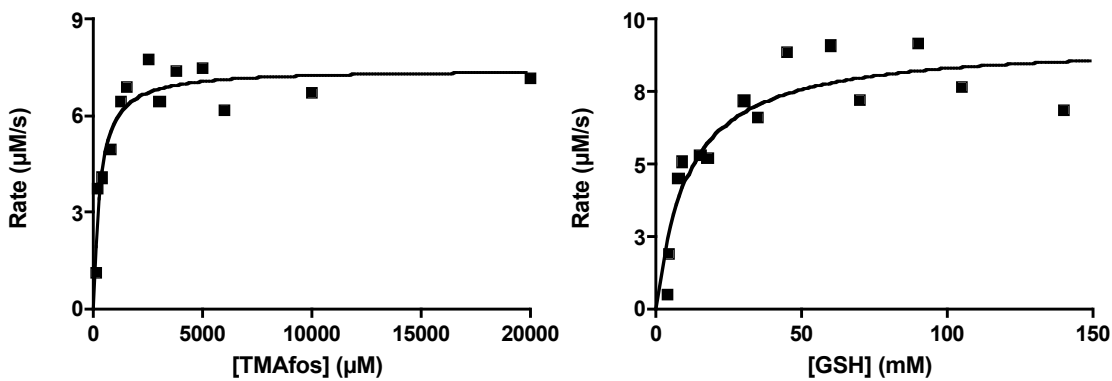


Figure 36.  Plots of kinetic data for T9V (A), T9S (B).
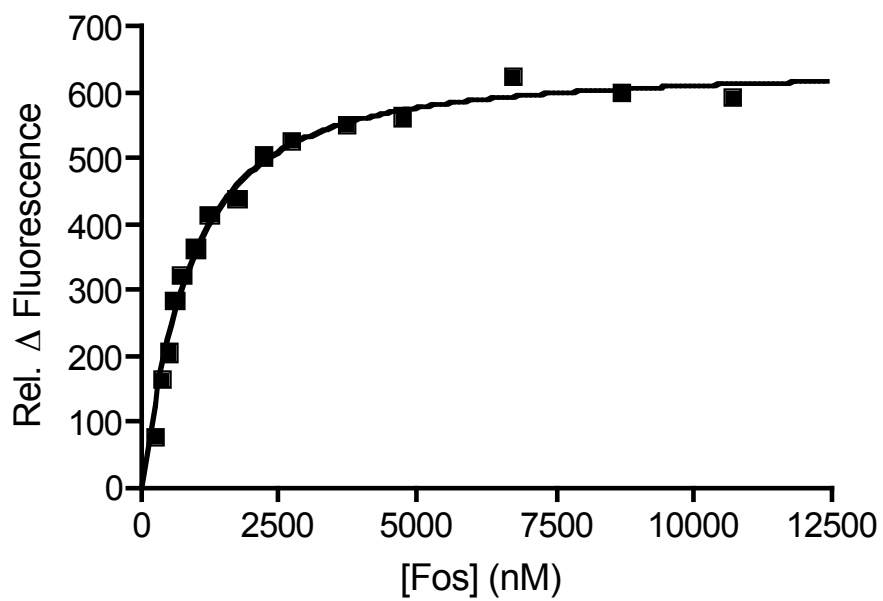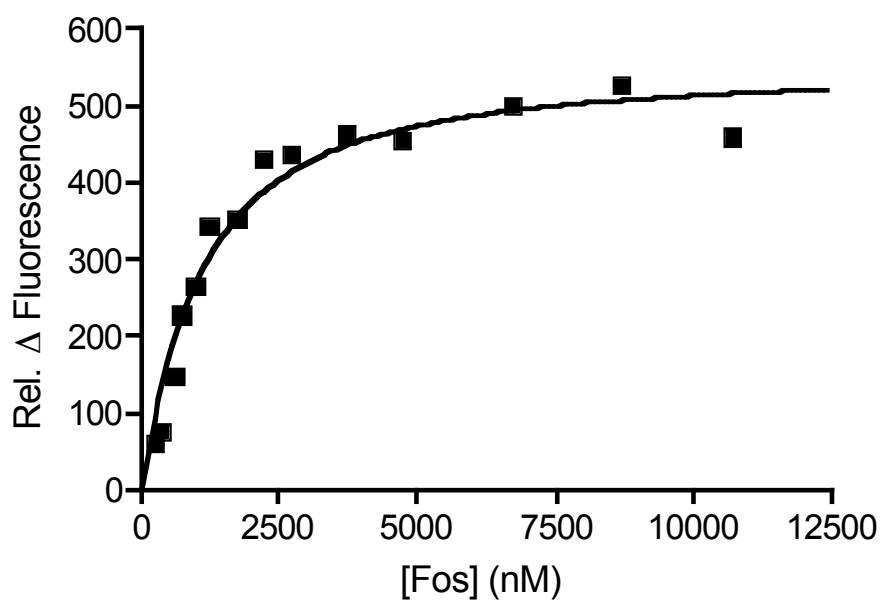
Figure 37. Plots of change in fluorescence upon titration of T9V (top) and T9S (bottom) with fosfomycin.
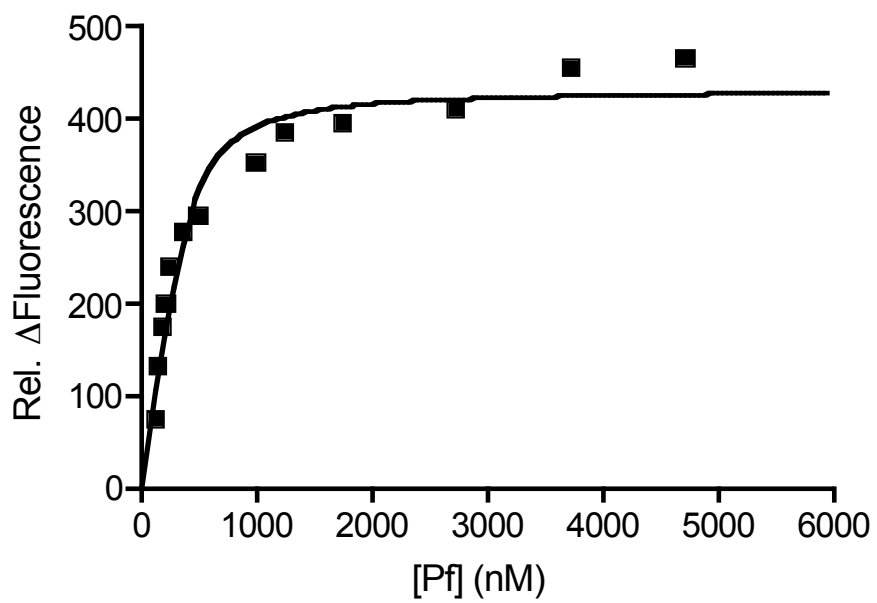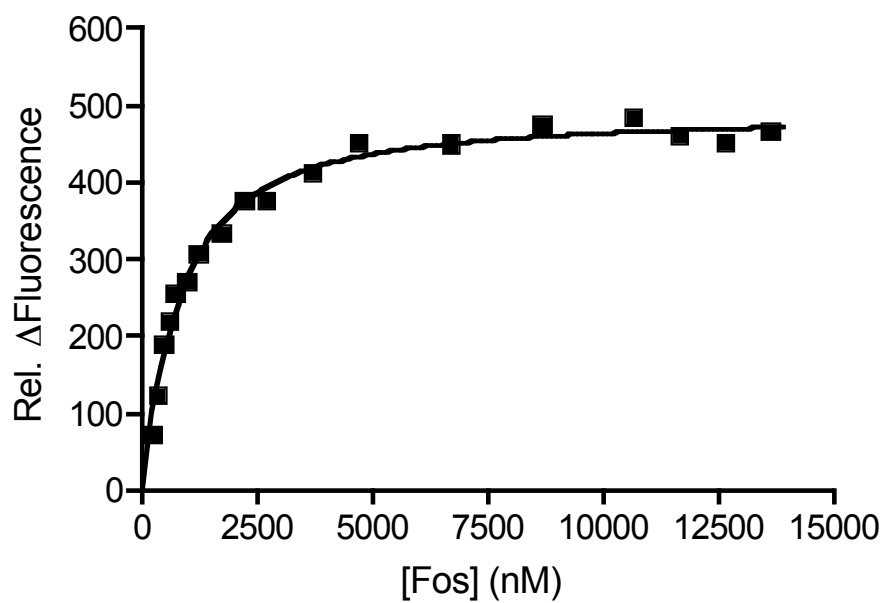
Figure 38. Plots of the change in fluorescence upon titration of PA1129 with fosfomycin (top) and phosphonoformate (bottom) in the absence of $K^+$.
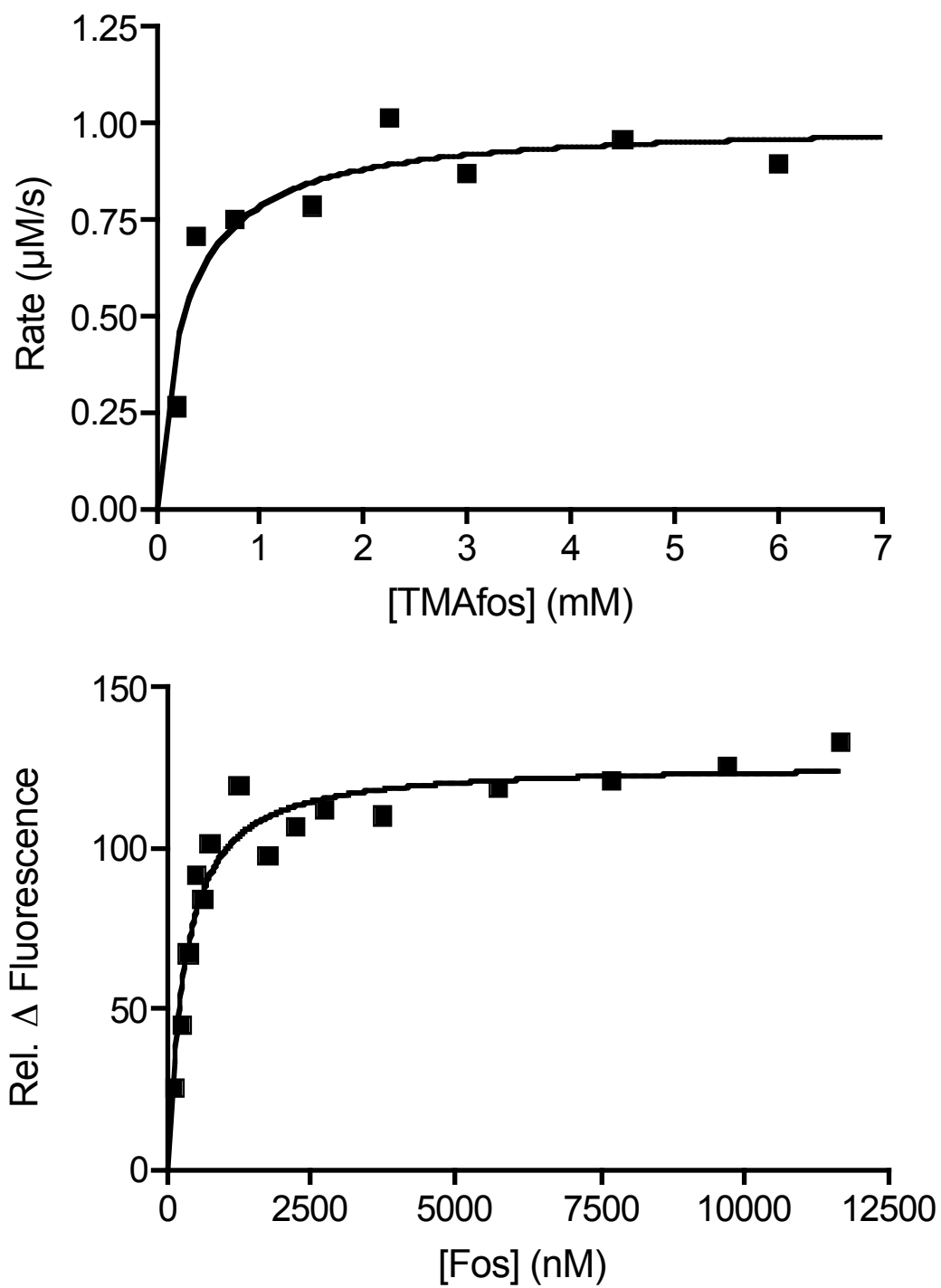
Figure 39.  K$^+$-loop mutant fosfomycin kinetic results (top) and relative change in protein fluorescence upon fosfomycin binding (bottom).

Figure 40. Relative change in intrinsic protein fluorescence upon titration of
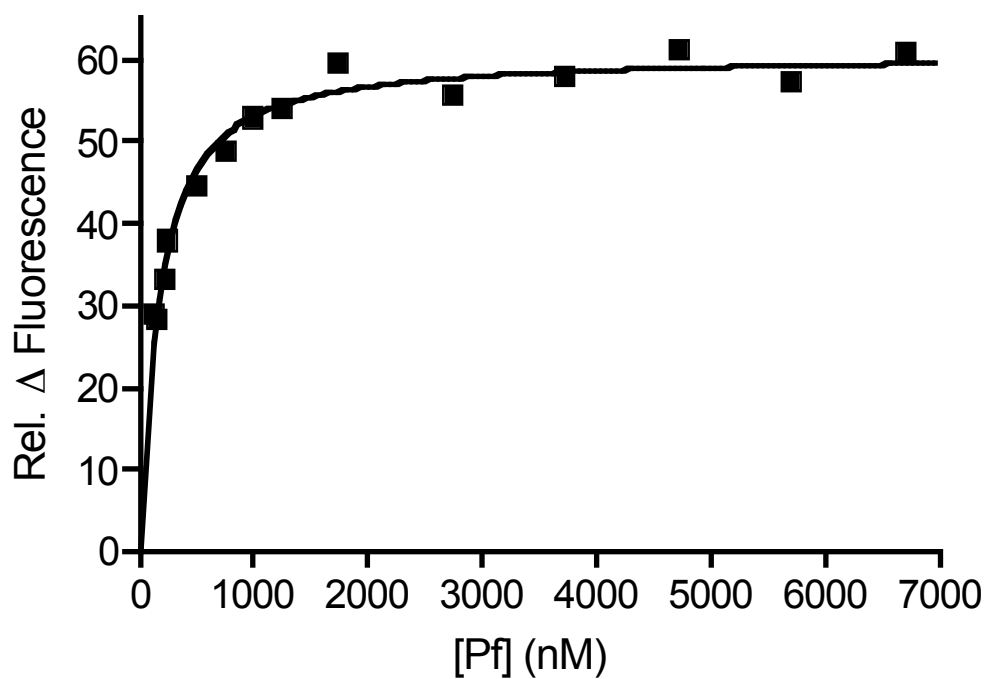


E•Mn(II)•K$^+$•GSH with phosphonoformate.

**Table 6.** Comparison of equilibrium binding constants for fosfomycin and phosphonoformate for PA1129 and mutants.

|  | $K_d^{Fos}$ (nM) | $K_d^{Pf}$ (nM) |
|---|---|---|
| Native | 730 ± 8 | |
| T9V | 790 ± 140 | |
| T9S | 510 ± 50 | |
| K$^+$-loop mutant | 250 ± 44 | |
| Native, no K$^+$ | 580 ± 40 | 65 ± 21 |
| Native, no K, + GSH | | 140 ± 10 |
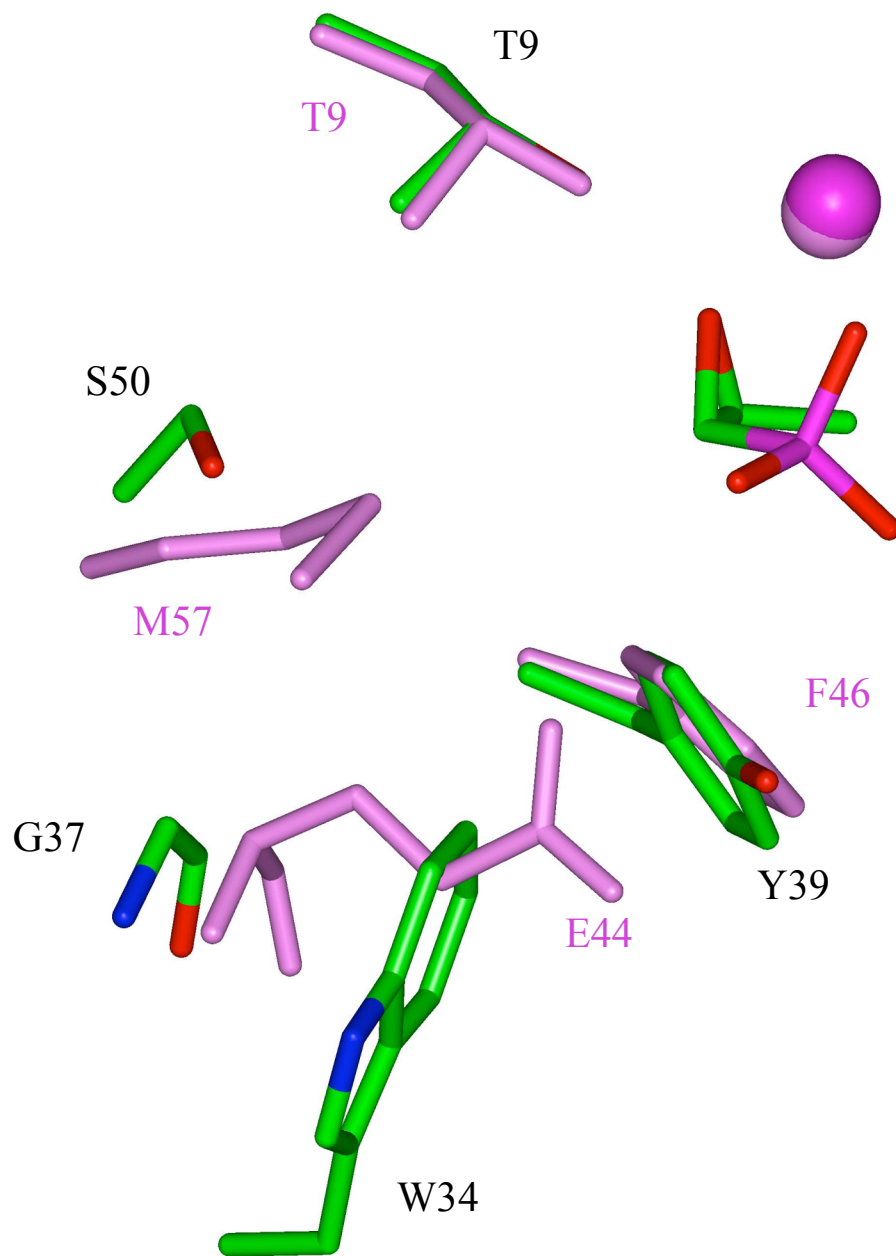
Figure 41. Overlay of active site residues from PA1129 (colored by atom) with *M. loti* FosX (pink). Mn(II) is shown as a purple (or pink) sphere. Numbers in pink correspond to FosX; those in black to FosA.

**A**



**B**                                              **C**
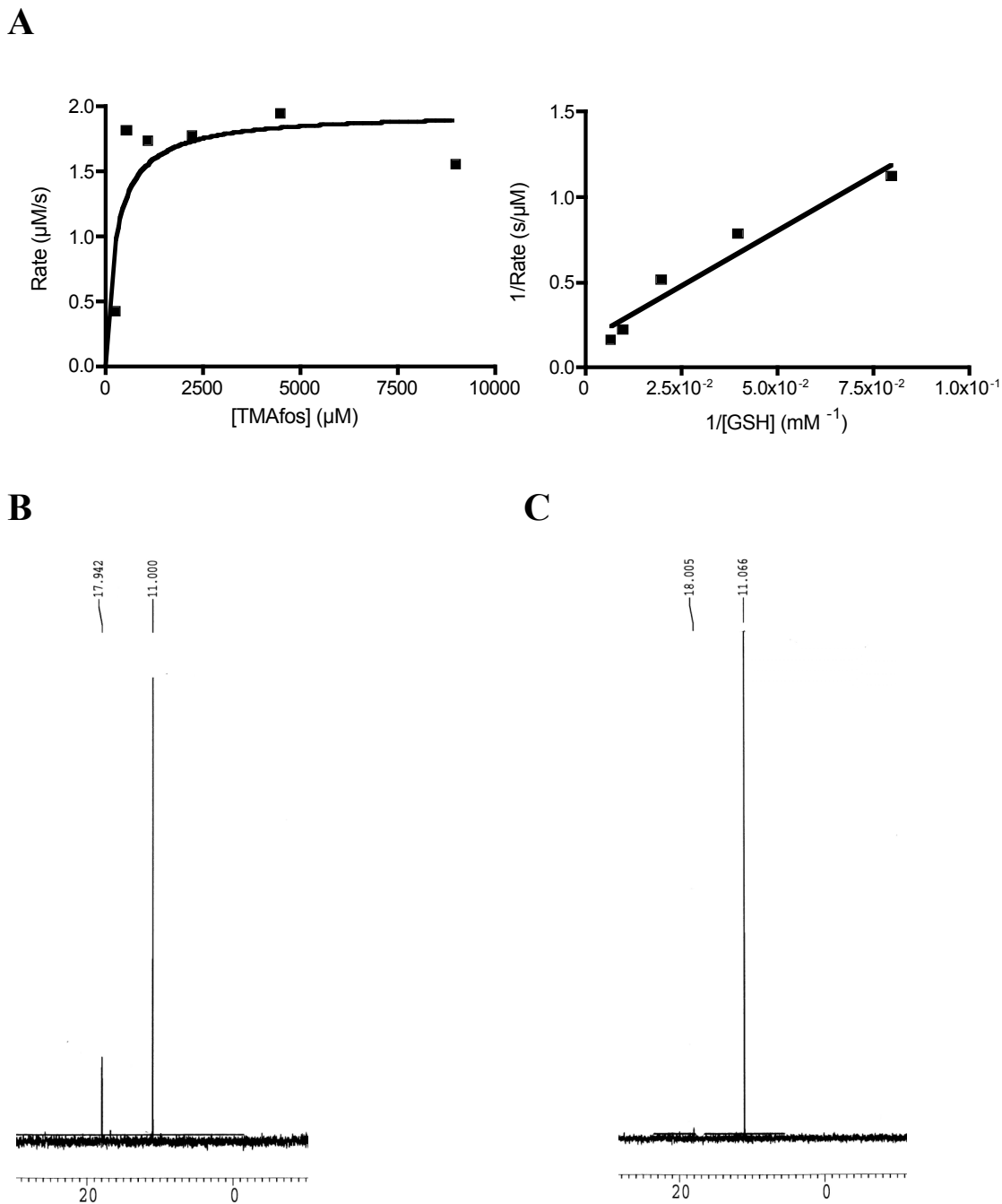


Figure 42.   A.   Plots of fosfomycin (left) and GSH (right) kinetic   data for the W34AG37E mutant.  B and C.  $^{31}$P NMR spectra of reaction mixtures showing catalysis by W34A/G37E/S50M and W34A/G37E/Y39E/S50M, respectively.            Fosfomycin resonance is seen at 11.1 ppm; GS-Fos is at 18.0.

**Table 7.** Turnover numbers for native and mutant enzymes for both FosA and X activities.

| | $k_{cat}^{FosA}$ (s$^{-1}$) | $k_{cat}^{FosX}$ (s$^{-1}$) | $K_m^{Fos}$ (µM) | $K_m^{GSH}$ (mM) |
|---|---|---|---|---|
| PA1129 | 180 ± 6 | ND* | 190 ± 30 | 5.0 ± 0.7 |
| G37E | 0.3 ± 0.04 | ND | | |
| W34A | 32 ± 3 | ND | 1500 ± 340 | 160 ± 30 |
| W34A/G37E | 2.0 ± 0.3 | ND | 280 ± 230 | 83 ± 12 |
| S50A | 134 ± 2 | ND | 76 ± 42 | 2.2 ± 0.1 |
| W34A/G37E/S50M | 0.46 | ND | | |
| W34A/G37E/Y39F/S50M | 0.0004 | ND | | |
| mlr3345 | 0.006 | 0.15± 0.02 | | |
| E44G | 0.0001 | 0.0002 | | |
| E44G/F46Y/M57S | 1.4 | ND | | |

*No detectable activity

*MIC determination for mutant proteins*

The minimum inhibitory concentration for fosfomycin for each mutant protein expressed in *E. coli* was determined by growing transformed bacteria on varying concentrations of fosfomycin. Plates are shown in Figure 44; data are listed in Table 9.

*Promiscuity*

Early studies of FosB proteins followed by discovery of the mlr3345 FosX protein revealed that, unlike the FosA proteins, which showed a high preference for GSH, these proteins were less selective in their choice of nucleophile (Tables 7 and 8) (*22*). The role

of $K^+$ in FosA in determining reaction selectivity was analyzed by comparing turnover numbers for catalysis using cysteine or GSH in the presence and absence of $K^+$ (Figure 43).  Results are shown in Table 8.

A
18.442
11.059

B
17.854
10.471

20    0        20    0
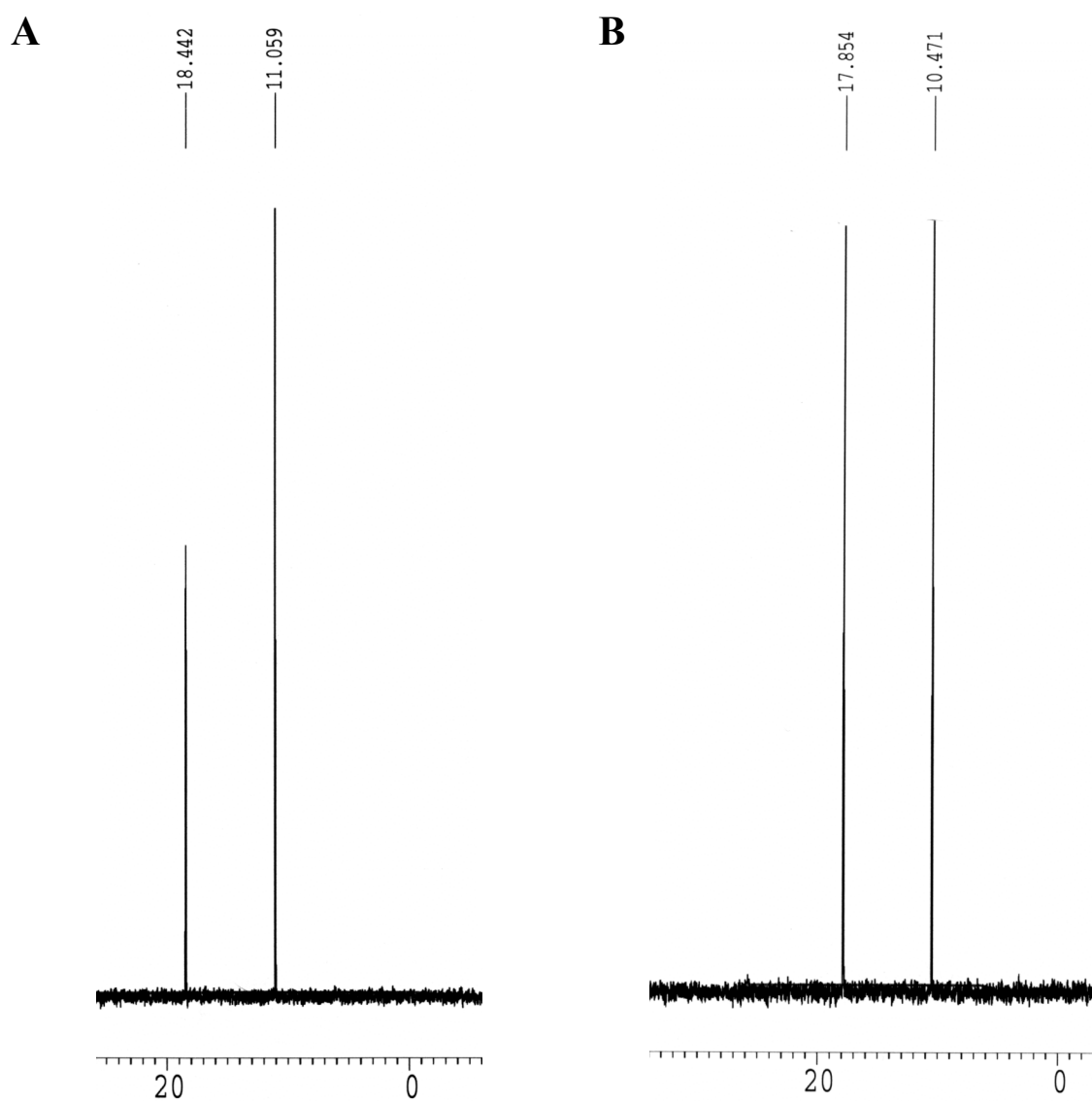
Figure 43.  $^{31}$P NMR spectra of the reaction of PA1129 with L-cysteine and fosfomycin in the presence (A) and absence (B) of $K^+$.

**Table 8.** Comparison of turnover numbers for catalysis by FosA and B with different thiols.

| | L-Cysteine | GSH | CoA |
|---|---|---|---|
| FosB$^{Sa}$ $k_{cat}$ (s$^{-1}$) | 5.0 | 0.06 | 0.02 |
| PA1129 $k_{cat}$ (s$^{-1}$) [+K$^+$] | 6.9 | 180 | -- |
| PA1129 $k_{cat}$ (s$^{-1}$) [-K$^+$] | 0.1 | 1.0 | -- |

**Table 9.** MIC values for fosfomycin for various PA1129 mutants.

| Protein | MIC (mg/mL) |
|---|---|
| W34A | > 20 |
| W34H | > 20 |
| G37E | ≈ 2.5 |
| W34A/G37E | ≈ 10 |
| W34A/G37E/S50M | < 1.25 |
| W34A/G37E/Y39F/S50M | < 1.25 |
| K$^+$-loop mutant | > 20 |
| W34A/G37E/Y39F/S50M in K$^+$-loop mutant background | 5 < MIC < 10 |
| T9S | > 20 |
| T9V | > 20 |
| Y39F | > 20 |
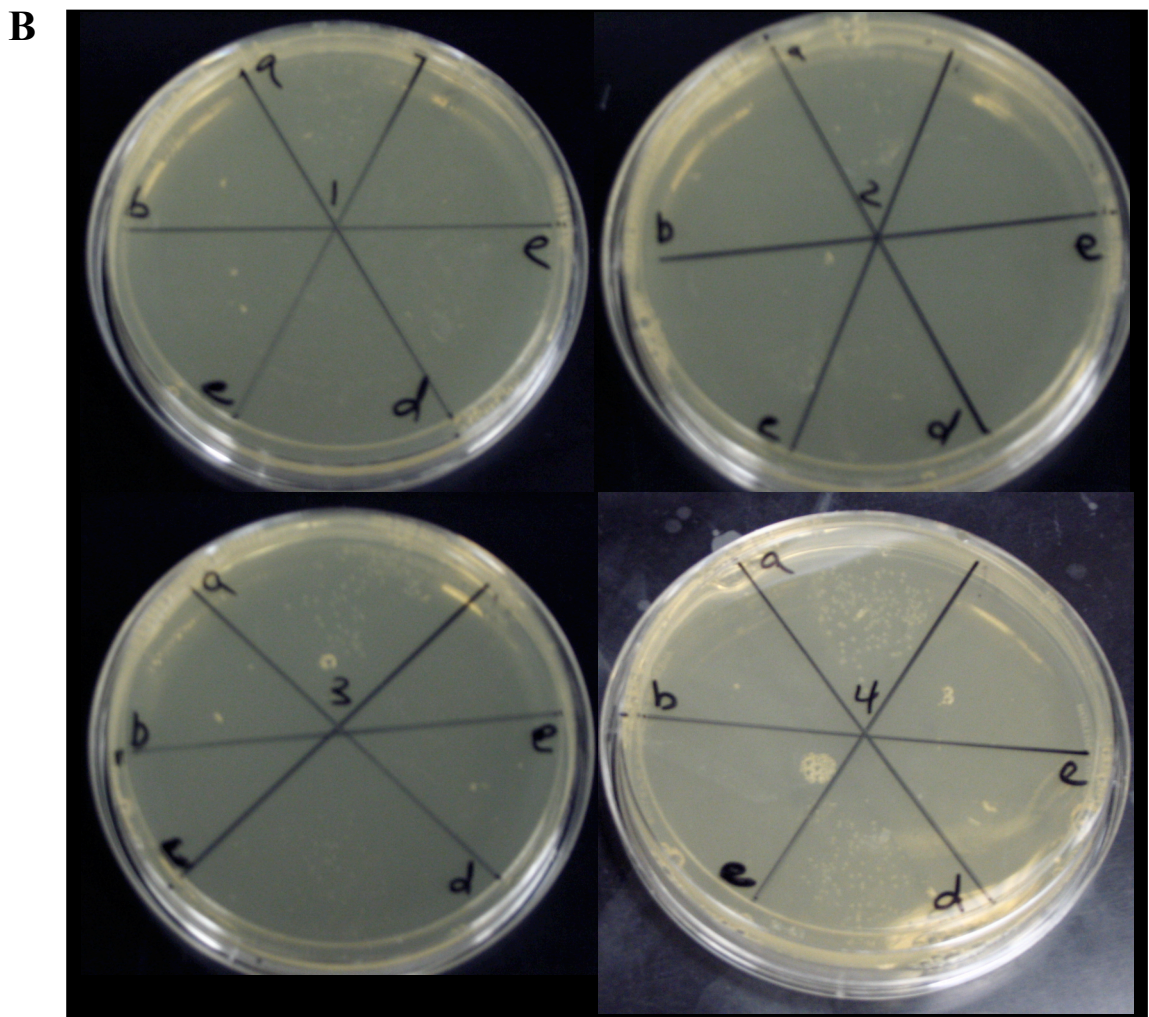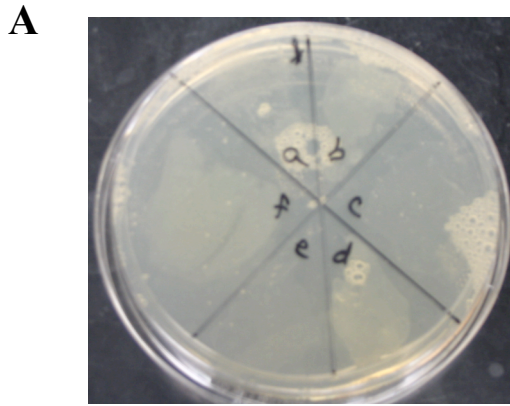
Figure 44. LB-agar plates showing growth of PA1129 mutants. A. Clockwise from *a* are *E. coli* transformed with expression plasmids for T9S, T9V, K$^+$-loop mutant, W34A, Y39F, and W34H expression plasmids. B. Counter-clockwise from *a*, *E. coli* transformed with W34A/G37E, W34A/G37E/S50M, W34A/G37E/Y39F/S50M, W34A/G37E/Y39F/S50M in the K$^+$-mutant background, and G37E expression plasmids.

*Conserved threonine provides important hydroxyl moiety*

It has been hypothesized that FosA Thr9 hydroxyl aids in protonation of fosfomycin during ring-opening. Interestingly, this residue is not conserved in the FosB proteins, which could partly explain their poor catalytic abilities. A recent study of FosA mutants functional in an *in vitro* resistance assay revealed strong preference for a hydroxyl moiety, either from Thr or Ser, at position 9 (*49*). Our own mutagenesis supports the importance of a hydroxyl moiety at this position, as the T9S mutant restores native activity lost by the T9V enzyme (Table 7). It would be interesting to investigate activity of a FosB mutant containing threonine at position 9. If this residue is indeed important in increasing catalytic efficiency, it could indicate that the FosB proteins have developed an alternate, albeit less-effective, means of supplying a proton to fosfomycin during catalysis. Consequently, adding a threonine could improve efficiency of these proteins. Why this seemingly important residue would not be retained during evolution is not understood.

*Phosphonate binding in the presence of thiol*

Although phosphonate binding to FosA had been studied in the presence and absence of $K^+$, it was not known if the presence of GSH affected phosphonate binding. Titration of PA1129•Mn(II)•$K^+$•GSH with Pf revealed that presence of GSH had no effect on changes in protein fluorescence or the equilibrium dissociation of phosphonate (Figure 40).

*K+-binding loop*

A unique property of FosA proteins is the truncation of one strand of the conserved βαββ structural motif, resulting in the formation of a potassium binding loop (*28*). Sequence alignments reveal the conservation of Ser94, the only residue to contact potassium through its side-chain, in FosA and FosX proteins (Figure 45). In fact, alignments show that the binding loop could have arisen from a simple three-residue deletion in the evolution of FosA proteins. A putatively non-functional binding loop mutant was prepared by inserting RVE residues into the FosA loop sequence. While structural information is not available to conclusively show that the mutant fails to bind K+, preliminary assays indicate that the mutant shows little, if any, activation by K+ (Brown and Armstrong, unpublished data). Alternatively, assays were carried out using native protein in the absence of small monovalent ions. Analyses of kinetic and fosfomycin binding assays revealed that while substrate affinity was unaffected, a severe loss in turnover occurred. This is indicative of the occurrence of non-productive substrate binding. Crystal structures have revealed that fosfomycin is oriented in the FosA active site with the negative phosphonate toward the K+. Structures of the protein in the presence of phosphate, phosphonoformate, and sulfate all support the presence of a favorable oxyanion binding site in this location (*28, 48*). However, in the absence of K+, or with a mutant incapable of binding K+, substrate binding could occur in alternate manners. In fact, analysis of FosX structures show product, sulfate, or citrate binding in the opposite manner as fosfomycin in the FosA structure (Fillgrove and Armstrong, unpublished data and Figure 45). Key interactions—coordination to the metal center and hydrogen bonding between Thr9 and Arg119 and substrate—occur in both structures.

**A**
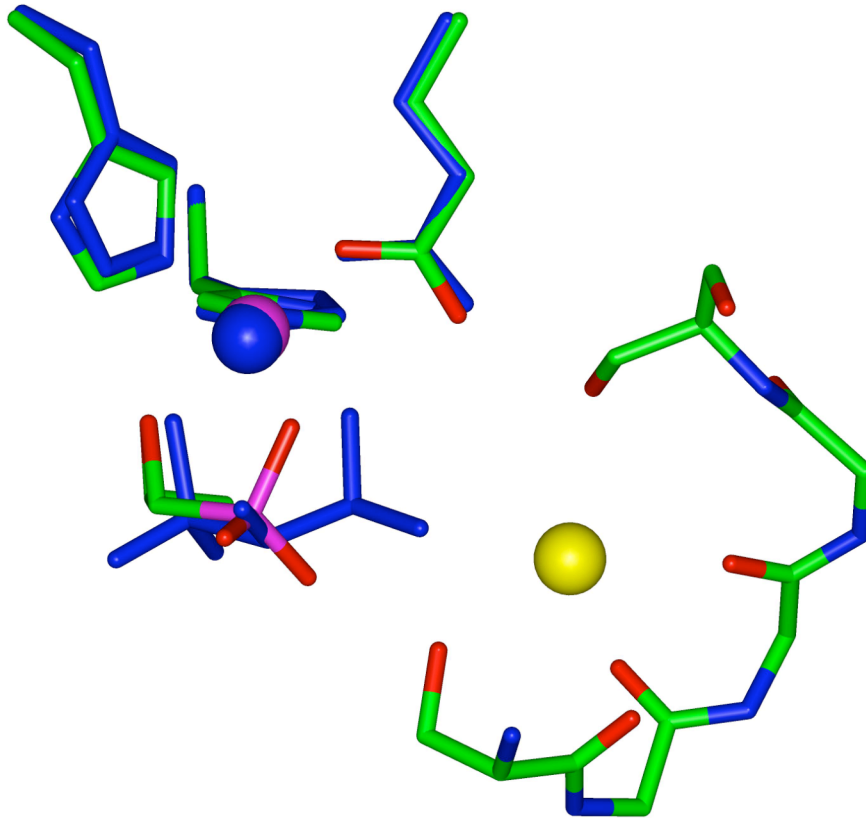


**B**

| | |
|---|---|
| PA1129 | [87]R E W K Q N R - - - S E G D S F Y F L [102] |
| FosA (Tn2921) | [89]T I W K Q N K - - - S E G A S F YF L[104] |
| *M. loti* FosX | [92]D M R P P R P R V E G E G R S I Y F Y[110] |
| *L. monocytogenes* FosX | [92]E I K P E R P R V Q G E G R S I Y F Y[110] |

Figure 45. A. Overlay of FosA and FosX (blue) active sites showing bound substrate (FosA) and product (FosX). Mn^{++} ions are shown in purple, and K^{+} ion is yellow. Note the difference in orientation of the phosphonates. B. Local sequence alignment showing residues involved in coordination of the K^{+} ion in FosA in red.

An obvious difference is the presence of $K^+$ in FosA. Developing the ability to coordinate a positive ion and thus eliminate non-productive binding events would certainly have allowed FosA proteins to proceed toward catalytic perfection.

*Reciprocal FosA and X mutants*

A series of reciprocal mutants of PA1129 and mlr3345 were prepared and analyzed for FosA (GSH transferase) and FosX (hydrolase) activity. The PA1129 W34A mutant has been discussed (Chapter V). The W34A/G37E mutant showed a severe decrease in catalytic activity and corresponding increase in $K_m^{GSH}$. In fact, limitations of the assay used prevented an accurate determination of $K_m^{GSH}$. Instead, a Lineweaver-Burk analysis was used to estimate the parameter. The G37E mutant was not analyzed except for a preliminary $k_{cat}$ determination. Neither the W34A/G37E/S50M or the W34A/G37E/Y39E/S50M mutants displayed hydrolase activity, and the GSH transferase activity was severely depressed.

*MIC determination for mutant proteins*

*In vivo* resistance assays revealed that some mutations to PA1129 had little effect on the ability to confer resistance to fosfomycin in *E. coli* (Table 9). However, the G37E single mutant and any multiple mutant containing G37E show depressed resistance to fosfomycin. Since the kinetic efficiency of these mutants is not very high, it is not surprising that resistance would be low. Interestingly, although the W34A mutant exhibits low catalytic activity and reduced GSH binding, it seems to retain sufficient activity to provide resistance *in vivo*.

*Promiscuity and evolution*

As proteins evolve, they must gain catalytic activity at the expense of substrate diversity. Steps to gain insight into the evolution of the fosfomycin resistance proteins have shown limited success. However, it appears that FosX and FosB proteins, which are less catalytically proficient than the FosA proteins, are also inherently more promiscuous (Tables 7 and 8). Mlr3345, the least active fosfomycin resistance protein, catalyzes the addition of nucleophiles, both water and GSH, to fosfomycin in addition to an as yet uncharacterized native activity. Other FosX proteins which have become more proficient in catalyzing fosfomycin hydrolysis (e.g. lmo1702) lack the ability to act as a thiol transferase. The modestly active FosB proteins developed in Gram positive bacteria to catalyze the addition of L-cysteine to fosfomycin. They show no hydrolase activity but also show low levels of catalysis with other cellular thiols, even one (GSH) which is not present in their native organisms. FosA, the most evolutionarily-advanced class of fosfomycin resistance proteins, shows a strong preference for GSH as thiol but can utilize the related cysteine, albeit not very efficiently. Interestingly, binding of $K^+$ by FosA dramatically changes the promiscuity ratio to only about a 10-fold preference for GSH over cysteine, indicating that acquisition of a cation binding loop played a significant role in the evolution of the FosA proteins (Table 8).

STUDIES OF FOSB HOMOLOGUES FROM *STAPHYLOCOCCUS AUREUS*
AND *BACILLUS SUBTILIS*


Results


*Purification of the FosB proteins*

The purification protocol for Bs_yndn protein was changed from previous

methods (Wang and Armstrong, unpublished data) to improve purity. Purification of the

FosB from *S. aureus* (FosB$^{Sa}$) successfully produced respectable yields of purified, active

enzyme. As expected from the calculated pI of 8.51 (EMBL WWW Gateway to

Isoelectric Point Service), protein interacted well with the cation exchange resin.
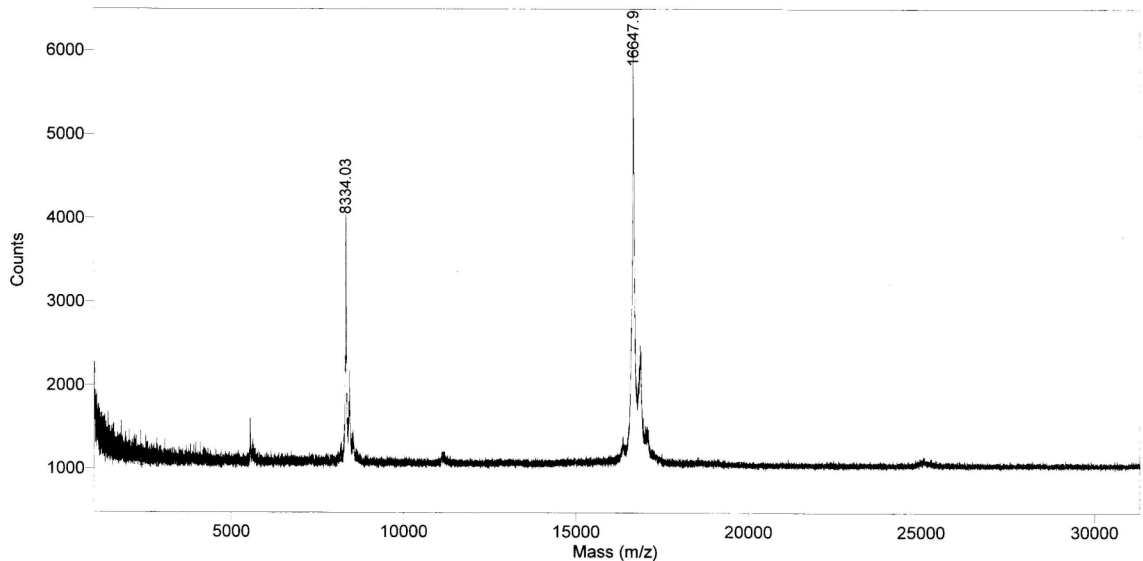



Figure 46. MALDI mass spectrum of purified FosB from *S. aureus*. The molecular
weight as calculated from primary sequence is 16,637 Da.

*Kinetic analysis of FosB$^{Sa}$ with L-cysteine and fosfomycin*

Preliminary assays revealed that, like the protein from *B. subtilis*, the *S. aureus* FosB preferred Mg$^{++}$ for catalysis (Figure 47). The protein also displayed kinetics very similar to the *B. subtilis* protein (Table 10).
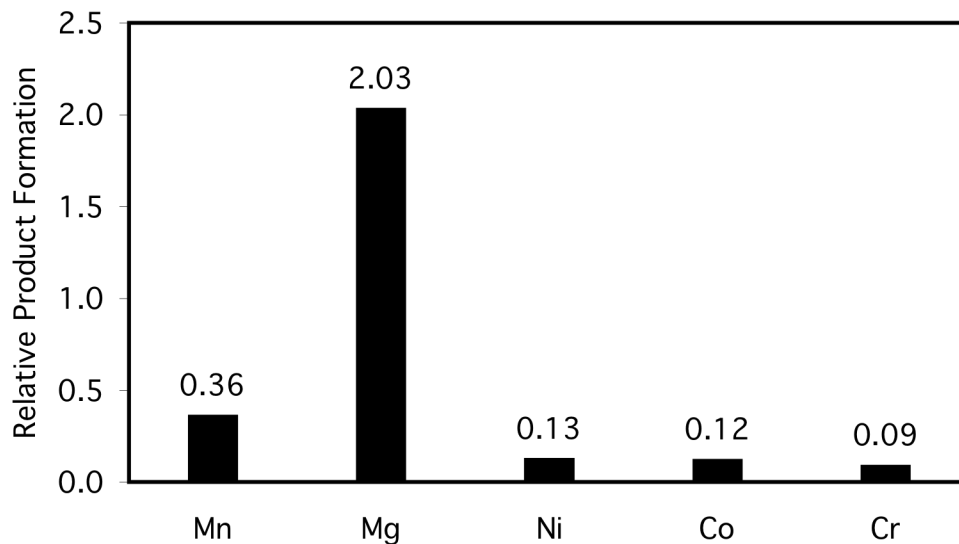


Figure 47. Metal ion preference as determined by relative product (Cys-fos) formation. Reactions contained 50 µM transition metal or 1 mM Mg$^{++}$, 100 mM K$^{++}$, 15 mM cysteine and fosfomycin, and 23 µM protein in 10 mM MOPS pH 7.0.

**A**
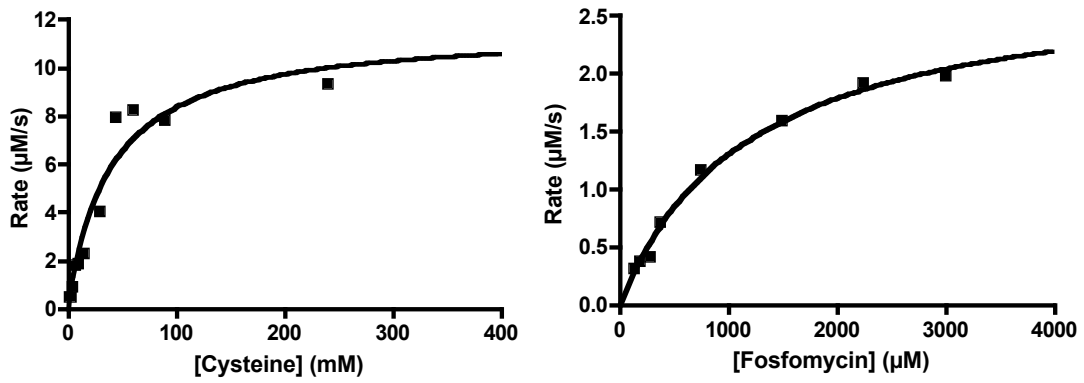


**B**
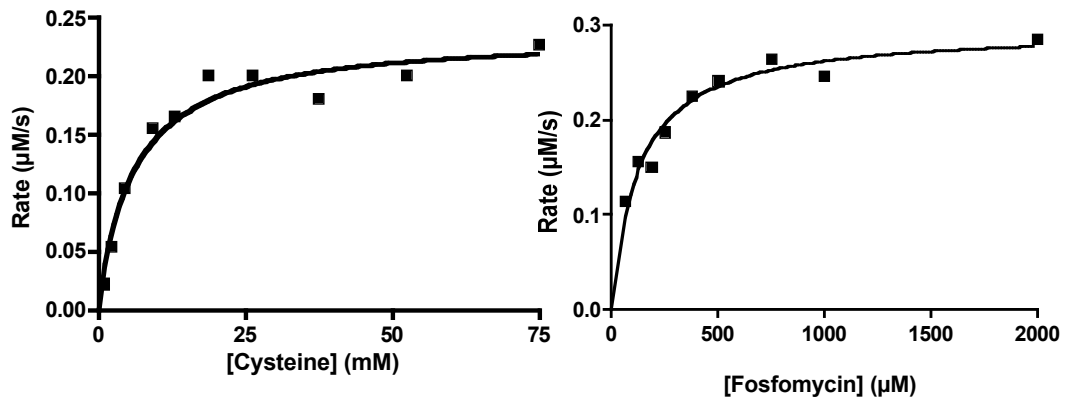


Figure 48.  Results of Michaelis-Menten plots of kinetic data for FosB from *Bacillus subtilis* (A) and *Staphylococcus aureus* (B).

**Table 10.** Kinetic parameters for FosB proteins from *S. aureus* and *B. subtilis*.

| | $k_{cat}$ (s$^{-1}$) | $K_m^{fos}$ ($\mu$M) | $k_{cat}/K_m^{fos}$ (M$^{-1}$s$^{-1}$) | $K_m^{cys}$ (mM) | $k_{cat}/K_m^{cys}$ (M$^{-1}$s$^{-1}$) |
|---|---|---|---|---|---|
| *S. aureus* | 0.98 ± 0.04 | 130 ± 20 | (7.7 ± 1.3) x 10$^3$ | 6.0 ± 1.2 | 160 ± 34 |
| *B. subtilis* | 4.8 ± 0.3 | 1190 ± 152 | (4.0 ± 0.6) x 10$^3$ | 40 ± 12 | 120 ± 40 |

Sequence alignments of FosB proteins with the FosA proteins revealed a conserved tyrosine which was investigated as a potential thiol ionizing residue (Appendix A). Evidence from an energy-minimized complex of GSH and PA1129 indicated that the residue was in an ideal position with respect to fosfomycin to activate GSH. The Y40F mutant of the FosB from *B. subtilis* was prepared by site directed mutagenesis, expressed, and purified. A preliminary kinetic analysis revealed that the mutant displayed severely depressed activity ($k_{cat}$ = 0.016 s$^{-1}$). Further evidence from the PA1129 Y39F mutant supports the notion that residue is in fact a common catalytic residue among the thiol-utilizing fosfomycin resistance proteins.

*Promiscuity of the FosB proteins*

Previous studies (Bernat and Armstrong, unpublished data) showed that FosB$^{Bs}$ was capable of catalyzing the addition of a variety of thiols (Figure 49) to fosfomycin, although not very efficiently. Substrate analysis of FosB$^{Sa}$ revealed that it too was a promiscuous enzyme, with L-cysteine being the preferred substrate (Figure 49, Table 11)
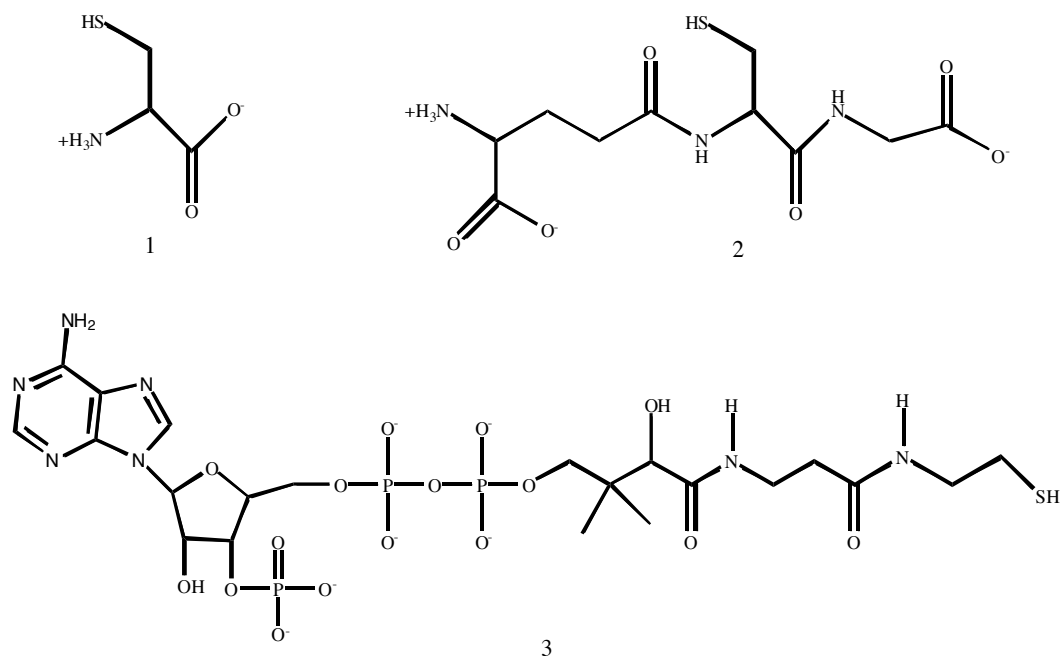
Figure 49. Thiols analyzed as FosB substrates. 1. L-cysteine. 2. Glutathione. 3. CoA.
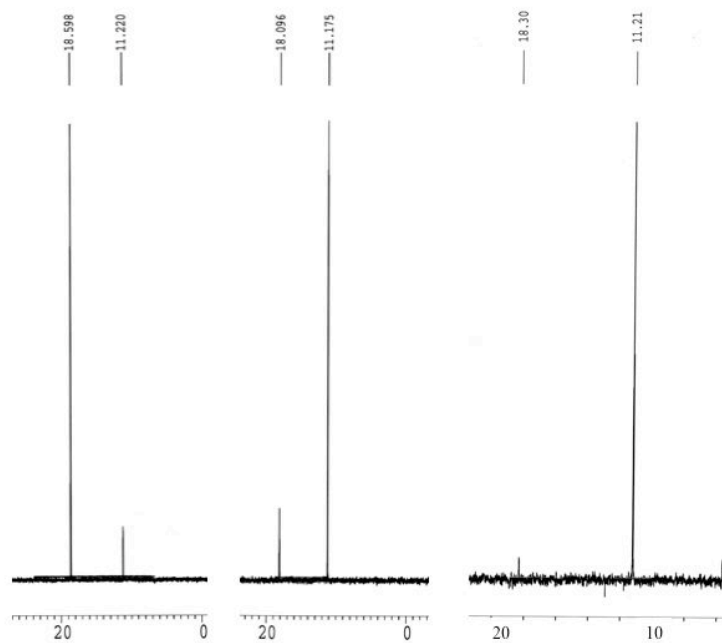


Figure 50. $^{31}$P NMR spectra showing results from incubations of FosB$^{Sa}$ with, from left to right, L-cysteine, GSH, and CoA showing formation of Cys-fos, GS-fos, and CoA-fos at 18.6, 18.1, and 18.3 ppm, respectively. The fosfomycin resonance is seen at 11.2 ppm.

**Table 11.** Turnover numbers for FosB$^{Sa}$ catalyzed addition of thiols to fosfomycin as estimated by $^{31}$P NMR.

| | L-Cysteine | GSH | CoA |
|---|---|---|---|
| k$_{cat}$ (s$^{-1}$) | 5.0 | 0.06 | 0.02 |

*Protein crystallography*

Several attempts have been made to crystallize the FosB proteins. Some crystals were obtained (Figure 51), but diffraction was poor.
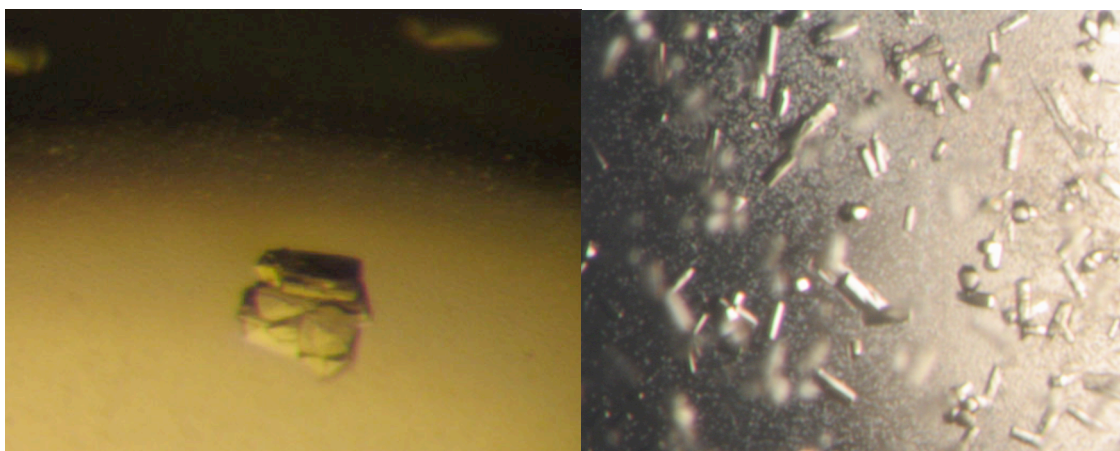


Figure 51. Left: Crystals of FosB$^{Sa}$ in 10% PEG 3350, 2% glycerol, 100 mM TRIS pH 7.0. Right: Crystals of FosB$^{Bs}$ in 14% PEG 3350 and 3% isopropanol and 100 mM TRIS pH 8.5.

*MIC for fosfomycin in E. coli*

The ability of the genomic fosfomycin resistance proteins to confer resistance *in vivo* has been approximated by determining MIC values for fosfomycin for *E. coli* transformed with plasmids expressing the resistance proteins (See Chapter III and Table

12).  Both FosB proteins produce respectable resistance in *E. coli* in the absence of the uptake inducer G6P.  However, in the presence of G6P, resistance is quite poor.

**Table 12.**  MIC values for fosfomycin (mg/mL) provided to *E. coli* transformed with expression plasmids for the indicated FosB protein.

|  | - G6P | + G6P |
|---|---|---|
| *B. subtilis* FosB | $12.8 < MIC < 25.6$ | $0.05 < MIC < 0.10$ |
| *S. aureus* FosB | $> 25.6$ | $0.20 < MIC < 0.40$ |

Discussion

*Kinetic analysis of FosB$^{Sa}$ with L-cysteine and fosfomycin*

Analysis of the FosB homologue from *S. aureus* revealed that it was a modestly active cysteine transferase specific for fosfomycin.  The enzyme prefers $Mg^{++}$ as its metal cofactor, which is similar to the homologous FosB protein from *B. subtilis*.

*Promiscuity of the FosB proteins*

The FosB proteins exhibit activity with a variety of thiol substrates, but their promiscuity is limited to thiol transferase reactions.  No hydrolase activity towards fosfomycin was observed.  Since no structural information exists for the FosB proteins, it is difficult to make many conclusions about how thiol promiscuity occurs.

*Protein crystallography*

Although attempts to crystallize the fosfomycin resistance proteins have generated high-resolution structures of PA1129 in the presence of metal, substrate, and inhibitor as well as structures of the plasmid-encoded FosA and several FosX proteins, no structure has been obtained for a FosB. The proteins do not crystallize readily by either vapor diffusion methods or under oil. Vapor diffusion trays yield poor results, generating crystals having low resolution diffraction and, in some cases, mosaicity. The proteins are not very amenable to NMR structural studies because their dimeric nature raises the effective molecular weight to over 30 kDa. Perhaps cloning another FosB homologue will enable a determination of structure if the new protein crystallizes more readily.

*MIC for fosfomycin in E. coli*

FosB proteins confer surprisingly poor resistance to fosfomycin when tested in *in vivo* assays using *E. coli* transformed with expression plasmids. The fact that these proteins prefer L-cysteine as a thiol donor, which is not readily available in *E. coli*, could explain their poor activity. The resistance which is seen probably results from the ability of the FosB proteins to utilize GSH in the absence of cysteine.

CHAPTER VIII


CONCLUSIONS


PA1129 has been shown to be a very efficient fosfomycin resistance protein of the FosA class, being a GSH transferase highly specific for fosfomycin. Like the plasmid-encoded protein, it prefers Mn(II) for catalysis and is activated by monovalent ions such as $K^+$. The protein has been structurally characterized via EPR and circular dichroism spectroscopy as well as x-ray crystallography. It retains the paired βαββ structural motifs characteristic of the VOC superfamily and utilizes its metal center in a similar manner to bind substrate and facilitate catalysis.

Early crystal structures of PA1129 indicated that small phosphonates might bind and effectively inhibit fosfomycin resistance proteins. Results reported here have established a stereoelectronic basis for the design of effective inhibitors of fosfomycin resistance proteins. The development of inhibitors that are effective *in vivo* is an attractive avenue for enhancing the efficacy of fosfomycin toward pathogens that harbor either plasmid or genomically encoded resistance proteins. Understanding substrate binding and catalysis can also aid in explanation of how the FosA proteins have become so catalytically efficient.

Evolution of the fosfomycin resistance proteins remains poorly understood. It is likely that FosX proteins developed from a promiscuous progenitor, since the nucleophile (water) is present at 55 M, a concentration far higher than other cellular nucleophiles. FosB proteins, which are more closely related to the progenitor than the FosA proteins,

could have developed the ability to utilize cysteine as a nucleophile in bacteria lacking GSH. Development of a $K^+$-binding loop and the ability to utilize GSH resulted in highly proficient FosA enzymes. The $K^+$ could serve to withdraw electron density from the metal center, making it more electrophilic and thus more reactive. Evidence reported here indicates it enhances catalysis by facilitating substrate binding. Essentially every mutant studied in attempts to more fully understand the FosA mechanism exhibited dramatic decreases in catalytic efficiency. This supports the notion that FosA enzymes have evolved to a state of near catalytic perfection, as any structural perturbation produces a protein with less activity.

The FosA proteins appear to have evolved a GSH binding site through convergent evolution when compared to the canonical GSH transferases. Many similarities, including critical hydrogen bonding interactions with the γ-glutamyl portion of the molecule, seem to have arisen. However, neither class of GSH transferase shows any cross-reactivity with electrophilic substrates utilized by the other class (e.g. fosfomycin, CDNB). Experiments to further validate the FosA GSH binding site are on-going.

Much remains to be learned about the FosB proteins, including analysis of various mutants (especially residue 9) and structural determinations. However, these results have conclusively shown that FosB proteins efficiently catalyze the addition of L-cysteine to fosfomycin in a $Mg^{++}$-dependant manner. Mutagenesis suggests that, like the FosA proteins, FosB enzymes utilize an active-site tyrosine (Y40 in the *Bacillus* protein) to assist in ionization of the thiol. Also, the FosB proteins exhibit less stringent requirements for thiol substrates, being able to utilize GSH and CoA in addition to cysteine.

*Future Work*

A large body of knowledge has been collected regarding the FosX fosfomycin resistance proteins. This includes a variety of crystal structures as well as an array of mutants. More work remains to be done to elucidate structural features of FosA and X proteins which determine substrate specificity and catalytic efficiency. The same can be said for the FosB proteins, whose structure and means of substrate binding remain elusive. Many intriguing questions remain regarding the evolution of these proteins. Why did only the FosA class develop a monovalent ion binding loop? How do the FosB proteins bind the alternate substrate CoA? Can GSH binding be improved in the FosX proteins by directed evolution? On-going research is attempting to answer these and other questions.

# APPENDIX

## A1. CLUSTAL W (1.81) Multiple Sequence Alignment

```
Consensus key
* - fully conserved residue          . - conservation of weak groups
: - conservation of strong groups      - no consensus


B_anthracis_FosB    -MLQGINHICFSVSNLEKSIEFYQKILQAKLLVKG-------RKLAYFDLNG-
BS_yndn             MEIKGINHLLFSVSHLDTSIDFYQKVFGAKLLVKG-------RTTAYFDMNG-
S_aureus_FosB       -MLKSINHICFSVRNLNDSIHFYRDILLGKLLLTG-------KKTAYFELAG-
LMO_ATCC            -MISGLSHITLIVKDLNKTTAFLQNIFNAEEIYSSGDKTFSLSKEKFFLIAG-
LMO_EGD             -MISGLSHITLIVKDLNKTTTFLREIFNAEEIYSSGDQTFSLSKEKFFLIAG-
B_melitensis        -MVQGLSHMTFIVRDLDRMEEILTTVFDARRVYDSGAETFSLSKERFFLIGNG
mlr3345             -MIEGLSHMTFIVRDLERMTRILEGVFDAREVYASDTEQFSLSREKFFLIGD-
C_botulinum         -MIERISHITFVVKNLDKTTQLFKELFNAKZVYYSGEKKHFLFKERFFIVGS-
P_fluorescens       -MLTGLNHLTLAVTDLDSSLAFYRDVLKLRVEAT-------WDAGAYLSLPG-
PA1129              -MLTGLNHLTLAVADLPASIAFYRDLLGFRLEAR-------WDQGAYLELGS-
TN2921              -MLQSLNHLTL-VSDLQKSVTFWHELLGLTLHAR-------WNTGAYLTCGD-
consensus           -ml-glnHitf-VrdLeksi-fy-dif-akll-----------k-ayf-lag-


B_anthracis_FosB    ---LWIALNVEEDIPRNE-IKQSYTHMAFTVTNEALDHLKEVLIQNDVNILP
BS_yndn             ---IWLALNEEPDIPRND-IKLSYTHIAFTIEDHEFEEMSAKLKRLHVNILP
S_aureus_FosB       ---LWIALNEEKDIPRNE-IHFSYTHIAFTIDDSEFKYWHQRLKDNNVNILE
LMO_ATCC            ---LWICIMEGDSLQER-----TYNHIAFQIQSEEVDEYTERIKALGVEMKP
LMO_EGD             ---LWICIMEGDSLQEQ-----TYNHIAFRIQSEEVDEYIERIKSLGVEIKP
B_melitensis        KEPIWIATMEGEPLPTR-----TNNHVAFKIANNEYEAYLKRIRALGLEVRE
mlr3345             ---IWVAIMQGEKLAER-----SYNHIAFKIDDADFDRYAERVGKLGLDMRP
C_botulinum         ---QWIAVMEDANILNR-----TYHHIAFKISNSDVDNYLDKIKTLNLELKP
P_fluorescens       ---LWLCLSLDPKRHPEP--AADYTHYAFSIGAADFPLFVQLLRAANVQEWR
PA1129              ---LWLCLSREPQ-YGGP--AADYTHYAFGIAAADFARFAAQLRAHGVREWK
TN2921              ---LWVCLSYDEARQYVPPQESDYTHYAFTVAEEDFEPLSQRLEQAGVTIWK
consensus           ---lWial-eee-I--------aytHiAF-i---efd-w--rlk-lgv-I-p


B_anthracis_FosB    GRERDERDQRSLYFTDPDGHKFEFHTGTLQNRLEYYKEDKKHMTFYI----
BS_yndn             GRERDERDRKSIYFTDPDGHKFEFHTGTLQDRLRYYKQEKTHMHFYDETAF
S_aureus_FosB       GRVRDIRDRQSIYFTDPDGHKLELHTGTLENRLNYYKEAKPHMTFYK----
LMO_ATCC            ERPRVQGEGRSIYFYDFDNHLFELHAGTLEERLKRYHE-------------
LMO_EGD             ERPRVEGEGRSIYFYDFDNHLFELHAGTLEERLKRYHE-------------
B_melitensis        GRSRVPGEGQSIYFYDDDNHMFELHTGTLDERLKRYGQGR-----------
mlr3345             PRPRVEGEGRSIYFYDDDNHMFELHTGTLTERLARKAKGLEAAQ-------
C_botulinum         PRRRVSGEGYSIYFYDYDNNLFELHTETLEKRLASYTKIDNI---------
P_fluorescens       DNR---SEGASFYFLDPDGHKLEAHVGDLASRLAACRQKPYAGMGFFNEP-
PA1129              QNR---SEGDSFYFLDPDGHRLEAHVGDLRSRLAACRQAPYAGMRFAD---
TN2921              QNK---SEGASFYFLDPDGHKLELHVGSLAARLAACREKPYAGMVFTSDEA
consensus           -r-r---eg-SiYF-DpDghkfElHtgtL--RL--yk--------y-----
```

REFERENCES

(1)     Heijenoort, J. v. (1998) Assembly of the monomer unit of bacterial peptidoglycan. *Cell. Mol. Life Sci. 54*, 300-304.

(2)     Hall, B. G. (2004) Predicting the evolution of antibiotic resistance genes. *Nature Reviews Microbiology 2*, 430-435.

(3)     Davies, J. E. (1997) Origins, acquisition and dissemination of antibiotic resistance determinants, in *Antibiotic resistance: origins, evolution, selection and spread* pp 15-27, John Wiley & Sons, Chichester.

(4)     Levy, S. B., and Marshall, B. (2004) Antibacterial resistance worldwide: causes, challenges and responses. *Nature Medicine 10*, S122-S129.

(5)     Walsh, C. (2003) Where will new antibiotics come from? *Nature Reviews Microbiology 1*, 65-70.

(6)     Hendlin, D., Stapley, E. O., Jackson, M., Wallick, H., Miller, A. K., Wolf, J. J., Miller, T. W., Chaiet, L., Kahan, F. M., Foltz, E. L., and Woodruff, H. B. (1969) Phosphonomycin, a new antibiotic produced by strains of *Streptomyces*. *Science 166*, 122-123.

(7)     Christensen, B. G., Leanze, W.J., Beattie, T.R., Patchett, A.A. (1969) Phosphonomycin: Structure and Synthesis. *Science 166*, 123-125.

(8)     Marquardt, J. L., Brown, E.D., Lane, W.S., Haley, T.M., Ichikawa, Y., Wong, C-H, Walsh, C.T. (1994) Kinetics, stoichiometry, and identification of the reactive thiolate in the inactivation of UDP-GlcNAc enolpyruvoyl transferase by the antibiotic fosfomycin. *Biochemistry 33*, 10646-10651.

(9)     Schönbrunn, E., Eschenburg, S., Krekel, F., Luger, K., and Amrhein, N. (2000) Role of the loop containing residue 115 in the induced-fit mechanism of the bacterial cell wall biosynthetic enzyme MurA. *Biochemistry 39*, 2164-2173.

(10)    Delano, W. L. (2002) The PyMOL Molecular Graphics System on the World Wide Web http://www.pymol.org.

(11)    Kadner, R. J., and Winkler, H. H. (1973) Isolation and characterization of mutations affecting the transport of hexose phosphates in *Escherichia coli*. *J Bacteriol 113*, 895-900.

(12)     Tsuruoka, T., and Yamada, Y. (1975) Charactertization of spontaneous
         fosfomycin (phosphonomycin)-resistant cells of *Escherichia coli* B in vitro. *J
         Antibiot (Tokyo) 28*, 906-11.

(13)     Kahan, F. M., Kahan, J.S., Cassidy, P.J. (1974) The mechanism of action of
         fosfomycin. *Ann. NY Acad. Sci. 235*, 364-386.

(14)     Kim, D. H., Lees, W. J., Kempsell, K. E., Lane, W. S., Duncan, K., and Walsh, C.
         T. (1996) Characterization of a Cys115 to Asp substitution in the Escherichia coli
         cell wall biosynthetic enzyme UDP-GlcNAc enolpyruvyl transferase (MurA) that
         confers resistance to inactivation by the antibiotic fosfomycin. *Biochemistry 35*,
         4923-8.

(15)     García-Lobo, J. M., and Ortiz, J. M. (1982) Tn2921, a transposon encoding
         fosfomycin resistance. *J. Bacteriology 151*, 477-479.

(16)     Llaneza, J., Villar, C. J., Salas, J. A., Suarez, J. E., Mendoza, M. C., and
         Hardisson, C. (1985) Plasmid-mediated fosfomycin resistance is due to enzymatic
         modification of the antibiotic. *Antimicrob. Agents Chemother. 28*, 163-164.

(17)     Arca, P., Rico, M., Brana, A. F., Villar, C. J., Hardisson, C., and Suarez, J. E.
         (1988) Formation of an adduct between fosfomycin and glutathione:  a new
         mechanism of antibiotic resistance in bacteria. *Antimicrob. Agents Chemother. 32*,
         1552-1556.

(18)     Arca, P., Hardisson, C., and Suarez, J. E. (1990) Purification of a glutathione S-
         transferase that mediates fosfomycin resistance in bacteria. *Antimicrob. Agents
         Chemother. 34*, 844-848.

(19)     Bernat, B. L., Laughlin, T., and Armstrong, R. N. (1997) Fosfomycin resistance
         protein (FosA) is a manganese metalloglutathione transferase related to
         glyoxalase I and the extradiol dioxygenases. *Biochemistry 36*, 3051-3055.

(20)     Armstrong, R. N. (2000) Mechanistic diversity in a metalloenzyme superfamily.
         *Biochemistry 39*, 13625-13632.

(21)     Pakhomova, S., Rife, C. L., Armstrong, R. N., and Newcomer, M. N. (2004)
         Structure of fosfomycin resistance protein FosA from transposon *Tn2921*. *Protein
         Science 13*, 1260-1265.

(22)     Cao, M., Bernat, B. A., Wang, Z., Armstrong, R. N., and Helmann, J. D. (2001)
         FosB, a cysteine-dependent fosfomycin resistance protein under the control of
         $\sigma^W$, an extracytoplasmic-function $\sigma$ factor in *Bacillus subtilis*. *J. Bacteriology
         183*, 2380-2383.

(23)     Reeves, D. S. (1994) Fosfomycin trometamol. *J. Antimicrob. Chemother. 34*, 853-858.

(24)     Matsumoto, T., Tateda, K., Miyazaki, S., Furuya, N., Ohno, A., Ishii, Y., Hirakata, Y., and Yamaguchi, K. (1997) Immunomodulating effect of fosfomycin on gut-derived sepsis caused by *Pseudomonas aeruginosa* in mice. *Antimicrob. Agents Chemother. 41*, 308-313.

(25)     Neu, H. C., and Kamimura, T. (1981) In vitro and in vivo antibacterial activity of FR-31564, a phosphonic acid antimicrobial agent. *Antimicrob. Agents Chemother. 19*, 1013-1023.

(26)     Daza, R., Gutiérrez, J., and Piédrola, G. (2001) Antibiotic susceptibility of bacterial strains isolated from patients with community-acquired urinary tract infections. *International J. Antimicrob. Agents 18*, 211-215.

(27)     Bernat, B. L., Laughlin, T., and Armstrong, R. N. (1999) Elucidation of a monovalent cation dependence and characterization of the divalent cation binding site of the fosfomycin resistance proteins. *Biochemistry 38*, 7462-7469.

(28)     Rife, C. L., Pharris, R. E., Newcomer, M. E., and Armstrong, R. N. (2002) Crystal structure of a genomically encoded fosfomycin resistance protein (FosA) at 1.19 Å resolution by MAD phasing off the L-III edge of Tl$^+$. *J. Am. Chem. Soc. 124*, 11001-11003.

(29)     Smoukov, S. K., Telser, J. A., Bernat, B. A., Rife, C. L., Armstrong, R. N., and Hoffman, B. M. (2002) EPR study of substrate binding to the Mn(II) active site of the bacterial antibiotic resistance enzyme FosA:  a better way to examine Mn(II). *J. Am. Chem. Soc. 124*, 2318-2326.

(30)     Ellman, G. L. (1959) Tissue sulfhydryl groups. *Archives Biochem Biophys 82*, 70-77.

(31)     Jakupovic, E., and Stenhede, J. (1997), Aktiebolaget Astra, United States.

(32)     McConnell, R. L. a. H. W. C., Jr. (1956) Preparation of 1-hydroxyalkylidenediphosphonates. *J. Am. Chem. Soc. 78*, 4450-2.

(33)     Hata, M. S. a. T. (1978) Convenient synthesis of unesterified acylphosphonic acids. *J.C.S. Chem. Comm. 7*, 285-286.

(34)     Franczyk, T. S. (2001)  (Office, U. S. P., Ed.), Monsanto Co, USA.

(35)     Dixon, M. (1953) The determination of enzyme inhibitor constants. *Biochem. J. 55*, 170-171.

(36)   Dirr, H., Reinemer, P., and Huber, R. (1994) X-ray crystal structures of cytosolic glutathione *S*-transferases: implications for protein architecture, substrate recognition and catalytic function. *Eur. J. Biochem. 220*, 645-661.

(37)   Ronald L. Dunbrack, J., and Karplus, M. (1993) Backbone-dependent rotamer library for proteins application to side-chain prediction. *J. Mol. Biol. 230,* 543-574.

(38)   Bayly, C. I., Cieplak, P., Cornell, W. D., and Kollman, P. A. (1993) A well-behaved electrostatic potential based method using charge restrains for determining atom-centered charges: the RESP model. *J. Phys. Chem. 97*, 10269-10280.

(39)   Case, D. A., Darden, T. A., T.E. Cheatham, I., Simmerling, C. L., Wang, J., Duke, R. E., Luo, R., Merz, K. M., Wang, B., Pearlman, D. A., Crowley, M., Brozell, S., Tsui, V., Gohlke, H., Mongan, J., Hornak, V., Cui, G., Beroza, P., Schafmeister, C., Caldwell, J. W., Ross, W. S., and Kollman, P. A. (2004), University of California, San Francisco, San Francisco.

(40)   Edelhoch, H. (1967) Spectroscopic determination of tryptophan and tyrosine in proteins. *Biochemistry 6*, 1948-1954.

(41)   Walsby, C. J., Telser, J., Rigsby, R. E., Armstrong, R. N., and Hoffman, B. M. (2005) Enzyme control of small-molecule coordination in FosA as revealed by ^{31}P pulsed ENDOR and ESE-EPR. *J. Am. Chem. Soc. in press*.

(42)   Daza, R., Gutiérrez, J., and Piédrola, G. (2001) Antibiotic susceptibility of bacterial strains isolated from patients with community-acquired urinary tract infections. *Int. Jnl. Antimicrob. Agts. 18*, 211-215.

(43)   Sigel, A., and Sigel, H. (2000) in *Metal ions in biological systems*, Marcel Dekker, New York.

(44)   Addison, A. W., and Rao, T. N. (1984) Synthesis, structure, and spectroscopic properties of copper (II) compounds containing nitrogen-sulphur donor ligands; the crystal and molecular structure of aqua [1,7-bis(*N*-methylbenzimidazol-2'-yl)-2,6-dithiaheptane] copper (II) perchlorate. *J. Chem. Soc. Dalton Trans.*, 1349-1356.

(45)   Armstrong, R. N. (1997) Structure, catalytic mechanism, and evolution of the glutathione transferases. *Chem. Res. Toxicol. 10*, 2-18.

(46)   Parsons, J. F., Xiao, G., Gilliland, G. L., and Armstrong, R. N. (1998) Enzymes harboring unnatural amino acids: mechanistic and structural analysis of the enhanced catalytic activity of a glutathione transferase containing 5-fluorotryptophan. *Biochemistry 37*, 6286-6294.

121

(47)   Bernat, B. L., Laughlin, T., and Armstrong, R. N. (1998) Regiochemical and stereochemical course of the reaction catalyzed by the fosfomycin resistance protein, FosA. *Journal of Organic Chemistry 63*, 3778-3780.

(48)   Rigsby, R. E., Rife, C. L., Fillgrove, K. L., Newcomer, M. E., and Armstrong, R. N. (2004) Phosphonoformate:  A minimal transition state analogue inhibitor of the fosfomycin resistance protein, FosA. *Biochemistry 43*, 13666-13673.

(49)   Beharry, Z., and Palzkill, T. (2005) Functional analysis of active site residues of the fosfomycin resistance enzyme FosA from *Pseudomonas aeruginosa*. *J. Biol. Chem. 280*, 17786-17791.

(50)   Liu, S., Zhang, P., Ji, X., Johnson, W. W., Gilliland, G. L., and Armstrong, R. N. (1992) Contribution of tyrosine 6 to the catalytic mechanism of isoenzyme 3-3 of glutathione-*S*-transferase. *J. Biol. Chem. 267*, 4296-4299.